

**DESIGN AND PERFORMANCE STUDY OF
HYDROPHILIC AND SUPER HYDROPHILIC CAPILLARY
VALVES FOR NOVEL MICROFLUIDICS SYSTEMS**

AMIN KAZEMZADEH

**FACULTY OF ENGINEERING
UNIVERSITY OF MALAYA
KUALA LUMPUR**

2015

**DESIGN AND PERFORMANCE STUDY OF
HYDROPHILIC AND SUPER HYDROPHILIC VALVES
FOR NOVEL MICROFLUIDICS SYSTEMS**

AMIN KAZEMZADEH

**THESIS SUBMITTED IN FULFILMENT OF THE
REQUIREMENTS FOR THE DEGREE OF DOCTORAL
OF PHILOSOPHY**

**FACULTY OF ENGINEERING
UNIVERSITY OF MALAYA
KUALA LUMPUR**

2015

UNIVERSITY OF MALAYA
ORIGINAL LITERARY WORK DECLARATION

Name of Candidate: AMIN KAZEMZADEH

Registration/Matric No: KHA130013

Name of Degree:

Title of Thesis (“this Work”):

DESIGN AND PERFORMANCE STUDY OF HYDROPHILIC AND SUPER
HYDROPHILIC VALVES FOR NOVEL MICROFLUIDICS SYSTEMS

Field of Study:

I do solemnly and sincerely declare that:

- (1) I am the sole author/writer of this Work;
- (2) This Work is original;
- (3) Any use of any work in which copyright exists was done by way of fair dealing and for permitted purposes and any excerpt or extract from, or reference to or reproduction of any copyright work has been disclosed expressly and sufficiently and the title of the Work and its authorship have been acknowledged in this Work;
- (4) I do not have any actual knowledge nor do I ought reasonably to know that the making of this work constitutes an infringement of any copyright work;
- (5) I hereby assign all and every rights in the copyright to this Work to the University of Malaya (“UM”), who henceforth shall be owner of the copyright in this Work and that any reproduction or use in any form or by any means whatsoever is prohibited without the written consent of UM having been first had and obtained;
- (6) I am fully aware that if in the course of making this Work I have infringed any copyright whether intentionally or otherwise, I may be subject to legal action or any other action as may be determined by UM.

Candidate’s Signature

Date: 28.11.2015

Subscribed and solemnly declared before,

Witness’s Signature

Date:

Name:

Designation:

UNIVERSITI MALAYA
PERAKUAN KEASLIAN PENULISAN

Nama: AMIN KAZEMZADEH

No. Pendaftaran/Matrik: KHA130013

Nama Ijazah:

Tajuk Tesis (“Hasil Kerja ini”):

REKABENTUK DAN PRESTASI KAJIAN HYDROPHILIC DAN SUPER
HIDROFILIK INJAP UNTUK SISTEM MICROFLUIDICS NOVEL

Bidang Penyelidikan:

Saya dengan sesungguhnya dan sebenarnya mengaku bahawa:

- (1) Saya adalah satu-satunya pengarang/penulis Hasil Kerja ini;
- (2) Hasil Kerja ini adalah asli;
- (3) Apa-apa penggunaan mana-mana hasil kerja yang mengandungi hakcipta telah dilakukan secara urusan yang wajar dan bagi maksud yang dibenarkan dan apa-apa petikan, ekstrak, rujukan atau pengeluaran semula daripada atau kepada mana-mana hasil kerja yang mengandungi hakcipta telah dinyatakan dengan sejelasnya dan secukupnya dan satu pengiktirafan tajuk hasil kerja tersebut dan pengarang/penulisnya telah dilakukan di dalam Hasil Kerja ini;
- (4) Saya tidak mempunyai apa-apa pengetahuan sebenar atau patut semunasabahnya tahu bahawa penghasilan Hasil Kerja ini melanggar suatu hakcipta hasil kerja yang lain;
- (5) Saya dengan ini menyerahkan kesemua dan tiap-tiap hak yang terkandung di dalam hakcipta Hasil Kerja ini kepada Universiti Malaya (“UM”) yang seterusnya mula dari sekarang adalah tuan punya kepada hakcipta di dalam Hasil Kerja ini dan apa-apa pengeluaran semula atau penggunaan dalam apa jua bentuk atau dengan apa juga cara sekalipun adalah dilarang tanpa terlebih dahulu mendapat kebenaran bertulis dari UM;
- (6) Saya sedar sepenuhnya sekiranya dalam masa penghasilan Hasil Kerja ini saya telah melanggar suatu hakcipta hasil kerja yang lain sama ada dengan niat atau sebaliknya, saya boleh dikenakan tindakan undang-undang atau apa-apa tindakan lain sebagaimana yang diputuskan oleh UM.

Tandatangan Calon

Tarikh: 28.11.2015

Diperbuat dan sesungguhnya diakui di hadapan,

Tandatangan Saksi

Tarikh:

Nama:

Jawatan:

ABSTRACT

The research in this PhD thesis is motivated by the importance of precise microflow control in transforming various laboratory-based chemical and clinical assays into portable centrifugal microfluidics based devices. The more specific aim is the development of inexpensive flow control and liquid routing techniques that can be used in sample preparative processes such as blood plasma separation, washing, metering, and analyte detection. Efficient and inexpensive flow control techniques based on new principles and operations are introduced and compared with state of the art industrial approaches. Unlike previously introduced techniques these novel flow control methods are not dependent on the direction of the disk rotation and do not require special surface treatments or external power sources. The hardware to enable these techniques is easy to implement and provides robust control of the flow in centrifugal microfluidic platforms.

Prior to designing new capillary valves, a comprehensive investigation of the relationship between contact angles and capillary dimensions on the performance of passive capillary valves was carried out. The results reveal, for example, that square capillaries have lower capillary forces compared to rectangular capillaries. The results also show that -contrary to earlier theoretical predictions- the capillary force at burst valves dramatically drops when the contact angle decreases.

For the first time, a new valving technique is introduced that exploits a geometrical effect on the surface tension to control and switch the flow direction. The valve is a frequency dependent device that is able to direct the flow to one direction (e.g., c.w.) at low frequencies and to the opposite direction (e.g., c.c.w.) at higher frequencies without using external power sources or applying surface treatments. The flow behavior of the new valve for distilled water as well as for liquids with different properties was investigated experimentally and numerically. The results show that the new valve is

able to control the flow direction on a spinning microfluidic platform for liquids of widely varying properties.

Another novel microvalve is presented that allows for the efficient routing of samples, switching and controlling the flow direction on centrifugal microfluidic platforms. The distinctive feature that makes this approach different from other types of passive capillary valves is the robust control of liquid movement, which is achieved by employing two adjustable sequential burst valves i.e., a primary and a secondary burst valve. The performance of this novel configuration was experimentally tested, the flow behavior was numerically studied using the VOF method and a theoretical model for their burst frequency was presented.

For the first time, the role of the effective moment of inertia of the liquid in centrifugal microfluidics – that can be used for pushing the liquid towards specific lateral or/and radial directions – was theoretically, experimentally and numerically investigated. The experiment results confirmed that utilizing the effective moment of inertia of the liquid i.e., as a result of a sudden reduction of the rotational speed (~ 45 Hz/s), propels the entire liquid volume from a chamber adjacent to the disc's periphery to a chamber close to the disc center.

ABSTRAK

Kajian dalam tesis PhD ini adalah didorong oleh kepentingan kawalan microflow yang tepat dalam transformasi pelbagai ujikaji kimia makmal kepada peranti berasaskan microfluidics empar mudah alih. Tujuan yang lebih khusus ialah pembangunan kawalan aliran murah dan teknik laluan cecair yang boleh digunakan dalam proses persiapan sampel seperti pemisahan plasma darah, pembasuhan, pemetaran dan pengesanan analit. Teknik kawalan aliran yang cekap dan murah berasaskan prinsip dan operasi baru diperkenalkan dan dibandingkan dengan keadaan seni pendekatan perindustrian. Tidak seperti teknik diperkenalkan sebelum ini, kaedah kawalan aliran novel ini tidak bergantung kepada arah putaran cakera dan tidak memerlukan rawatan permukaan khas atau sumber kuasa luaran. Perkakas yang diperlukan untuk membolehkan teknik-teknik ini mudah untuk dilaksanakan dan menyediakan kawalan aliran yang mantap dalam platform microfluidic empar.

Sebelum mereka bentuk injap kapilari baru, siasatan menyeluruh mengenai kaitan di antara sudut hubungan dan dimensi kapilari kepada prestasi injap kapilari pasif telah dijalankan. Keputusan menunjukkan bahawa kapilari segi empat mempunyai daya rerambut yang lebih rendah berbanding dengan kapilari segi empat tepat. Keputusan juga menunjukkan bahawa berbanding dengan teori sebelum ini daya rerambut pada injap pecah jatuh mendadak apabila sudut kenalan berkurangan.

Buat pertama kalinya, satu teknik injap baru diperkenalkan dengan mengeksploitasi kesan geometri pada ketegangan permukaan untuk mengawal dan menukar arah aliran. Injap ini adalah alat yang bergantung kepada kekerapan dan mampu mengarahkan aliran ke satu arah (contohnya, cw) pada frekuensi rendah dan ke arah bertentangan (contohnya, CCW) pada frekuensi yang lebih tinggi tanpa menggunakan sumber kuasa luaran atau menggunakan rawatan permukaan. Kelakuan aliran injap baru bagi air

suling dan juga untuk cecair dengan ciri-ciri yang berbeza telah disiasat secara eksperimen dan juga secara perangkaan. Keputusan menunjukkan bahawa injap yang baru ini mampu untuk mengawal arah aliran dalam platform microfluidic berputar secara meluas untuk cecair-cecair yang mempunyai sifat berbeza.

Satu lagi microvalve baru yang dibentangkan untuk membolehkan penghalaan sampel yang cekap, penukaran dan mengawal arah aliran pada platform microfluidic empar. Ciri-ciri yang tersendiri injap tersebut yang membuat pendekatan ini berbeza daripada injap jenis kapilari pasif yang lain adalah kawalan cecair pergerakan yang mantap, yang dicapai dengan menggunakan dua injap pecah boleh-laras yang berurutan iaitu, injap pecah yang pertama dan kedua. Prestasi konfigurasi baru ini telah diuji secara eksperimen manakala kelakuan aliran dikaji secara berangka menggunakan kaedah VOF dan model teori bagi kekerapan pecah mereka telah dibentangkan.

Buat pertama kalinya, peranan momen inersia cecair dalam microfluidics empar yang boleh digunakan untuk menolak cecair ke arah tertentu arah sisi atau / dan jejarian telah disiasat secara teori, uji kaji dan berangka. Keputusan eksperimen mengesahkan bahawa menggunakan momen inersia berkesan ini, iaitu cecair, akibat daripada pengurangan secara tiba-tiba kelajuan putaran (~ 45 Hz/s), menggerakkan isipadu cecair keseluruhan dari ruang yang bersebelahan dengan pinggir cakera ke ruang berhampiran dengan pusat cakera.

bersebelahan dengan pinggir cakera ke ruang berhampiran dengan pusat cakera.

ACKNOWLEDGEMENTS

I would like to express my sincere appreciation to Dr. Poo Balan Ganesan for his supports and encouragements in the early stages of my PhD study and his valued thoughts and and suggestions during my research. I would also like to thank Prof. Ibrahim for her finical supports and her encouragements and suggestion during my study.

I like to heartedly acknowledge and appreciation and thank to Prof. Madou for his excellent guidance, suggestions and supervision of my study. His great, vivid thoughts have added much value to my study and critical thinking skills.

University of Malaya

TABLE OF CONTENTS

Abstract	iv
Abstrak	vi
Acknowledgements	viii
Table of Contents	ix
List of Figures	xiv
List of Tables.....	xviii
List of Symbols and Abbreviations.....	xix
CHAPTER 1: INTRODUCTION.....	1
1.1 Research background.....	1
1.2 Problem Statement.....	3
1.3 Research aims and objectives	3
1.3.1 Research aims.....	4
1.3.2 Research objectives	4
1.4 Scope	4
1.5 Thesis Outline.....	5
CHAPTER 2: LITERATURE REVIEW.....	6
2.1 Microfluidic platforms.....	6
2.2 Materials and Fabrication	7
2.2.1 Materials	7
2.2.1.1 Silicon.....	7
2.2.1.2 Glass	8
2.2.1.3 Polymers.....	8
2.2.2 Fabrication.....	9

2.3	Centrifugal microfluidics.....	10
2.3.1	Theory of Centrifugal Microfluidics	14
2.3.1.1	Centrifugal and Coriolis forces	14
2.3.1.2	Capillary pressure.....	16
2.3.2	Flow type.....	18
2.3.3	Microvalves and Micropumps.....	18
2.3.3.1	Passive techniques.....	19
2.3.3.2	Active techniques	26
2.4	Computational fluid dynamics studies.....	28
2.5	Summary and research gap.....	31

CHAPTER 3: EXPERIMENTAL SETUP AND COMPUTATIONAL FLUID DYNAMICS METHODS 33

3.1	Disc designs.....	33
3.2	Fabrication.....	33
3.2.1	PMMA fabrication	33
3.2.1.1	Laser cutting.....	33
3.2.1.2	CNC machining.....	35
3.2.2	Pressure sensitive adhesive (PSA) cutting	37
3.2.3	Assembly.....	37
3.3	Testing setup.....	38
3.4	Computational fluid dynamics (CFD) method	39
3.4.1	Fundamental of numerical methods	39
3.4.2	Volume of fluid (VOF) method.....	40
3.4.3	Governing equations.....	41

CHAPTER 4: INVESTIGATION OF THE PERFORMANCE OF HYDROPHILIC AND SUPER HYDROPHILIC CAPILLARY VALVES..... 44

4.1 Introduction..... 44

4.2 Boundary conditions and Numerical method 46

4.3 Mesh 47

4.4 Simulation Cases 48

4.5 Experimental set up 49

4.6 Results and discussion 50

 4.6.1 Validation 50

 4.6.2 Flow sequence in a super hydrophilic capillary 51

 4.6.3 Effect of dimensions of the capillary channel 53

 4.6.4 Effect of contact angles on burst frequency 58

4.7 Summary..... 61

CHAPTER 5: DESIGN OF GATING VALVE, A MICROVALVE TO SWITCH THE FLOW DIRECTION..... 63

5.1 Introduction..... 63

5.2 Concept..... 64

5.3 Experimental set up 64

5.4 Characterization..... 65

5.5 Numerical analysis..... 67

5.6 Results 69

 5.6.1 Validation 69

 5.6.2 Fluid motion 71

 5.6.3 Burst frequency in GVs..... 73

 5.6.4 Flow switch 75

5.7 Summary..... 79

**CHAPTER 6: DESIGN OF GUIDED ROUTING VALVE, A MICROVALVE
FOR FLOW SWITCH AND ROUTING..... 81**

6.1	Introduction.....	81
6.2	Concept.....	83
6.3	Fabrication and Experimental setup	84
6.4	Theory	86
6.5	Numerical analysis	90
6.6	Results	91
6.6.1	Flow behavior.....	91
6.6.2	Guided Routing applications	94
6.6.2.1	Flow switch	94
6.6.2.2	Fluid distribution	97
6.7	Summary.....	100

**CHAPTER 7: THE EFFECT OF MOMENT OF INERTIA AND
HETEROGENEITY 102**

7.1	Introduction.....	102
7.2	Moment of inertia in centrifugal microfluidics	102
7.2.1	Concept.....	103
7.2.2	Theory	104
7.2.3	Fabrication method and experiments.....	106
7.2.4	Preliminary results.....	107
7.3	Effect of surface heterogeneity on the liquid flow	108
7.3.1	Concept.....	108
7.3.2	Numerical method and simulation cases	109
7.3.3	Flow behavior.....	110
7.4	Summary.....	112

CHAPTER 8: CONCLUSIONS.....	113
8.1 Suggestions for future study	116
REFERENCES.....	118
LIST OF PUBLICATIONS AND PAPERS PRESENTED	131

University of Malaya

LIST OF FIGURES

Figure 2.1: Process of the formation of a centrifugal microfluidic foil (Focke et al., 2010).	10
Figure 2.2: An injection-molded LabDisc used for ELISA (He et al., 2009).	13
Figure 2.3: A metering microstructure based on capillary valving (Steigert et al., 2005).	13
Figure 2.4: Switching the flow direction by Coriolis force, (Brenner et al., 2005).	13
Figure 2.5: Partial top view of a liquid plug in a channel on a disc of radius r spinning at ω , the length of the plug is characterized by its boundaries r_2 and r_1	15
Figure 2.6: Schematic of the meniscus development in rectangular capillary, Chen et al. (2008).	18
Figure 2.7: A schematic of different types of capillary valves, a) Sudden expansion of microchannel, b) Hydrophobic patch generated by surface treatment methods, c) Siphoning.	22
Figure 2.8: The effect of aspect ratio on the burst frequency of capillary valves for $\sigma_{la}=0.072$ N/m, $\theta = 68^\circ$. The solid and the dashed lines are theoretically obtained values for capillary width of $300 \mu\text{m}$ and $400 \mu\text{m}$, respectively (Chen et al., 2008).	22
Figure 2.9: The effect of expansion angle on the burst pressure in terms of the liquid volume for a square channel ($w=h=300 \mu\text{m}$) and $\sigma_{la}=0.072$ N/m and $\theta = 68^\circ$ (Chen et al., 2008).	24
Figure 2.10: Liquid trigger valve (Melin et al., 2004).	24
Figure 2.11: Sequences of siphoning on a LabDisc, (Ducrée et al., 2007).	25
Figure 2.12: The schematic of Centrifugo-pneumatic pumping. (Gorkin III et al., 2012).	27
Figure 2.13: The schematic of using external source to apply periodic air and control the flow direction on the spinning disc (Kong & Salin, 2011).	28
Figure 2.14 Reversing the position of the red and blue liquids at 50 rad/s (Ducrée et al., 2006).	29
Figure 2.15: Mixing of red and blue colors in a zigzag micro (Ren & Leung, 2013). ...	30
Figure 2.16: Filling process A) the circle shape micro chamber B) the oval shaped micro chamber (Chen et al., 2006).	30

Figure 3.1: Different defects caused by long laser pulse (Madou, 2002).	35
Figure 3.2: An image of CNC router/engraver machine used to fabricate centrifugal microfluidics.	36
Figure 3.3: The cutter plotter used to fabricate PSA layers.	37
Figure 3.4: The spinning system and the high-speed camera.	38
Figure 4.1: Top view of Geo. 1 and Geo. 2 used in the simulations b) Computational mesh adjacent to the outlet of capillary channel of Geo 1 and Geo 2.....	48
Figure 4.2: Experimental setup: controlling computer system connected to a high-speed camera and a digital rpm meter.	49
Figure 4.3: Comparison between the present study and experimental and numerical data from Gliere et al. (2006), a) for DI-water (surface tension of 0.072 N/m) and b) biological buffer (surface tension of 0.03 N/m).....	54
Figure 4.4: Sequences of the fluid motion in a, a) hydrophilic and b) super hydrophilic capillary.....	55
Figure 4.5: Burst frequency of the CFD model and Equation from Chen et al (2008) versus aspect ratio for Cases 5-10.....	56
Figure 4.6: The distribution of the burst frequencies using Equation from Chen et al. (2008) versus different capillary height where the capillary width is kept constant of $300 \mu\text{m}$ for a contact of 70.	57
Figure 4.7: Burst frequency from the CFD model, Equation from Zeng et al. (2000b) and Equation from Chen et al. (2008) versus contact angles for Cases 11-18. Experiment results from He et al. (2009) is also given.....	59
Figure 4.8: Burst frequencies from the CFD model, Equations from Zeng et al. (2000b) and Chen et al. (2008) versus contact angles for Cases 19-26.....	59
Figure 4.9: The distribution of the burst frequencies from the CFD model and Equation from Chen et al. (2008) with respect to different aspect ratios and contact angles for Cases 27-42.	60
Figure 5.1: A sketch of (a) a conventional capillary valve (b) a Gating valve and (c) isometric view of GV.....	65
Figure 5.2: Partial top view of the liquid motion in a clockwise rotating disc a) conventional valve b) GV for capillary width of $400 \mu\text{m}$ and $G=400 \mu\text{m}$	67
Figure 5.3: Computational mesh adjacent to the outlet of capillary channel.....	68

Figure 5.4: Comparison between numerical data and theoretical expression from Chen et al. (2008).	69
Figure 5.5: Sequences of the liquid motion and meniscus propagation in a a) conventional and b) GV ($G=50 \mu m$).	70
Figure 5.6: The distribution of burst frequencies for different capillary heights and various G s between 0 and $50 \mu m$	71
Figure 5.7: The distribution of burst frequencies for different capillary heights and various G s between 50 and $250 \mu m$, for a constant capillary height ($200 \mu m$) and contact angle (68°).	71
Figure 5.8: Switching the flow direction by increasing the rotational speed.	79
Figure 6.1: A sketch of 3D view, top and side views of a conventional capillary and a GR valve. Fabrication and Experimental setup.	85
Figure 6.2: The custom-made experimental setup.	86
Figure 6.3: An exploded view of the disc assembly, Guided routing valves (GR) are located on layer fourth and fifth of the assembled disc.	86
Figure 6.4: Partial view of a disc spinning at ω containing GR valve of the auxiliary inlet and outlet length of λ_i and λ_o respectively, a liquid plug exposed to radial centrifugal and transversal Coriolis force.	90
Figure 6.5: The burst frequencies of GR valve a) primary burst occurring at the auxiliary inlet when λ_i is equal to the microchannel height, b) secondary burst at the auxiliary outlet.	90
Figure 6.6: Three dimension view of the possible methods of fabricating capillary valves.	92
Figure 6.7: Numerically obtained sequential images of meniscus advancement in response to increasing the rotational frequency.	93
Figure 6.8: switch and switching back the flow direction in centrifugal microfluidics. .	96
Figure 6.9: A partial view of a rotating disc indicate showing the distribution of the liquid by using GR valve.	99
Figure 6.10: Free body diagram of a GR with two branch channels splitting at a junction.	100
Figure 6.11: Numerically obtained velocity magnitudes in branch channels.	100

Figure 7.1: A partial top view of the liquid flow.	104
Figure 7.2: Propelling liquid towards the disc center using Euler and inertial forces. .	107
Figure 7.3: Top view of a heterogeneous micro chamber, $\theta = 70^\circ$ and $\beta = 120^\circ$	111
Figure 7.4: Top view of a trapezoid heterogeneous micro chamber.....	112

University of Malaya

LIST OF TABLES

Table 4.1: Details of simulations, r_1 , r_2 are kept the same as those used in Chen et al. (2008).....	49
Table 4.2: Comparison between the numerical and experimental burst frequencies with dimensions and positions of the capillary valves on the disk.	53
Table 4.3: A comparison between burst frequencies of square and rectangular capillary valves.....	57
Table 5.1: Details of the simulation cases, where, \hat{r} , θ , σ_{1a} are distance from the disc center, contact angle and surface tension of the liquid, respectively.	68
Table 5.2: Comparison between the numerical and experimental burst frequencies of the conventional capillary valves and GVs on the disc.	70
Table 5.3: Burst and switching frequencies of different liquids before and after protein adsorption.	78
Table 6.1: The effect of GR on the burst frequency for different liquids for $\hat{r}=39\text{mm}$...	96
Table 6.2: The response of flow to the auxiliary inlet and outlet dimensions and experimental flow switch frequencies.....	97
Table 7.1: Simulation cases used to study the effect of heterogeneity on the flow pattern.	110

LIST OF SYMBOLS AND ABBREVIATIONS

F_f	:	Friction force
F_{cen}	:	Centrifugal force
F_{co}	:	Coriolis force
F_{Eu}	:	Euler force
G	:	Asymmetric distance
I	:	Moment of Inertia
m	:	Mass
μ	:	Viscosity
ρ	:	Density
n	:	Normal vector
Q	:	First moment of Inertia
r	:	Mean radial position
r_1	:	Radial position close to the center
V	:	Shear force
α	:	Angular acceleration
β	:	Expansion angle
γ	:	Surface tension
μ_s	:	Friction coefficient
σ	:	Normal stress
τ	:	Shear Stress
θ, φ	:	Contact angle
ω	:	Angular velocity

CHAPTER 1: INTRODUCTION

1.1 Research background

Conventional clinical diagnostic tasks and many chemical processes usually consist of a series of sequenced procedures carried out by skillful operators until the final analytical results are obtained (Lee et al., 2001b; Madou et al., 2006; Madou et al., 2001; Zoval & Madou, 2004). These processes are time consuming and highly dependent on the skills of trained and experienced operators. Alternatively, Lab-on-a-Chip (LOC) devices are attracting more attention as possible platforms for automating complex clinical and chemical processes with comparable cost. They provide portable desktop form factor, reduced time-to-results, reduced amount of sample needed and increased possibility of multiplexing (simultaneous run of multiple test from the same sample) as compared to standard lab assays (Godino et al., 2013; Lee et al., 2009; Lee et al., 2011; Lee et al., 2013).

Today, many steps of chemical and clinical assays such as sample preparation (Li et al., 2014; Nan et al., 2014; Reboud et al., 2012), amplification/detection of nucleic acid targets (Jenison et al., 2014; Ma et al., 2014) and hybridization steps as well as integrated sample-to-answer procedures are developed on LOC devices (Ritzi-Lehnert et al., 2011; Schumacher et al., 2012). Centrifugal microfluidic devices (LabDisc) are realization of LOC concept on spinning platforms (typically in a geometric shape of a disc) that contain chambers for samples, reagents and waste connected by a network of fabricated microchannels. Centrifugal microfluidic platforms do not affect the important physicochemical properties of fluids such as pH or ionic strength and therefore they are attractive candidates for applications of various chemical/clinical procedures such as blood plasma separation, disease screening, drug testing, cellular and chemical analysis, etc. (Auroux et al., 2002; Madou et al., 2006; Oh & Ahn, 2006; Reyes et al., 2002). In centrifugal microfluidics, assays are mainly carried out in a sequence of microfluidics

operations e.g., metering, aliquoting, etc., starting from the center side of the disc and progressing radially outward due to unidirectional nature of the flow in centrifugal microfluidics (i.e., in the direction of centrifugal force).

The ability to employ multi-directional flow on centrifugal microfluidics allows for better use of disc's real estate and increases flexibility of fluidic operations. The flow manipulation and multidirectional propelling of the flow are imperative tasks for complex operational sequences on the centrifugal microfluidic platforms (such as sample preparation such as fractionation and DNA extraction, reagent mixing, volume definition, etc.) (Brenner, 2005; Jinlong et al., 2008; Kim et al., 2008; Kong & Salin, 2011; Lin, 2010; Steigert et al., 2005). To date, several passive and active techniques (i.e., need external power sources) have been introduced in order to develop multidirectional flow on the centrifugal microfluidics such as Coriolis force, siphoning, thermo pneumatic pumping and "centrifugo-dynamic inward pumping (Abi-Samra et al., 2011a; Brenner et al., 2005; Kim et al., 2008; Madou et al., 2006; Zehnle et al., 2012). An active flow switch method employing a periodic air supply in order to change the flow direction has been proposed by Kong et al. (2011). Although this method is able to change the flow without changing the spinning direction of the disc, portability reduction and the increase in the system cost, making it less desirable especially for clinical applications. In a different approach, Lin et al. (2010) has introduced a passive micro structure that evenly distributes the liquid at the T-junctions which can be used in the centrifugal ELISA chips. Given the limitations of the existing flow switching methods, and due to the diversity of clinical and chemical assays there is a clear need for development of new valving techniques. This study introduces novel techniques, which provide more control on the flow in centrifugal microfluidics that allows for the efficient use of the disc real estate and more sophisticated microfluidic operations on centrifugal microfluidics.

1.2 Problem Statement

Naturally, the liquid flow in centrifugal microfluidics is in the direction of the centrifugal force at relatively lower rotational speeds and in the direction of Coriolis force at relatively higher rotational velocities. The unidirectionality of flow on centrifugal microfluidics is a major obstacle in the design and development of complex clinical and chemical processes which are often comprised of series of consecutive microfluidic unit operations such as mixing, metering and separation (Haeberle et al., 2012). Propelling liquid in the directions opposite to the centrifugal and Coriolis forces allows for the efficient use of the disc space and conducting more microfluidic unit operations on the disc (Madou et al., 2006). To date, several techniques have been developed for propelling liquids towards the disc center e.g., applying surface treatments (Handique et al., 1997), pneumatic and thermo-pneumatic techniques (Abi-Samra et al., 2011a; Gorkin III et al., 2012) or against Coriolis force e.g., reversing the disc rotation and supplying periodic air pressure (Brenner et al., 2003; Kong & Salin, 2011). However, there is a need for new techniques due to the variety of clinical assays and chemical operations and also due to the shortages and disadvantages of many existing techniques. For example, applying surface treatment, using periodic air pressure supply or thermo-pneumatic techniques are not robust and reproducible techniques and/or impose additional cost to LOC devices.

1.3 Research aims and objectives

This study focuses on the flow control and liquid routing on the spinning platforms and aims to introduce new methods for liquid routing and flow control on centrifugal microfluidic devices.

1.3.1 Research aims

This study aims to introduce novel methods to control flow and route liquids on spinning microfluidic platforms without employing external power source or applying surface treatments. With this regard, the effect of contact angle and microchannel dimensions in centrifugal microfluidics on the performance of the capillary valves are studied in order to provide a holistic insight of the flow pattern which assists in the design and development of novel flow control devices.

1.3.2 Research objectives

The objectives of this study are as follow:

1. To investigate the flow pattern in capillary channels (different dimensions) of various contact angles on centrifugal microfluidic platforms experimentally and numerically.
2. To develop novel passive valving techniques for centrifugal microfluidic systems to switch and to switch back the flow direction at capillary T-junctions.

1.4 Scope

This study is delimited to the numerical simulation of hydrophilic and super hydrophilic capillary channels for a wide range of contact angles due to the limitation in fabrication and the unjustified cost of experimentally testing of a wide ranges of materials with different contact angles. It focuses on the passive flow manipulation techniques due to their simplicity and their high chance of commercialization and integration into various LOC devices. The study will emphasis on the passive methods to switch the flow direction because of its importance in flow preparation on many LOC devices and also due to very limited numbers of currently available flow switch methods. The novel flow switch techniques that will be presented in this study will be

only tested for liquids which are widely used in biomedical and biochemical applications. The reproducibility and the functionality of these valves will be experimentally tested by repeating the experiments under various operational conditions. The mechanism of valves will be theoretically discussed and the fluid motion in these valves will be numerically explained.

1.5 Thesis Outline

This thesis begins with the Introduction chapter that overviews the most important and the state-of-art flow manipulation techniques and highlights the research gaps. It continues with the Methodology chapter that include the numerical and experimental setup that will be used for conducting the simulations and experiments. Chapter 4, 5 and 6 present the results of a comprehensive study on functionality of the hydrophilic and super hydrophilic different capillary valves, a novel flow switch and the improvement of the presented novel flow switch technique, respectively. In Chapter 7, the preliminary results of the effect of moment of inertia and the surface heterogeneity on the fluid flow will be presented. The last chapter includes the conclusions of the thesis and the suggestion for future study.

CHAPTER 2: LITERATURE REVIEW

This section introduces the background and the state-of-the-art of centrifugal microfluidic platforms and indicates the current trends in development of different liquid handling techniques to perform various microfluidic unit operations. It provides an overview of several integrated centrifugal microfluidic platforms with particular emphasis on the methods of controlling and manipulating flow. It includes the effect of advances in micro technology on performing clinical assays and chemical operations, fabrication methods, the description of the components of microfluidic platforms specifically centrifugal microfluidics and describes the relevant forces and parameters involved. It also reviews most of the studies on the flow control and manipulation on centrifugal microfluidics.

2.1 Microfluidic platforms

Micro technology has assisted researchers to develop brand new products that can replace their counterparts at remarkably smaller sizes and higher efficiencies. In the academic research especially in the field of clinical and biomedical the influence of micro technologies has been increasing during the past years. The emerge of microfluidics dates back to when efforts have been made for dispensing Nano liter liquids to be used later in ink-jet technology (Haeberle et al., 2012). The miniaturization of the gas chromatograph system on a silicon wafer, for the first time has realized the transportation of fluids through sub millimeter cross section channels (Terry et al., 1979). Afterwards the liquid propulsion and transport in sub millimeter and micro channels have been studied by several researchers in various fields (Duffy et al., 1999; Madou & Kellogg, 1998; Manz et al., 1990). The specific aspects of flow in micro channels such as high surface-to-volume ratio allows for the employment of surface related phenomena such as capillarity, fast thermal response and so on. These features

have been used to enhance many of the analytical procedures in clinical and chemical assays e.g., by reducing the size of the samples, more accurate control on the samples and reducing the reactions time. Based on such advantages of microfluidics Manz et al. (1990) have proposed the concept of miniaturized total chemical analysis systems (TAS) which is now known better as micro-TAS or laboratories on a chip (LOC) as proposed by Harrison et al. (1992). A lab on a chip is a microfluidic device that integrates clinical or chemical operations on a single chip of millimeter or centimeter size.

2.2 Materials and Fabrication

2.2.1 Materials

The most common materials used in fabricating microfluidic systems are silicon, glass and polymers that are used in bio medical or biological microelectromechanical systems (BioMEMS). The advantages and disadvantages of the abovementioned materials are briefly reviewed in this section.

2.2.1.1 Silicon

The fabrication methods of silicon materials such as lithography and etching have been extensively developed since the last four decades (Madou, 2002). Silicon made LOCs can withstand high temperature and have high thermal conductivity, which makes them suitable for high temperature sterilization applications and polymerase chain reaction (PCR) where heat transfer is an important factor. The low transparency is one of the disadvantages of silicon, which creates problems for optical-based detection methods. The silicon raw material is expensive and requires series of preparation steps such as cleaning, coating and so on, which extends the fabrication time and increases the cost. In addition, proteins, DNA and biomolecules tend to stick and adsorb on the surface of silicon based microfluidic devices because of the hydrophobic property of the

material. The fabrication of micro channels with high aspect ratios (the ratio of the height to width) and intricate cross sections is challenging due to the isotropic property of the silicon.

2.2.1.2 Glass

Glass is a biocompatible material that can endure high temperature. Its high thermal conductivity and electric insulation have made glass-based microfluidics suitable for applications, which are based on heat transfer (e.g., PCR) and those require high electric field (electroosmosis). In comparison with silicon, glass is a highly transparent material with no light absorbance, which makes it a perfect material for visualization of liquid movements and optical-based detection methods. However, it is fragile and has low impact strength and the fabrication of glass-based microfluidics has the similar problems and limitation to silicon-based microfluidics.

2.2.1.3 Polymers

In comparison with the abovementioned materials, the raw material of polymers is significantly cheaper and they can be easily processed by many different production techniques such as molding, machining and so on. Different polymers can be produced with a variety of physical properties, which make them suitable for a wide range of chemical and biomedical applications. They are electric insulator and transparent which makes them suitable materials for electrophoresis applications and optical detections. However, polymer based microfluidics may not be used for applications that require heat transfer or high temperature due to their low thermal conductivity and lower resistance to high temperature. At high temperatures, polymer-based microfluidics are unstable and prone to deformation. Polymers are transparent (which is important in detection processes), biocompatible, electric insulator and have less thermal conductivity ($\sim 0.1 \text{ W/mK}$) in comparison with silicon and glass (more than 1 W/mK). In

general, polymers compared to other materials are less expensive and can be fabricated cost effectively with various fabrication methods, which makes them the preferable material in most microfluidics devices.

2.2.2 Fabrication

For prototyping where the surface quality of several micrometers is satisfactory CNC machining can be used to fabricate microfluidic platforms. When dimensions that are more precise are needed, laser ablation can be used in fabrication of polymer-based materials. In the later method, the laser energy is used to cut out different geometries with the precisions of few hundred nanometers in the x-y directions and $0.1\mu\text{m}$ in the depth direction (Pethig et al., 1998; Schwarz et al., 1998). The mass production of glass and silicon based microfluidics is usually based on different types of lithography techniques such as electro-projection lithography, X-ray lithography and so on, while hot embossing and injection molding are the typical mass production method for polymer-based microfluidics. Figure 2.1 shows an example of the process of a moulding-based technology used for fabrication of polymer-based centrifugal microfluidics.

Several research groups have described different molding and casting techniques that are cost-effective to replicate microfluidic platforms made from polymethylmethacrylate (PMMA) and polydimethylsiloxane (PDMS) (Duffy et al., 1999; Lee et al., 2001a; Madou et al., 2001). The advantage and disadvantages of various fabrication methods of microfluidic platforms in general and centrifugal microfluidics in particular are critically reviewed and discussed by Focke et al. (2010). Figure 2.1 shows the process of formation of a centrifugal microfluidic foil. Figure 2.1 (a) shows that PMMA master is milled, cast with PDMS mould and cured at 80°C . Figure 2.1 (b) shows that after a post curing at 200°C (in order to obtain the desired tool

condition) the PDMS is placed in a hot embossing machine and evacuated after curing at 190°C. Figures 2.1 (c) to (e) show clamping of the foil in vacuum machine, pressurizing the foil through gradually injection nitrogen from the top and creating a pressure difference and demoulding PDMS after cooling. In addition, various types of microvalves for the specific use in microfluidic platforms can be designed and fabricated with different fabrication techniques for plastic materials (Feng & Chou, 2011; Glière & Delattre, 2006; Jeon et al., 2002; Koch et al., 1997; Madou et al., 2001).

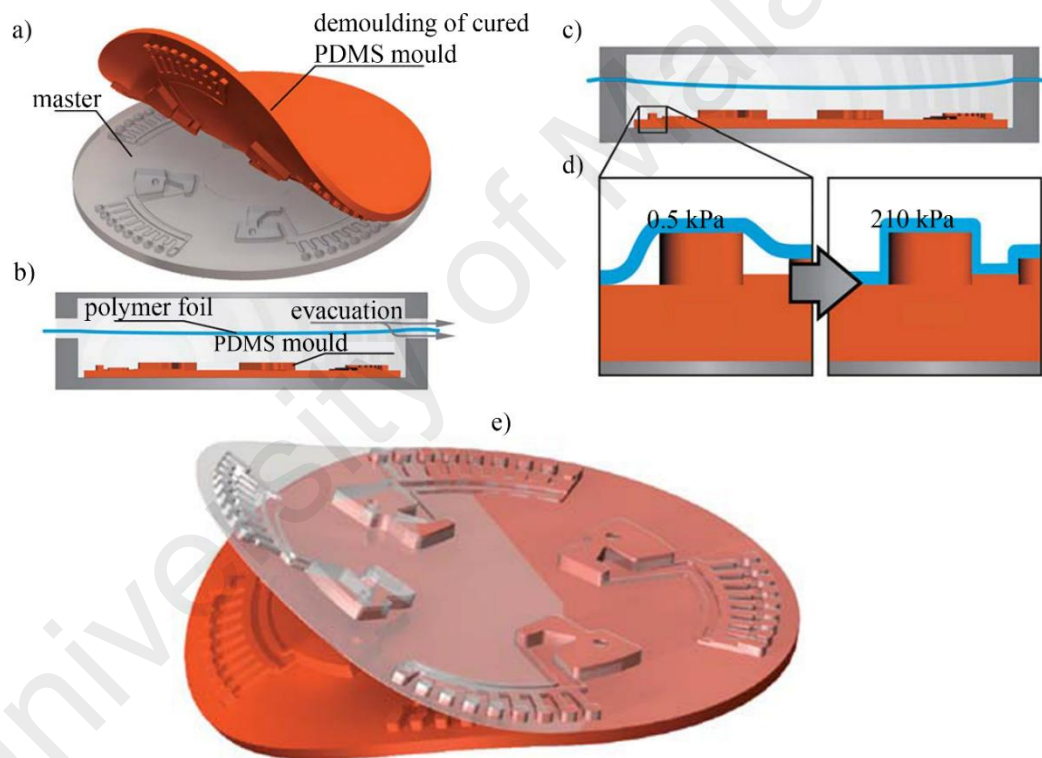


Figure 2.1: Process of the formation of a centrifugal microfluidic foil (Focke et al., 2010).

2.3 Centrifugal microfluidics

The centrifugal microfluidic platform is one of the various types of lab-on-a-chip devices that often has a CD-like shape, which it is mounted on a rotating system and exploits the centrifugal force for propelling liquids. Centrifugal microfluidics, also called lab-on-a-disc, is an attractive option for various biomedical and chemical

applications such as blood plasma separation, disease screening, and drug testing, cellular, etc. They require minimal external instrumentation to propel and manipulate fluids and its fabrication is a well-established art. The approach of using centrifugal force in processing liquid samples for biomedical applications dates back to the late 1960s where centrifugal analyzers were used to process and mix samples and reagents in the microliter volumetric range (Anderson, 1969; Burtis et al., 1972). The advancement in micro technology and micro fabrication has assisted in the emergence of a modern generation of centrifugal platforms, where the length scale less than few hundred micrometers enables parallel processing of a large magnitude of microfluidic unit operations on a disc (Duffy et al., 1999; Ekstrand et al., 2000; Madou & Kellogg, 1998; Madou et al., 2001). With this regard, centrifugal microfluidics platforms (LabDiscs) are a branch of LOC devices that minimize the external power sources used to propel liquid samples by realization of the microfluidic unit operations on a spinning platform often in the shape of a disc. The reagents/samples are dispensed into the inlet chambers and are propelled by the centrifugal force to travel radially towards the disc periphery. Today various fluid handling operations including sample lysis, homogenization (Leung & Ren, 2013; Ren & Leung, 2013), metering (Bouchard et al., 2010), volume definition and valving (Hwang et al., 2011; Kazarine & Salin, 2014; Ouyang et al., 2013) have been developed on centrifugal microfluidic platforms. Therefore, the technology is considered mature enough for applications such as disease screening, drug testing and polymerase chain reaction (Aguirre et al., 2014; Brogger et al., 2012; Lee et al., 2013; Marchalot et al., 2014; Strohmeier et al., 2014; Ymbern et al., 2014). The integration of various microfluidic unit operations such as mixing, separating and detecting into centrifugal microfluidics, results in automation of many intensive manual operations. For instance, He et al. (2009) have presented a low-cost fully automated centrifugal based ELISA that is able to carry out multiple operations

with high precision in parallel. Centrifugal microfluidic platforms are particularly important in the integration of clinical process such as ELISA and polymerase chain reaction (PCR) (Aguirre et al., 2014; Amasia et al., 2012; Focke et al., 2010; He et al., 2009; Lee et al., 2009). Figure 2.2 shows an injection-molded centrifugal microfluidics that is able to integrate the process of the clinical assays such as ELISA. A centrifugal microfluidic platform is mounted on a spinning motor and it is comprised of a network of microchannels, vessels and microvalves and sometimes micropumps. These elements on the platforms are to carry out the basic as well as complex parallel microfluidic unit operations, which are required in clinical and chemical assays. The basic microfluidic unit operations are liquid transport, metering, flow switch, separation and valving (Gorkin et al., 2010; Haeberle et al., 2012). Liquid transport towards the rim of the disc can be scaled over a wide range of flow rates by considering the hydraulic resistance of the microchannels and spinning frequency of the disc. The metering is a preparative task on centrifugal microfluidics that is used when a defined volume of sample needed to be separated from the whole part. Figure 2.3 shows a typical metering technique where a) an undefined volume of liquid is dispensed into the inlet when disc is set to rotate, b) once the metering chamber is filled the rest of the liquid is cutoff, c) the centrifugal force overcomes the capillary valve and the liquid passes through the valve.

The flow switch is required in many preparative protocols where different solutions e.g., wash, sample, etc. have to be directed to the waste or a receiving chamber after passing a common stationary phase (Beebe et al., 2002; Gorkin et al., 2010; Lai et al., 2004; Oh & Ahn, 2006). Figure 2.4 shows a flow switching technique on centrifugal microfluidic platforms based on Coriolis force. The liquid streams into the left reservoir following the direction of rotation (Figure 2.4 (a)) and switching the direction of rotation renders liquid to stream into the other reservoir (Figure 2.4 (b)). Valving and pumping operations are reviewed in more details in the next section due to their

importance, which facilitate the implementation of several complex processes on centrifugal microfluidics.



Figure 2.2: An injection-molded LabDisc used for ELISA (He et al., 2009).

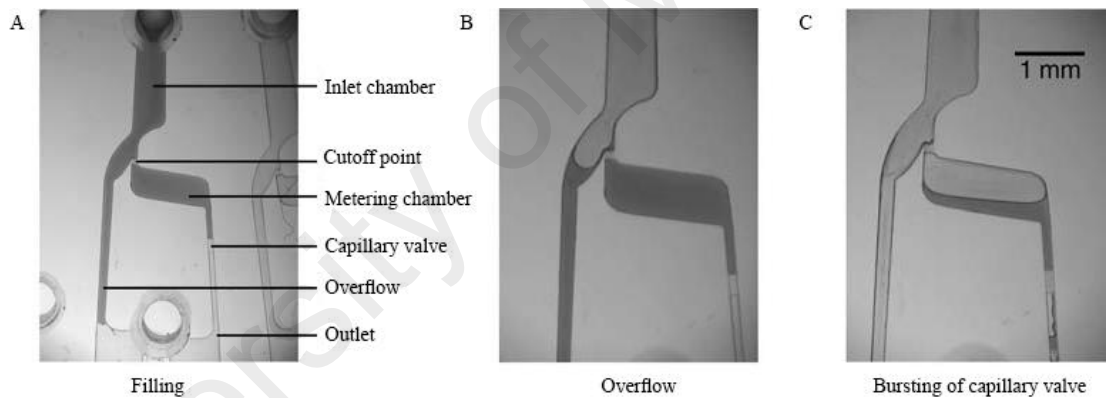


Figure 2.3: A metering microstructure based on capillary valving (Steigert et al., 2005).

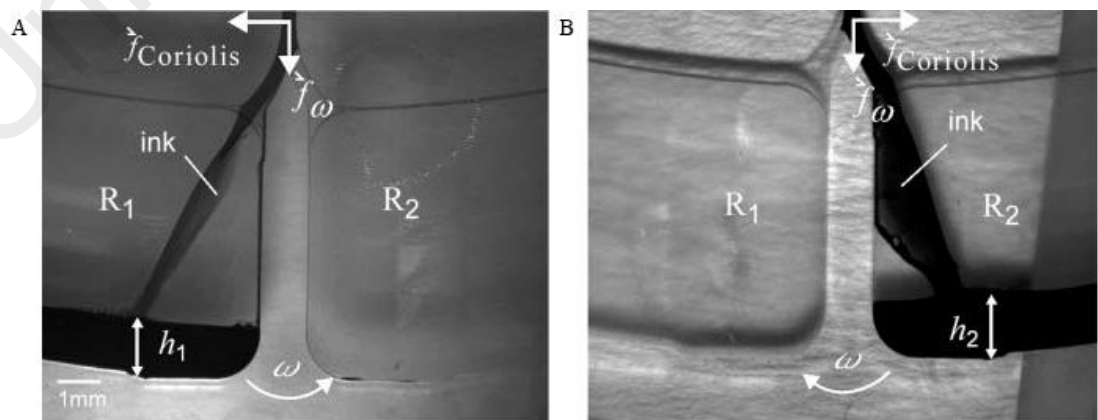


Figure 2.4: Switching the flow direction by Coriolis force, (Brenner et al., 2005).

2.3.1 Theory of Centrifugal Microfluidics

2.3.1.1 Centrifugal and Coriolis forces

Navier-Stokes equation is used to describe the fluid dynamics on the centrifugal microfluidic platforms. The Eulerian form of Navier-Stokes equation for incompressible, Newtonian fluids is (Ducrée et al., 2007):

$$\rho \left(\frac{\partial \vec{u}}{\partial t} + (\vec{u} \cdot \nabla) \vec{u} \right) = -\nabla P + \mu \nabla^2 \vec{u} \quad [1]$$

where, ρ , u and μ are the density, velocity and the viscosity of the fluid. In a non-inertial reference frame rotating at constant spinning frequency, the material derivation of liquid velocity on the right hand side of Eq. 1 is written as:

$$\frac{\partial u}{\partial t} + \vec{\omega} \times (\vec{\omega} \times \vec{r}) + 2\vec{\omega} \times \vec{u} \quad [2]$$

Substitution of Eq. 2 into Eq. 1, we can write:

$$\rho \left(\frac{\partial}{\partial t} u + u \cdot \nabla u \right) = -\nabla P + \mu \nabla^2 u + \rho \omega \times \omega \times r + 2\rho \omega \times u \quad [3]$$

Which contains two pseudo forces (see Figure 2.5), the Centrifugal force (density):

$$F_{cen} = \rho \omega \times (\omega \times r) \quad [4]$$

And Coriolis force (density):

$$F_{cor} = 2\rho \omega \times u \quad [5]$$

The average centrifugal force (density) acting on the liquid plug, depends on its radial position and can be calculated by integrating the centrifugal force over the radial length of the liquid:

$$F_{cen} = \frac{1}{l} \int_{r_1}^{r_2} \rho \omega^2 r dr = \frac{1}{l} \rho \omega^2 (r_2^2 - r_1^2) = \rho \omega^2 \bar{r} \quad [6]$$

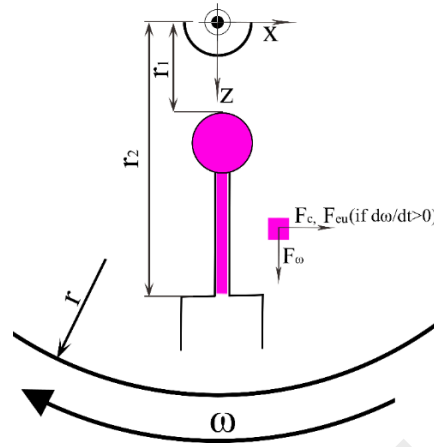


Figure 2.5: Partial top view of a liquid plug in a channel on a disc of radius r spinning at ω , the length of the plug is characterized by its boundaries r_2 and r_1 .

Where, l is the radial length of the liquid and \bar{r} is the mean radial position of the liquid. In order to calculate Coriolis force, the maximum radial velocity is obtained by writing Navier-Stokes equation in the plane parallel to the disc surface. Typically, the gravitational force is significantly smaller than other forces on spinning disc and thus can be ignored. We also assume fluid of constant density and since the walls are impermeable, liquid is confined to flow in z -direction and there exist no changes of the velocity except in the direction of flow:

$$-\rho \omega^2 \bar{r} + \mu \left(\frac{\partial^2 u_z}{\partial x^2} + \frac{\partial^2 u_z}{\partial z^2} \right) = \rho (u_z \frac{\partial u_z}{\partial z}) \quad [7]$$

Considering that the flow is fully developed, the velocity of the fluid in the direction of the flow is constant:

$$-\rho \omega^2 \bar{r} + \mu \left(\frac{\partial^2 u_z}{\partial x^2} \right) = 0 \rightarrow u_z = \rho \omega^2 \bar{r} \frac{1}{2\mu} x^2 + C_1 x + C_2 \quad [8]$$

Due to no-slip at the wall, $v_z=0$ at $x=0$ and $x= w$:

$$u_z = \rho\omega^2\bar{r} \frac{1}{2\mu} x(x-w) \quad [9]$$

The maximum velocity is at $x=0.5w$ and it is equal to:

$$u_z = \frac{\rho\omega^2\bar{r}}{8\mu} w^2 \quad [10]$$

Where, w is the microchannel width. At this point Coriolis force can be obtained by equation 5.

2.3.1.2 Capillary pressure

The capillary pressure has been investigated in several theoretical, experimental and numerical studies (Chen et al., 2008; Cho et al., 2004; Duffy et al., 1999; Man et al., 1998). It is a function of the microchannel width, height and surface properties and can be derived from thermodynamics in terms of interfacial free energy (Whitesides, 2006):

$$U_T = A_{sl}\sigma_{sl} + A_{sa}\sigma_{sa} + A_{la}\sigma_{la} \quad [11]$$

Where, A_{sl} , A_{sa} and A_{la} are solid-liquid, solid-air and liquid-air interface, σ_{sa} , σ_{sa} , σ_{sa} are their corresponding surface tension forces. The surface tension forces per unit length are function of the contact angle and given by Young-Laplace equation (Frederick, 1964):

$$\sigma_{sa} = \sigma_{sl} + \sigma_{la} \cos\theta_c \quad [12]$$

After using Young-Laplace equation and subtracting the constant sum of the solid-liquid and solid-air interfaces the total energy will be (Chen et al., 2008):

$$U_T = \sigma_{la}(A_{la} + A_{sa}) + A_{la}\sigma_{la} - A_{sl}\sigma_{la} \cos\theta_c$$

where

$$U_0 = \sigma_{la}(A_{la} + A_{sa}) \quad [12a]$$

U_o is a constant energy since the sum of the solid–liquid and solid–air interfaces remains constant. The pressure acting on the liquid plug can be obtained from the changes of the interfacial energy of the system with respect to the changes in the liquid volume and can be calculated as:

$$\Delta P = \frac{dU_T}{dV_i} = \sigma_{la} \left(\frac{dA_{sl}}{dV} \cos \theta_c - \frac{dA_{la}}{dV} \right) \quad [13]$$

The capillary barrier pressure changes as the liquid volume changes and can be categorized and calculated in three main regimes which are when the liquid is pinned in the microchannel, when it is pinned at a sudden change in the surface properties and at the point when the centrifugal pressure is equal to capillary pressure. Figure 2.6 shows stages of meniscus advancement in a rectangular capillary; stage 1 is when $x_c < L$, stage 2 is defined when $x_c = L$ and stage 3 is when the meniscus is bulged and $x_c > L$. The parameters w , θ_c , and β are the width of the capillary, the contact angle and the capillary expansion angle. However, it is at the latest regime that we require to calculate the capillary pressure barrier on the centrifugal microfluidics. The capillary barrier pressure at this regime is called capillary burst pressure and for a rectangular microchannel it has been given by references (Chen et al., 2008; Leu & Chang, 2004a):

$$\Delta P = \frac{2\sigma_{la}}{w} \left(-\frac{w}{h} \cos \theta_c - \cos(\theta_c + \beta) \right) \quad [14]$$

Where, w , h and β are the microchannel width, height and the angle of the expansion of the microchannel.

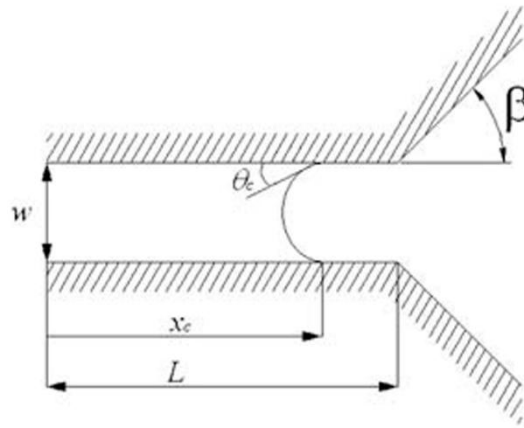


Figure 2.6: Schematic of the meniscus development in rectangular capillary, Chen et al. (2008).

2.3.2 Flow type

The capillary number $Ca = \frac{\mu U}{\sigma}$ is used to define the flow type in microfluidics; when $Ca \ll 1$ the surface tension effect is the predominant force and the flow is called surface tension dominant flow. The flow in most LOC devices including centrifugal microfluidics is the surface tension dominant flow with a low Re number i.e., typically below or on the order of 1 and $Ca \ll 1$. In the surface tension dominant flow, the effect of viscous forces consisting of flow viscosity, the flow path length and the fluid viscosity is insignificant in comparison with the effect of capillary force (Fulcher et al.; Shrivanthi et al., 2005; Wang et al., 2014; Wang & Dimitrakopoulos, 2012). This type of fluid movement allows for applying the most significant operation on centrifugal microfluidics, which is called capillary valving.

2.3.3 Microvalves and Micropumps

In the past two decades a large number of studies have been focused on developing new microfluidic valving mechanisms for liquid transport, flow control, mixing etc. (Grumann et al., 2005; Haeberle et al., 2012; Madou & Kellogg, 1998; Oh & Ahn, 2006; Shoji & Esashi, 1994). Microvalves are the main components of LabDisc that are

used to control and manipulate flow on the spinning platforms. Their applications such as flow regulations, switching and sealing of fluids are vital in performing clinical and chemical processes on centrifugal platforms. They are mainly classified into passive i.e., do not need external power sources and active valves, which require external power sources to actuate. This section briefly overviews the most important microvalves as well as the latest introduced valves and their mechanisms and applications in centrifugal microfluidics. It reviews different types of the passive valves (consist of mechanical and non-mechanical) as well as various types of active valves and their advantages and disadvantages.

2.3.3.1 Passive techniques

Passive valves are the most popular valves on centrifugal microfluidics (i.e., due to the ease of fabrication) and can be categorized into mechanical and non-mechanical valves. The simplest non-mechanical passive valves are capillary valves, which are based on the interaction between the capillary and the centrifugal forces. Capillary valves are based on a pressure barrier that develops when cross-section or surface properties of the capillary changes abruptly (Duffy et al., 1999; Leu & Chang, 2004a; Man et al., 1998). The fundamental theory, design and fabrication of capillary valves have been reported in a study conducted by Man et al. (1998) as well as in other studies (Johnson et al., 2001; Madou & Kellogg, 1998; Madou et al., 2001). Figure 2.7 shows a schematic of various possible types of capillary valves. Capillary valves are constructed in three different methods, which are: a) by a sudden expansion/contraction of a hydrophilic/hydrophobic channel, b) by generating hydrophobic patches on hydrophilic channels and c) by constructing siphoning structure. The first two types of capillary valves are normally closed valves that block the liquid flow i.e., induced by the centrifugal force. Increasing the spinning frequency generates a larger centrifugal force,

which ultimately overcomes the capillary barrier pressure of the valve (Cho et al., 2004; Erickson et al., 2002; Man et al., 1998; Zeng et al., 2000a; Zeng et al., 2000b). The spinning frequency that generates a centrifugal force equal to or greater than the capillary pressure barrier is called burst frequency of the capillary valve. Burst frequency of the capillary valves varies within a wide range of spinning frequencies that allows for sequential implementation of various clinical/chemical processes (Madou et al., 2006). The hydraulic resistance and the surface properties of the channel together with the position of the valve relative to the disc center determine the burst frequency of a capillary valve (Cho et al., 2004; Erickson et al., 2002; Leu & Chang, 2004a; Man et al., 1998; van Remoortere & Joos, 1991; Zeng et al., 2000a; Zeng et al., 2000b). The theory and principles of the capillary valving have been studied by Cho et al. (2007a) focusing more on the relation between the contact angle of the liquid on different surfaces. The hydraulic resistance of the capillaries and the effect of capillary dimensions on the burst frequency of the capillary valve for a constant contact angle was experimentally and theoretically studied by Chen et al. (2008). Their study shows that for a given contact angle the height of the capillary has a greater effect on the performance of the valve in comparison with its width. Figure 2.8 shows the effect of aspect ratio (ratio of capillary height to capillary width) on the burst frequency for constant capillary width of 300 μ m and 400 μ m. The effect of capillary expansion angle β on the burst frequency of capillary valves is shown in Figure 2.9.

In addition, the effect of the surface topologies on wetting behavior and on the fluid flow has been studied by Kunert et al. (2008). Capillary valves are reported to be used in order to form sequential valves, perform flow switch as well as mixing different liquids (Noroozi et al., 2011; Soroori et al., 2013; Steigert et al., 2005). For instance, an inlet and an outlet chamber connected by a hydrophilic channel was used to produce a reciprocating flow that is used in mixing different liquids (Noroozi et al., 2011). The

technique employs the centrifugal pressure to push the liquid towards the rim of the disc and uses the capillary action when the disc is at rest to draw the liquid back to the center. Capillary valves can also be designed to be actuated at the centrifugal pressures lower than their burst pressure by introduction a secondary liquid flow that make contact with the other liquid at the capillary junctions (Melin et al., 2004). The mechanism of their technique is shown in Figure 2.10 where at (i, ii) liquid 1 flows towards the junction and stops, (iii) liquid 2 flows towards the junction and make contact with liquid 1 at the junction (vi) liquid 1 and 2 proceed to fill the outlet

The effects of pseudo-forces such as Euler and Coriolis forces on the flow behavior and their applications in the spinning platforms have been also studied. As one of the significant examples, the effect of Coriolis force on the liquid transporting by the microchannels was employed to control the flow direction when a micro channel meets an outlet chamber (Brenner et al., 2005; Brenner et al., 2003; Ducreé et al., 2004). At sufficiently high spinning frequencies (i.e., when Coriolis force is much greater than the centrifugal force) the liquid completely flow in the direction of Coriolis force and the flow direction is reversed by reversing the direction of the disc rotation. A liquid can also be routed first into one branching channel and then into a different branching channel when asymmetrical channels and chambers are used. When the liquid is filling a first chamber the liquid rises to a level that prevents the connection of the air in the branching channel with the vent hole and the fluid in the main channel will be routed to a second reservoir (Kim et al., 2008). Capillary valves have been used in order to produce equal flow rates in two outlet destinations branched out from a main capillary channel (Lin, 2010). The equal flow rate allows for duplicating the identical fluidic operations, which can reduce the sample consumption and the cost of the assay.

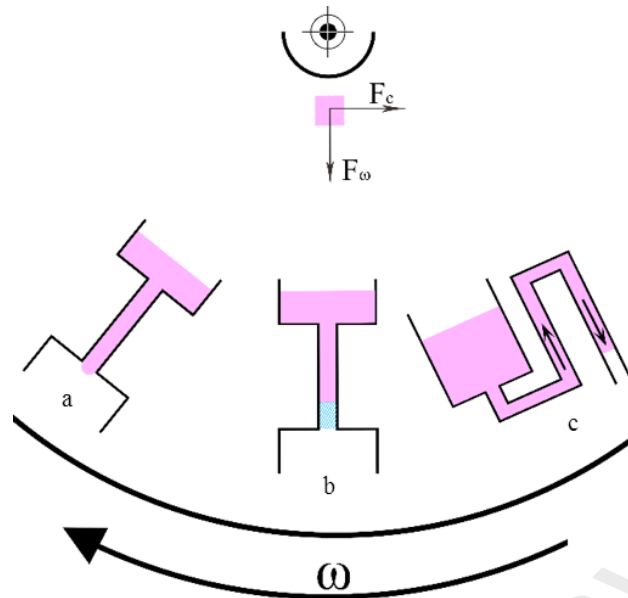


Figure 2.7: A schematic of different types of capillary valves, a) Sudden expansion of microchannel, b) Hydrophobic patch generated by surface treatment methods, c) Siphoning.

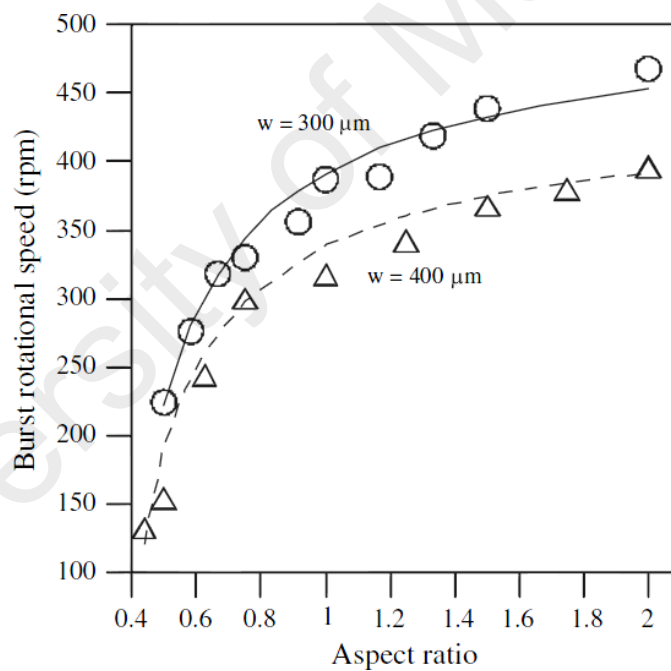


Figure 2.8: The effect of aspect ratio on the burst frequency of capillary valves for $\sigma_{la}=0.072 \text{ N/m}$, $\theta=68^\circ$. The solid and the dashed lines are theoretically obtained values for capillary width of $300\mu\text{m}$ and $400\mu\text{m}$, respectively (Chen et al., 2008).

The use of hydrophobic patches (hydrophobic capillary valves) is traced back to the study by Handique et al. (1997) and McNeely et al. (1999) where specific hydrophobic regions were defined on specific locations in a LOC device (by restriction in a

hydrophobic channel or applying surface treatments) to create and control the movements of liquids. Although, hydrophobic capillaries on centrifugal microfluidics require especial surface treatments which can make them less attractive compared to the other types of capillaries, Ouyang et al. (2013) have recently introduced a low-cost method hydrophobic capillary valve. They have used the laser printer lithography to pattern hydrophobic patches on a polyester films and shown that the value of the contact angle can be adjusted by the intensity of the toner as well as its color.

The siphoning technique, which has been employed in many applications such as separation, sedimentation etc., is consisted of an inlet chamber and an outlet connected together by a hydrophilic channel (Ducrée et al., 2007; Gorkin et al., 2012; Siegrist et al., 2010b). The hydrophilic channel allows for a positive capillary pressure, which is able to draw liquid towards the desired direction that is often towards the center of the disc. The specific structure of siphon allows for complete drainage of the liquid in a vessel located far from the disc center towards the chamber closer to the disc center at low spinning frequencies (see Figure 2.11). Figure 2.11 (a) shows equalizing of the liquid level in the inlet chamber and the hydrophilic channel at high spinning frequency. Figure 2.11 (b) shows the stopping of the disc and rising of the liquid in the hydrophilic channel. Figures 2.11 (c), (d) show spinning of the disc when the retracting meniscus reaches the crest point of the hydrophilic channel and drainage of the inlet chamber. However, most of the polymeric materials used to construct microfluidic platforms are hydrophobic in nature that challenges employment of the siphoning technique. A method that uses the pressure difference between the advancing and retracting liquid (which is created during liquid transport from the inlet to the outlet chamber) in the capillary has been introduced which improve siphoning for the use in a hydrophobic platform (Gorkin et al., 2012).

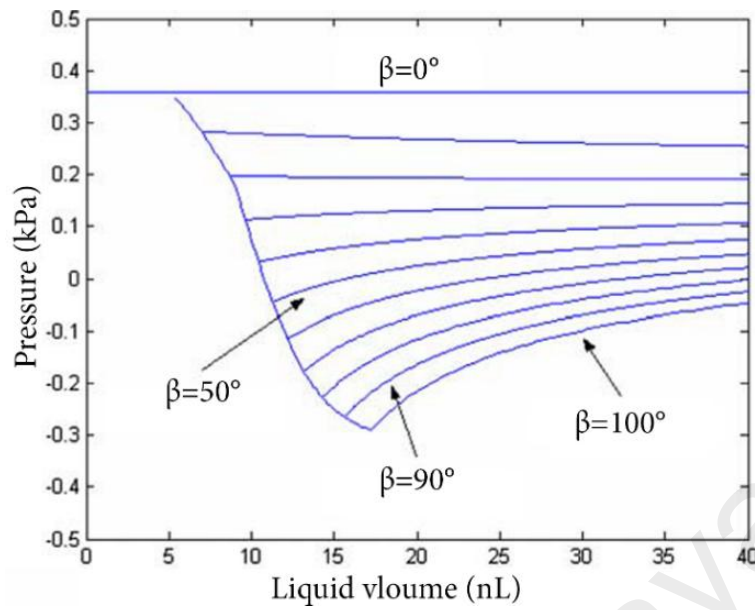


Figure 2.9: The effect of expansion angle on the burst pressure in terms of the liquid volume for a square channel ($w=h=300\mu m$) and $\sigma_{la}=0.072$ N/m and $\theta=68^\circ$ (Chen et al., 2008).

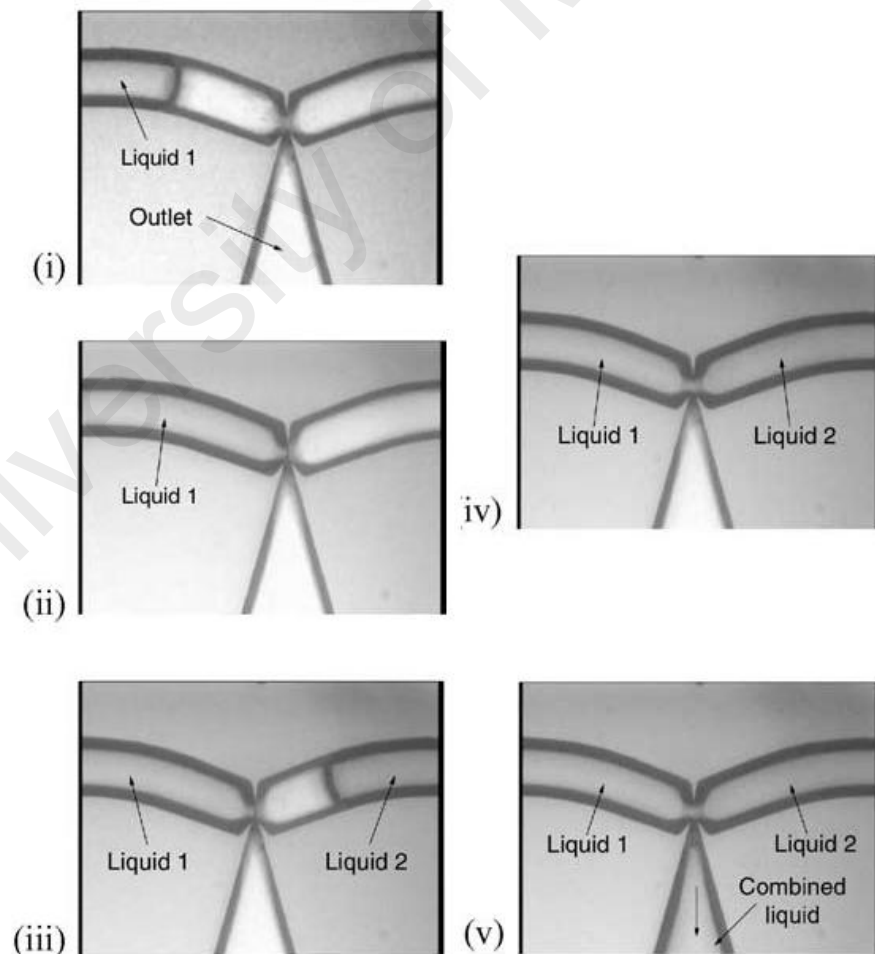


Figure 2.10: Liquid trigger valve (Melin et al., 2004).

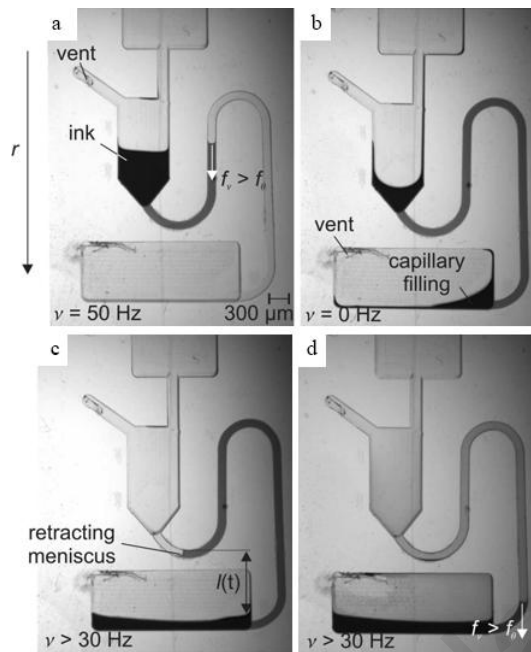


Figure 2.11: Sequences of siphoning on a LabDisc, (Ducrée et al., 2007).

Furthermore, mechanical passive valves are based on the reciprocal displacement of mechanical moving parts such as elastic membranes, flaps, spherical balls, and other mobile structures (Ansgar et al., 2001; Guo-Hua & Eun Sok, 2004; Hwang et al., 2011; Leslie et al., 2009; Mohan et al., 2011; Tingrui et al., 2005; Yamahata et al., 2005; Zengerle et al., 1995). Hwang et al. (2011) have recently integrated thin elastomeric films into a disc that enables more accurate control over the flow rate of the liquid passing through the valve in comparison with the conventional capillary valves. The elastomeric film is designed to provide a weak blockage against the flow and deflect in response to the increase in the centrifugal pressure. Gorkin et al. (2012) have constructed an intermediate compression chamber that acts like a barrier between a dissolvable films and the liquid in order to improve the valve actuation and widen the operational range of this type of valves. However, passive valves typically benefit from their cost-efficiency, ease of fabrication and have allowed for conducting several biomedical assays due to the variety of chemical and clinical procedures employing external power sources to develop more sophisticated type of valves are inventible (Haeberle et al., 2012).

2.3.3.2 Active techniques

Active valves employ various types of external power sources such as heat, magnetic field, and pneumatics (Madou et al., 2006). The incentives for using external power sources are to enhance the capability, durability and precision of valves and to efficiently use the disc's real estate, which is limited due to the unidirectionality of the flow on centrifugal microfluidic platforms. In regard with the improvement on performance of capillary valves, waxing and ice valving techniques are introduced (Abi-Samra et al., 2011b; Amasia et al., 2012; Garcia-Cordero et al., 2009; Lin & Jing, 2004). These types of valves are normally closed and frequency independent valves which are activated (melted) by external heat sources such as air-guns and laser beams. The difference in the melting points of various types of waxes allows for sequencing different process on the disc. Abi-Samra et al. (2011b) have used paraffin waxes actuating by infrared radiation in order to store and release samples. The ice valving technique is based on freezing a section of liquid in the microchannel to block the flow (Lin & Jing, 2004). The first utilization of the technique in an integrated centrifugal microfluidics was demonstrated by Amasia et al. (2012) to reduce the evaporation rate in polymerase chain reaction (PCR). Recently, several active techniques such as pneumatic and thermo-pneumatic methods have been presented in order to push liquid against the centrifugal force (from the disc rim to the disc center) or against Coriolis force on centrifugal microfluidics (Haeberle et al., 2012). The concept of utilization of compressed air in a chamber to propel the fluids dated back to a study by Handique et al. (2001). They demonstrated that 10 °C heating the air trapped in a chamber of 100nL size can produce the pressure equal to 7.5 kN/m² and the rate of pumping can be controlled by the rate of heating. The utilization and the analytical model of thermal expansion of the air in centrifugal microfluidics has been presented by Abi-Samra et al. (2011a). However, the existence of the centrifugal force allows for compressing the air

in an sealed chamber and use the stored pneumatic energy to pump liquids from a radial outward position to a radial inward position (Zehnle et al., 2012).

Figure 2.12 shows the sequential schematic of pumping liquid towards the disc center based on the interaction between centrifugal force and the pneumatic energy stored in the compression chamber. Figures 2.12 (a), (b) show that liquid is dispensed into the chamber and disc is rotated at high rotational frequency and fills the compression chamber. Figures 2.12 (c), (e) show the balance between the centrifugal pressure and the stored pneumatic pressure, fast reduction of the disc spinning frequency and the expansion of the compressed air which propel the liquid mainly through the outlet channel and the termination of the pumping process. In a different approach Kong et al. (2011) has introduced a technique to push liquid towards to disc center or against Coriolis force by applying external periodic air supply. In their method, an external air supplier is required to blow the air at the specific locations on a rotating disc and propel the liquid (see Figure 2.13).

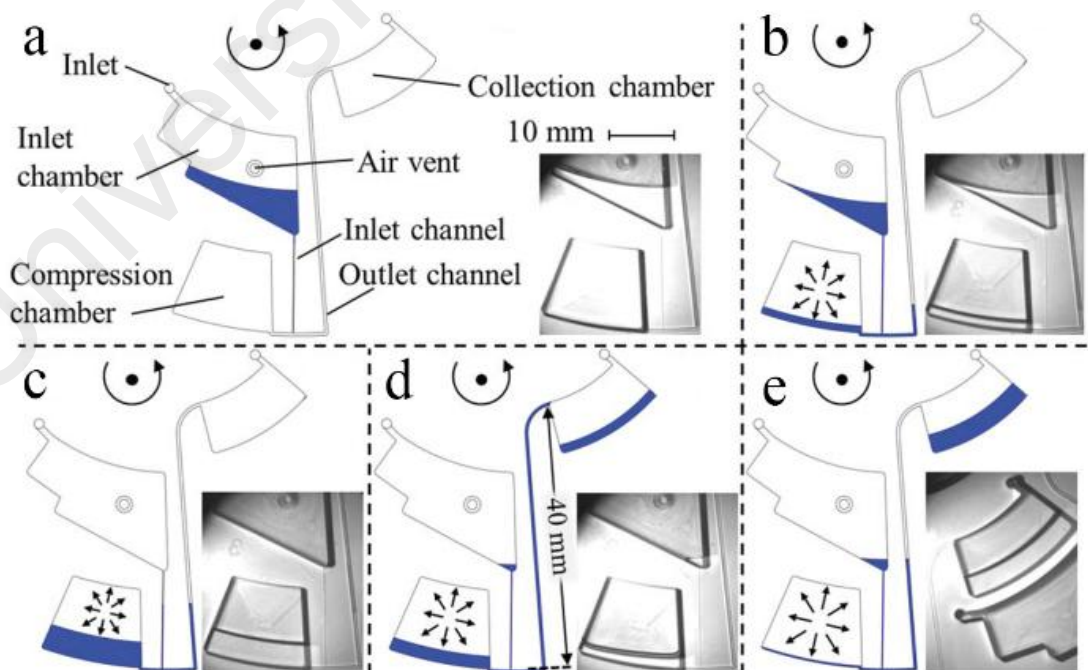


Figure 2.12: The schematic of Centrifugo-pneumatic pumping. (Gorkin III et al., 2012).

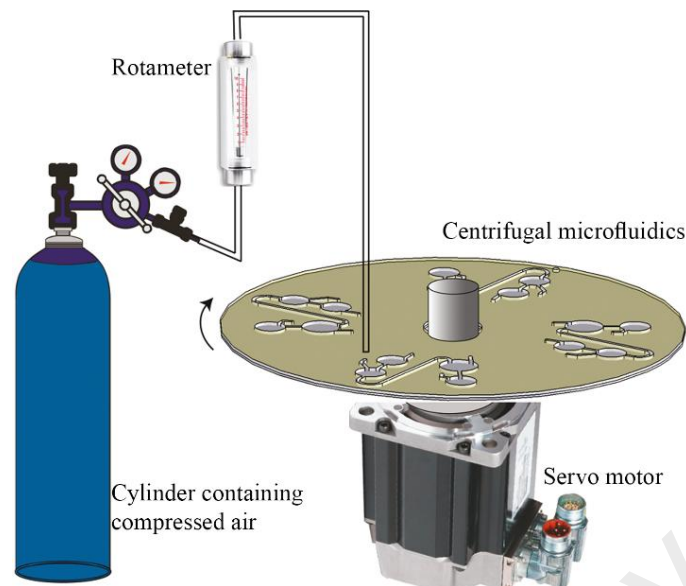


Figure 2.13: The schematic of using external source to apply periodic air and control the flow direction on the spinning disc (Kong & Salin, 2011).

2.4 Computational fluid dynamics studies

The fluid flow on centrifugal microfluidics has been numerically investigated by several research groups (Brenner et al., 2005; Brenner et al., 2003; Ducrée et al., 2006; Ducrée et al., 2007; Glière & Delattre, 2006; Grumann et al., 2005; Jens et al., 2007; Leung & Ren, 2013; Meijer et al., 2009; Siegrist et al., 2010a; Zeng et al., 2000b). Most of these studies have employed volume of fluid (VOF) method (Hirt & Nichols, 1981) to study the effect of the capillary pressure, and Coriolis force on the flow behavior and mixing progress in rotating platforms. In order to simulate the flow on a rotating microstructure, the most significant parameter that has to be taken into account is the changes of the contact angle, which varies due to the transient nature of liquid flow. The VOF method considers the effect of contact angle changes on the flow that enables a precise prediction for most of capillary flow problems. Several comparisons between the numerical models developed based on the static and those based on the dynamic contact angle has been carried out by different research groups such as Ashish et al. (2009) and Mitra et al. (2009). The interaction between the centrifugal force and the capillary pressure barriers, which is a criterion to design the sequential microfluidic processes, has been numerically studied since the last two decades. One of the first

numerical studies on the nature of the capillary action in centrifugal platforms was carried out by Zeng et al. (2000b) who derived a model describing the pressure barrier development occurring in capillary valves. Their model, which was needed in the design and construction of capillary valves, was later improved by many other researchers to obtain more accurate results of capillary pressure barrier and predict the flow behavior (Ducreé et al., 2007; He et al., 2009; Jens et al., 2007; Zeng et al., 2000b). The effect of surface roughness which is an inevitable disadvantage of microfluidics fabrication methods such as CNC machining on the flow behavior has been studied by Kunert et al. (2008).

The Coriolis force induces a lateral deflection on the flow, which can be used in mixing, and flow direction control on the spinning discs. The effect of Coriolis force on the flow direction when the fluid reaches a T-junction and its applications on mixing different liquids have been investigated by using VOF method (Brenner et al., 2005; Ducreé et al., 2006). Figure 2.14 shows the effect of Coriolis force on two separate liquids, blue and red that can be used in mixing liquids. The liquids are separated under the influence of Coriolis force in a straight radial channel of $100 \times 100 \mu\text{m}$ cross-section, and 2.1 cm length.

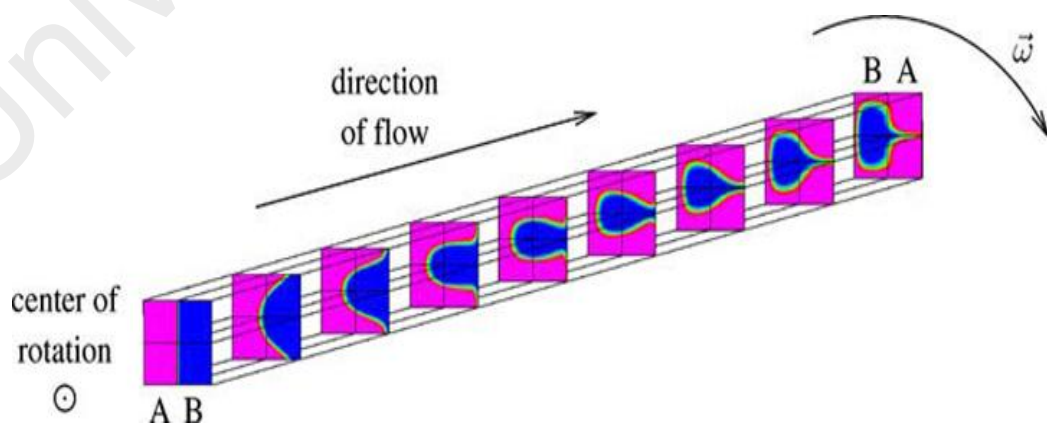


Figure 2.14 Reversing the position of the red and blue liquids at 50 rad/s (Ducreé et al., 2006).

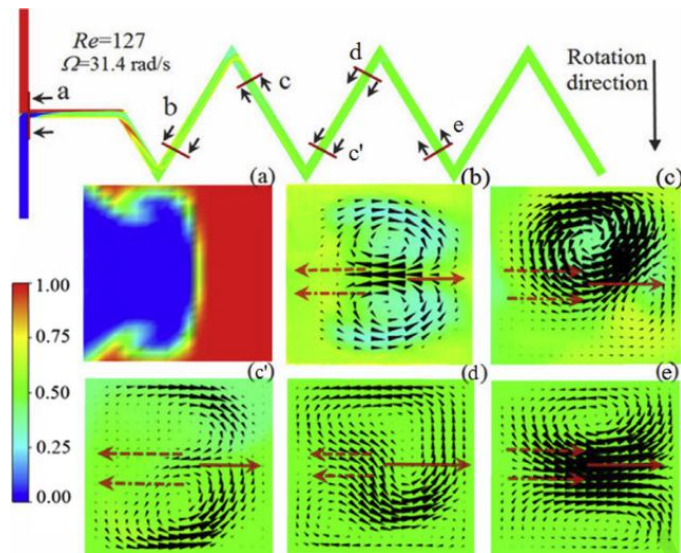


Figure 2.15: Mixing of red and blue colors in a zigzag micro (Ren & Leung, 2013).

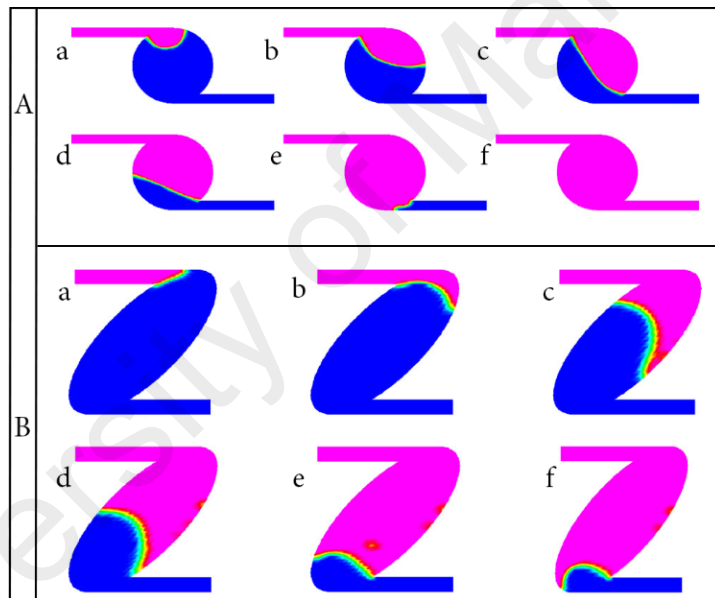


Figure 2.16: Filling process A) the circle shape micro chamber B) the oval shaped micro chamber (Chen et al., 2006).

The effect of Coriolis in mixing fluid in microchannels with various geometrical structures has also attracted attention in the last decade (Ducrée et al., 2006; Leung & Ren, 2013; Meijer et al., 2009; Ren & Leung, 2013). For example, Figure 2.15 shows a zig-zag channel on a centrifugal microfluidic platform when the disc spins at 31.4 rad/s and $Re=127$. The investigated cross-sectional plane, the viewing direction, the direction of centrifugal and cross-flow acceleration the direction of are shown by red line, black arrow, red dot dash line arrow; red dash line arrow. Insets (a) to (e) indicate the cross-sectional planes

(Ren & Leung, 2013). The liquid in a zigzag micro channel is under the influence of consistent changing of the direction of Coriolis force that expedites the mixing process.

In addition to above parameters, the uniform filling of micro chambers on the centrifugal microfluidics where the liquid-gas interface and surface tension forces vary consistently is an important parameter in design and construction of microfluidic networks e.g., in microfluidic PCR. The filling of various shapes of oval micro chambers by different micro channel sizes has been analyzed by Chen et al. (2006). They have studied the effects of the width of the feeding channels, the Reynolds number, Weber number and contact angles on the flow characteristics. Figure 2.16 shows the sequential filling process for a circle and an oval shape micro chamber studied by Chen et al. (2006). A critical comparison between different numerical approaches used to investigate the filling process of micro chambers in centrifugal microfluidics shows that the numerical results have good agreement with the experimental results in both static and dynamic modeling (Siegrist et al., 2010a).

2.5 Summary and research gap

The background of LOC devices and the theory of the centrifugal microfluidics have been reviewed. The main components of a centrifugal microfluidic platform (microvalves and micropumps) and the common operation units such as flow switch, siphoning metering and so on have been thoroughly reviewed. The review shows that capillary valves are the most common valves in many centrifugal microfluidic devices. It implies that there are extensive theoretical, experimental and numerical studies on describing the performance of capillary valves for hydrophobic materials. The theoretical models developed to predict the performance of the capillary valves have been mostly experimentally validated for a narrow range of materials which have the

contact angles of $>70^\circ$ and the performance of capillary valves for hydrophilic materials ($<90^\circ$) has not been comprehensively studied.

This review implies that there are less numbers of passive techniques in comparison to active methods for propelling liquid against the centrifugal and particularly Coriolis forces. The existing passive and active techniques to propel liquid against the Coriolis force are very limited. The latest passive techniques are based on trapping air inside a secondary chamber and use the hydro resistance to direct liquid to the opposite direction which have their own drawbacks such as high sensitivity and reducing the disc real estate. The newest active technique is based on gusting periodic air pressure on designated vent hole which significantly imposes additional costs to the whole system and disturbs the portability of the centrifugal microfluidics. In general, both existing passive and active techniques have not been able to alleviate fluids flow against Coriolis force which is a necessary microfluidic unit operation of many preparative protocols in clinical and biochemical tasks. Therefore, in next chapters the methodology of this study in order to develop novel techniques to switch the flow against the Coriolis force will be presented and the novel methods will be experimentally tested for various liquid properties. The mechanism of the novel flow switch techniques will be theoretically studied and numerically discussed.

CHAPTER 3: EXPERIMENTAL SETUP AND COMPUTATIONAL FLUID DYNAMICS METHODS

In this chapter, the method used for the fabrication of centrifugal microfluidics, the experimental setup employed to carry out various tests and the CFD method used to investigate the flow pattern and burst frequency of capillary valves is described.

3.1 Disc designs

Autodesk computer aided drawing software was used to create different disc's designs contacting various microfluidic features such as capillary valves, vessels and air holes. In general, several designs have been created and tested prior to final design. The final design then was used to fabricate several discs in order to test the repeatability and the durability of the designs.

3.2 Fabrication

The two methods of laser and CNC machining that were used to fabricate PMMA centrifugal microfluidics are described in this section. In both methods the PMMA discs are fabricated layer by layer according to a given design and bounded by using pressure sensitive adhesive (PSA) layers.

3.2.1 PMMA fabrication

3.2.1.1 Laser cutting

A short mode laser machine which provides a pulse length of normally greater than 10 ns, is used to cut PMMA substrate. The most important parameters that require attention in laser cutting are: the wavelength, the depth and the minimum diameter of the concentrated laser beam (spot size), the average intensity of the laser beam and the pulse length. A rapid and complete laser ablation requires the deposition of high energy in a small volume, which is possible by selecting a wavelength with the minimum

absorption depth. The ablation process at short wavelength (~200 nm) is mainly due to the absorption of a highly energetic photon by the material that can cause a fast ablation of the material. At wavelengths longer than 300 nm, the energy of the absorbed photon is not enough to break the absorption and a more number of photons must be considered.

The precision of the ablation region is highly dependent on the spot size of the laser beam, the smaller the spot size the more precise the surface. The control of the spot size relies on several factors however; the smallest possible spot size is usually about half of the wavelength used. The size of ablation region may differ from the desire size and sloped sidewalls can be formed if the spot size is not in the right range. In the ideal condition (lens is perfect) for more precise fabrication the spot size can be calculated based on the wavelength, the focal and diameter of the beam at the concentrating lens (Madou, 2002). The laser focus depth needs to be taken into account when the surface of the work piece is not precisely flat, for such surfaces a focus depth auto ranging device is to be used.

Finally, laser pulse length is the most important parameter in micro fabrication especially in long pulse laser ablation regime. The heat created in the process diffuses away in the duration that can be lower or greater than the laser pulse duration. The quality of the product and the machining efficiency will be reduced if the heat diffusion time is larger than the duration of the laser pulse. The heat diffusion will cause small globes remaining on the surface after the machining which are difficult or impossible to remove without damaging the work piece. The heat diffusion longer than the laser pulse can melt the surface around the removed material, which reduces the accuracy of the machining. Figure 3.1 shows various possible defects caused by undesirably long laser pulse.

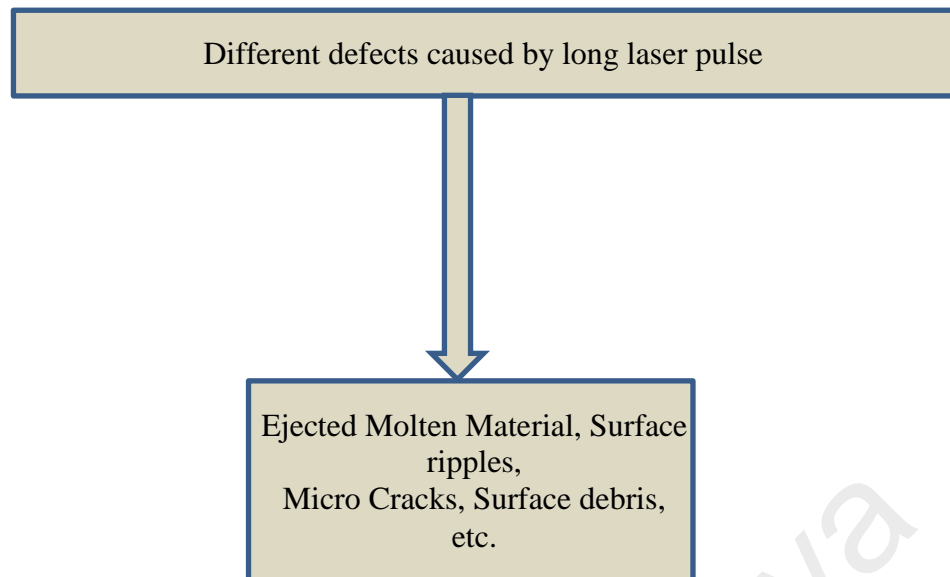


Figure 3.1: Different defects caused by long laser pulse (Madou, 2002).

3.2.1.2 CNC machining

In mechanical machining, mechanical energy from a cutting tool is applied for drilling, engraving and milling materials. The material is mechanically removed when the stress exerting from the cutting tool overcomes the material strength and therefore the dimensional precision is depending on the ratio of the stress applied and the residual stress to the yield stress. In addition, deformation of the work piece and cutting tool, improper fixture or tool selection and inaccuracies of machine tools are important parameters that affect accuracy of the products. The centrifugal microfluidic platforms for this research were mainly fabricated using a Computer Numerical Control (CNC) machine i.e., model VISION 2525, by Vision Engraving and Routing Systems, USA (Figure 3.2). The machine is capable of performing various applications such as drilling, contouring, routing, milling and engraving. The computer-aided designs of centrifugal microfluidic platform are imported into a software package released by “Vision Engraving and Routing Systems Incorporation”, which provide a flexible interaction between the user and the machine. The centrifugal microfluidics are often fabricated in three and five PMMA layers dependent on the complexity of the design and their applications. In the three layers designs all the microstructures including capillaries,

inlet and outlet chambers and especially designed valves are cut out on a PMMA. That PMMA layer is next sandwiched by two other PMMA and PSA layers which one covers the cut out from the top side (often containing air holes) and the other covers the cut outs from the bottom. For more complicated designs, where the microstructures on one PMMA layer are connected to microstructures on the other layers the number of PMMA layers increases to five or more layers. Note that, both five layers and three layers designs can be made with less number of PMMA layers by engraving microstructures instead of cutting them out. In the engraving technique, the microstructures (mostly vessels) are carved out from the PMMA layer with a depth lower than the thickness of the PMMA layer, which enables the elimination of the layer that is used to cover the microstructures in the cut out method. However, the engraving is more time consuming and the surface of engraved micro structures are of lesser quality than those cut out. The quality of the product adds more parameters (e.g., surface roughness) into the liquid flow investigation and also affects the quality of the video recorded by the camera of the testing setup.



Figure 3.2: An image of CNC router/engraver machine used to fabricate centrifugal microfluidics.

3.2.2 Pressure sensitive adhesive (PSA) cutting

The designs conforming to those used in fabrication of a PMMA layer are drawn by a computer aid design software such as Autodesk and imported (with proper format) to CorelDraw software. The conforming centrifugal microfluidic designs are cut on PSA sheets by a cutter plotter machine (FLEXcon, USA). The PSA is supplied in the form of three layer sheets comprised of two non-sticking plastic layers and a PSA layer sandwiched between the two plastic layers. Figure 3.3 shows the cutter plotter machine used to cut out the microstructures on the PSA layer.



Figure 3.3: The cutter plotter used to fabricate PSA layers.

3.2.3 Assembly

The PMMA discs fabricated by CNC machine are bounded to each other using PSA layers. The PSA layer is separated from the non-sticking plastics and carefully laid on the PMMA discs containing the conforming microstructures. A custom-made disc holder has been made in order to facilitate bounding PMMA discs, which enables precise conformity between the microstructure on different PMMA layers and microstructures on the PSA layers. The same procedures are repeated until all PMMA layers are bounded together by PSA layers. The centrifugal microfluidic platform is

next placed in a custom-made screw press and is pressurized and the disc fabrication process is accomplished.

3.3 Testing setup

The investigation of flow behavior and testing the performance and efficiency of different microfluidic valving techniques are carried out on a custom made experimental setup. The experimental setup is comprised of a sophisticated spinning system, which allows for spinning the disc up to 7000rpm. The spinning system allows for acceleration and deceleration of the disc as well as periodic and programmed increment in spinning velocity based on previously defined values. The spinning system is connected to a personal computer and controlled by the user-friendly interactive software. The user is able to control the disc spinning speed and program the speed for sequential operations through the software. A high-speed camera is placed on top of the disc holder and the position of the camera is adjusted according to the experiments requirements. The camera is able to capture the flow movement in the defined microstructures as per disc revolution. Figure 3.4 shows the experimental setup comprised of a high-speed camera and a spinning system.

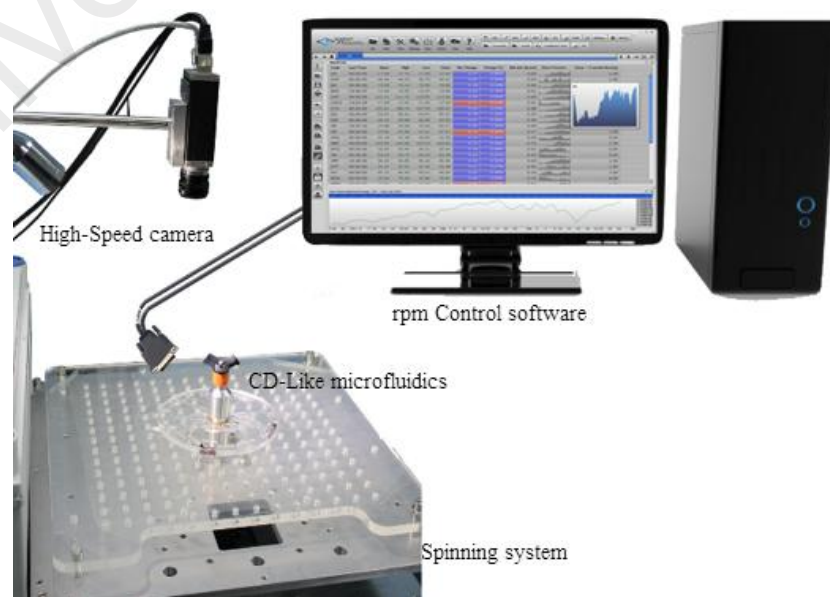


Figure 3.4: The spinning system and the high-speed camera.

3.4 Computational fluid dynamics (CFD) method

3.4.1 Fundamental of numerical methods

Today, numerical methods such as CFD are used more and more due to rapid growing computer technologies, which solve mathematic problems faster and more reliable. The governing equations for a fluid are derived based on the fundamental laws of mechanics, which are the conservation of mass, the conservation of momentum and conservation of energy equation. These equations form a set of coupled, nonlinear partial differential equations, which are difficult to be solved analytically for most of engineering problems. Nevertheless, it is possible to find approximate computer-based solutions to the governing equations in order to solve engineering problems. Computational fluid dynamics (CFD) uses the numerical methods and algorithms to analyze fluidic problems. In general, the aim of CFD methods is to simplify and replace continues domain problems to discrete domains by using grids. The difference between the numerical and analytical method can be shown by comparing continues pressure and discrete pressure in one-dimensional domain. The pressure in an analytical model is:

$$p = p(x) \quad 0 < x < 1$$

and for a discrete domain is:

$$p_i = p(x_i) \quad i = 1, 2, \dots, N$$

In a CFD solution, the relevant flow variables are directly solved only at the grid points and the other location values will be defined by interpolation of the values at the grid points. Therefore, defining the initial and boundary conditions are significant requirements to numerically solve fluid mechanic problems. The governing partial differential equations and boundary conditions in exact solution are defined in terms of the continuous variables such as pressure, velocity and so on. In a discrete domain,

these parameters can be approximated in terms of the discrete variables. The discrete system is a large set of coupled, algebraic equations in terms of discrete variables. Setting up the discrete system and solving it involves a large number of repetitive calculations and ANSYS-Fluent is one of the useful computational fluid mechanic software for analyzing fluid flows. There are two methods of discretization, which are finite-difference and finite-volume method. The finite-volume method is used by the most CFD software such as ANSYS-Fluent. In this method, the integral form of the conservation equations will be applied to the control volume, which is defined by a cell, and the discrete equations of the cell are obtained. Software such as ANSYS-Fluent conserve each cell to find solutions and variable values of the flow are solved at center of cells and the solutions at other locations are obtained by interpolation.

3.4.2 Volume of fluid (VOF) method

The volume of fluid (VOF) method from the commercial ANSYS-Fluent CFD package, version 13.1 is used to investigate the flow pattern and to predict the burst frequency in centrifugal microfluidic platforms. This method is computationally inexpensive and provides reliable results for liquid gas interaction problems (ANSYS-FLUENT, 2011; Hirt & Nichols, 1981; Tseng et al., 2002). In the VOF algorithm, the dynamic contact angle is automatically calculated as part of the solution via finite volume method from the basic equilibrium of forces in the numerical method (Brackbill et al., 1992; Hirt & Nichols, 1981). The contact angle is the angle formed between the moving liquid interface and the solid interface at three-phase contact line (Blake, 2006; van Remoortere & Joos, 1991), The VOF algorithm computes the macroscopic effect of surface tension by tracking the contact line and does not impose a constant contact angle at the surface. In other words, the predefined contact angle is continuously changing based on the velocity and the direction of the contact line (Rosengarten et al., 2006). However, since the contact line tracked in the VOF algorithm is based on the

macroscopic level of interaction between the three-phase, it is necessary to ensure the viability of the algorithm in the simulation of capillary flows. Saha et al. (Ashish & Mitra, 2009) have used the VOF method to investigate the fluid flow in capillary channel made of PDMS using both the static and the dynamic contact angles. The latter was calculated using eight different types of theoretical models from literature e.g., Blake, Bracke, Newman and Shikhmurzaev (Grader, 1986; Popescu et al., 2008) and incorporated into Fluent via a User Defined Function (UDF). However, no significant difference was found in results due to the use of the two types of contact angles. The study was carried out for contact angles of 0° , 36° and 72° and various surface tensions and viscosities. Therefore, the physics occurring in the Nano-scale level at the three-phase contact line can be addressed quite well in the VOF method (Brackbill et al., 1992; Hirt & Nichols, 1981; Rosengarten et al., 2006). Note that, the cases studied in Saha et al. (Ashish & Mitra, 2009) are spontaneous wetting cases. Forced wetting problems e.g., flow in centrifugal microfluidic platforms have the same underlying mechanisms and are described in an equivalent way to a spontaneous wetting problem since they are basically instances of moving contact lines (Ashish & Mitra, 2009; Shikhmurzaev, 1997).

3.4.3 Governing equations

In the VOF method, the position of the interface between the fluids of interest is tracked in a fixed Eulerian mesh domain. A single set of Navier-Stokes equations is solved for the computational domain and the volume fraction of each fluid is tracked by using an additional transport equation. The volume fraction (α) in each cell in the computational domain is between 0 and 1. For control volume, the sum of the volume fraction of all phases is set to unity. Therefore, any given cell represents either a mixture of phases ($0 < \alpha < 1$) or a pure phase ($\alpha = 1$) flow. The continuity and momentum equations

for laminar, incompressible, Newtonian, and isothermal flow employed in the current study are as follows (Feng et al., 2003):

$$\nabla V = 0 \quad [15]$$

$$\rho \frac{\partial u}{\partial t} + \nabla u \cdot u = -\nabla P + \nabla \mu \nabla u + \nabla^T u + F_v \quad [16]$$

where, V , P , t , F_v , ρ and μ are the velocity of the mixture, pressure, time, volumetric forces, density and viscosity, respectively. The continuity equation of a multiphase immiscible flow in Fluent is solved solely for the secondary phase q_{th} , which has the following form (ANSYS-FLUENT, 2011):

$$\dot{m}_{pq} \frac{\partial y}{\partial t} (a_q \rho_q) + \nabla (a_q \rho_q \vec{v}_q) = \sum_{p=1}^n (\dot{m}_{pq} - \dot{m}_{qp}) \quad [17]$$

where, \dot{m}_{pq} is the mass transfer from phase p to phase q and \dot{m}_{qp} is the mass transfer in the reverse direction. The primary-phase volume fraction is computed using the following constraint:

$$\sum_{q=1}^n a_q = 1 \quad [18]$$

The average values of variables and properties of the mixture are defined based on the volume fraction of each phase at a given location (ANSYS-FLUENT, 2011). For instance, the average values of density and viscosity of the mixture in a computational cell are (ANSYS-FLUENT, 2011):

$$\rho = a\rho_2 + (1-a)\rho_1 \quad [19]$$

$$\mu = a\mu_2 + (1-a)\mu_1 \quad [20]$$

The continuous surface force model (CFS) is used to reformulate surface tension into an equivalent body force (Brackbill et al., 1992). For a two-phase system, the volumetric force due to surface tension at the interface between phases 1 and 2 is given as:

$$F_v = 2\sigma \frac{\rho k \nabla a}{\rho_1 + \rho_2} \quad [21]$$

where, ρ is the volume-averaged density computed using Eq. 5, ρ_1, ρ_2 are the density of phase 1 and 2, respectively. According to the CSF model, the surface curvature k is computed from local gradients in the surface normal to the interface, which is given as:

$$k = \frac{1}{|n|} \left[\left(\frac{n}{|n|} \cdot \nabla \right) |n| - \nabla \cdot \hat{n} \right] \quad [22]$$

where $n = \nabla A$ is the normal vector. Wall adhesion is included in the model through the contact angle:

$$\hat{n} = \hat{n}_w \cos \theta + \hat{t}_w \sin \theta \quad [23]$$

where \hat{n} is the unit vector normal to the surface, $\hat{n} = \frac{n}{|n|}$, \hat{n}_w , \hat{t}_w represents the unit vector normal and tangent to the wall, respectively.

CHAPTER 4: INVESTIGATION OF THE PERFORMANCE OF HYDROPHILIC AND SUPER HYDROPHILIC CAPILLARY VALVES

4.1 Introduction

Today, in spite of the development of various types of passive and active techniques, capillary valves are still the most common valves in the centrifugal microfluidics and this is due to their simplicity and ease of fabrication. Flow in capillary valves is controlled by the interaction between the centrifugal and the capillary forces. When a capillary meets abrupt changes in its geometry a pressure barrier is built and the fluid advancement in the capillary is stopped. In the centrifugal microfluidic platforms, the pressure required to overcome this pressure barrier is provided by the centrifugal force. The maximum centrifugal force needed to overcome this pressure barrier is referred to as the burst pressure and the corresponding disc rotational speed is called the burst frequency. The burst frequency is the main parameter for designing of capillary valves as well as for flow sequencing and flow control in centrifugal microfluidics. A number of theoretical models to calculate the burst pressure in a centrifugal microfluidic platform have been presented and reviewed in chapter two (Chen et al., 2008; Cho et al., 2007b; He et al., 2009; Kim et al., 2002; Man et al., 1998; Zeng et al., 2000b). For example, the effects of capillary dimension, expansion angle and capillary shapes on burst frequencies in hydrophobic microstructures have been thoroughly studied and several theoretical models to predict the burst frequency have been presented (Chen et al., 2008; Cho et al., 2007b). The burst frequency in super hydrophobic capillaries has also been investigated and a theoretical model that considered the capillary dimension and expansion angle has been developed (He et al., 2009). In general, these theoretical models have been experimentally validated for limited contact angles, usually one contact angle. Therefore, employing these equations universally for predicting the burst frequency for capillaries of different range of contact angles may not be applicable. In

particular, flow behaviors in super hydrophilic, less hydrophilic capillaries have not been studied, and using these equations to predict burst frequency in such capillaries cannot be recommended specially when they have not been compared with experimental or numerical results.

In this chapter the effect of capillary dimension and the effect of contact angle on the burst frequency of super hydrophilic and less hydrophilic capillaries and the flow behavior in the centrifugal microfluidics are investigated numerically and experimentally. Herein, the super hydrophilic and less hydrophilic capillaries are referred to as the cases where the contact angle between the surface of the capillary and di-water is $20^\circ < \theta < 60^\circ$ and $60^\circ < \theta < 90^\circ$, respectively. The results obtained from this investigation provide a holistic insight into the performance of capillary valves and assist in their design and fabrication on the centrifugal microfluidic devices made from super hydrophilic and less hydrophilic materials. In this experimental and numerical investigation, the capillary dimensions of various capillary structures are varied from 150 μm to 450 μm to study the effect of dimensions and the contact angle on the burst frequency. The volume of fluid method within version 13.1 of commercial code of ANSYS-Fluent is used for solving the governing fluid mechanics equations. In order to validate the implementation of the numerical model our experimental data and existing experimental data in the literature are compared to the present computed data. Some of the results of this investigation have been published (Kazemzadeh et al., 2013).

This section begins with the governing equations, geometries and boundary conditions taken into account in simulation of the fluid flow in super hydrophilic/less hydrophilic centrifugal microfluidics. It continues with presenting the results of the effect of capillary dimensions and contact angles on super hydrophilic and less hydrophilic centrifugal microfluidics.

4.2 Boundary conditions and Numerical method

Two common types of microstructures, named Geo. 1 and Geo. 2 are used to study the effect of contact angles and capillary dimensions on burst frequency (see Figure 4.1 (a)). Geo. 1 features square chambers and Geo. 2 features circular chambers. In both structures, a capillary channel is located between the two chambers and fluid flows from the left chamber to the right one. The left chamber (close to the CD center) is referred to as the entry chamber and the right one as the outlet chamber. The distance of the capillary valve from the center of the rotation (r_2), this is also the center of the disk, for Geo. 1 and Geo. 2 is 31.5 mm and 43.57 mm, respectively. The surface tension of water is set at 0.072 N/m. These parameters in addition to the value of advancing and equilibrium contact angles are the same as those used in the experiments carried out by Chen et al. (2008) and He et al. (2009) and will be used for validation of our numerical data. The contact angle at solid walls has been specified according to the cases listed in Table 1. The computational domains of Geo. 1 and Geo. 2 are set to rotate clockwise using a single rotational frame (SRF) (ANSYS-FLUENT, 2011) in order to propel the fluid from the left chamber to the right chamber through the capillary channel. The rotational speed starts from a low frequency, i.e. 25rpm and it is gradually increased at intervals of 50rpm. All the solid boundaries of the domain are treated as walls with zero slip velocity. A zero pressure gradient is assumed from fluid entrance on the left to fluid exit on the right. The left chamber is filled with a sufficient volume of water such that the water consistently occupies the capillary channel until it bursts and fills some volume in the right chamber. In order to reduce the computational time simulations begin when half of the capillary is filled with the water. In addition, we have investigated a case where left chamber is filled with water allowing it to flow from the left chamber into the capillary channel before bursting to the right chamber. However,

our numerical data show that there is no difference in the results between the above two types of initial conditions.

The Pressure Implicit Split Operators (PISO) method, which uses the splitting of operations in the solution of the discretized momentum and pressure equations is used for coupling of pressure and velocity (Issa, 1986). The convection terms are spatially discretized using a second order upwind discretization method, which is an advanced finite difference scheme fully accounting for surface tension and wall adhesion forces. The body-force-weighted interpolation scheme is used in order to take into account the explicit body forces (e.g., Coriolis, centrifugal, etc.). Zonal discretization with a compressive slope limiter was set in order to have a sharper interface. An under-relaxation factor of 0.25 is used in the calculation of the pressure, density, body forces, and momentum and volume fraction. This factor reduces the rate of solution changes during the iteration to stabilize the convergence behavior of the momentum and continuity equations. The equations were solved using the unsteady model in Fluent with a time step of 1×10^{-5} s to 5×10^{-5} s for various cases of the current study. A convergence criterion of 1×10^{-6} was used to specify the relative error between two successive iterations was specified.

4.3 Mesh

The mesh used was based on quad grids with an element size of 0.01mm. Grids in the area of the waterfront and the edges adjacent to expansion areas i.e., at the water outlet to the right chamber were refined to smaller element size of 0.005mm. Mesh dependency tests were carried out for each case and the meshes eventually used were justified by the quality of the results. For instance, increasing the original mesh by 100% to obtain finer grids does not give any significant difference for the burst frequency (<1.3%). The quality of the grids used for Geo. 1 and Geo. 2 at the outlet of

the right chamber is shown in Figure 4.1 (b). The total number of cells in Geo. 1 and Geo. 2 is 437,980 and 314,852, respectively.

4.4 Simulation Cases

Forty-four simulation cases were created from Geo. 1 and Geo. 2 by varying the ratio of height/width (aspect ratio) and the contact angle (θ°). The range of these parameters, as listed in Table 4.1, represents a large sample of centrifugal microfluidic platforms scenarios. Simulation cases 1-4, 11, 32 and 37-44 are used to validate the implementation of the VOF method. These cases coincide with the experimental investigations from Chen et al. (2008), He et al. (2009) and Gliere et al. (2006) and consist of various contact angles and capillary dimensions. Cases 5-10 are used to study the effect of the height and width dimensions of the capillary channel on the burst frequency. Here one of the dimensions is varied from 180 μm to 450 μm while the other dimension and the contact angle are kept constant at 300 μm and 68 $^\circ$, respectively. Cases 11-36 are used to study the effect of varying contact angles (from 20 $^\circ$ to 90 $^\circ$) on the burst frequency using Geo. 1 and Geo 2.

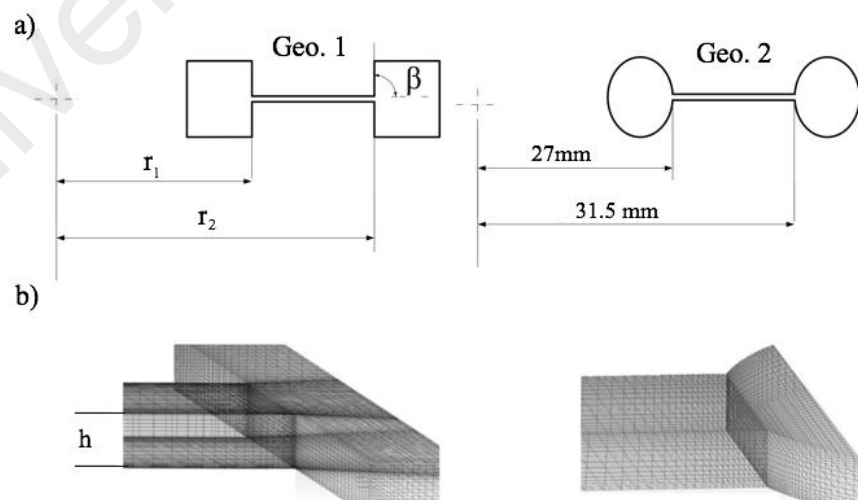


Figure 4.1: Top view of Geo. 1 and Geo. 2 used in the simulations b) Computational mesh adjacent to the outlet of capillary channel of Geo 1 and Geo 2.

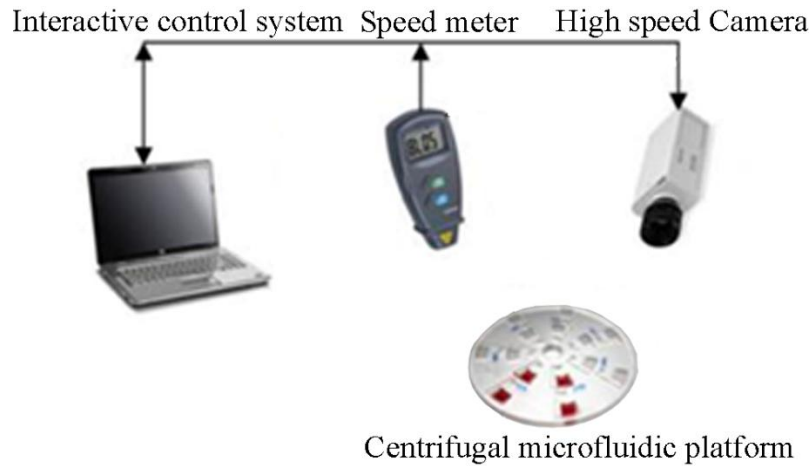


Figure 4.2: Experimental setup: controlling computer system connected to a high-speed camera and a digital rpm meter.

Table 4.1: Details of simulations, r_1 , r_2 are kept the same as those used in Chen et al. (2008)

Num. Cases	Aspect ratios h/w	θ°	Geo.	Remarks
1-4	$\frac{180}{300}, \frac{300}{300}, \frac{400}{300}, \frac{450}{300}$ $(\frac{h}{w}=0.6, 1, 1.33, 1.5)$	68	1	These cases are used for validation and are the same to that used in Chen et al. (2008).
5-10	$\frac{300}{450}, \frac{300}{400}, \frac{300}{360}, \frac{300}{300}, \frac{300}{240}, \frac{300}{180}$ $(\frac{h}{w}=0.6, 1, 1.33, 1.5)$	68	1	These cases are used to study the effect of: capillary dimensions on burst frequency and h/w is the inverse of that used in Chen et al. (2008).
11-18 ,19-26 27-31	$\frac{157}{426}, \frac{426}{157}, \frac{h}{w}$ ($\frac{h}{w}=0.37, 2.71$)	20:10:80 and 93	2	These cases are used to study the effect of θ on burst frequency, where: $h/w=157/426$ and $h/w=426/157$ is the same to and the inverse of that used in He et al. (2009) respectively.
,32-36	$\frac{157}{426}, \frac{157}{314}, \frac{h}{w}$ ($\frac{h}{w}=0.37, 0.5$)	45:10:85	1	

4.5 Experimental set up

The rectangular microstructures were fabricated using a Computer Numerical Control (CNC) machine (model VISION 2525, by Vision Engraving and Routing Systems, USA). The micro structures were engraved on compact disc-like platforms layer made of a 2mm thick Polymethyl methacrylate (PMMA) and bonded by Pressure Sensitive Adhesive (PSA) material (by FLEXcon, USA) to a 2mm PMMA layer with

venting holes cut through. A cutter plotter (model PUMA II, by GCC, Taiwan) was used to cut the microfluidic design in the PSA layers corresponding to the design of the PMMA layer. A custom-made system consists of a digital disk Spin Test System, laser sensor and a high-speed camera was used to perform the experiments (see Figure 4.2).

4.6 Results and discussion

4.6.1 Validation

Several experimental studies (Chen et al., 2008; Glière & Delattre, 2006; He et al., 2009) have been used in order to validate our numerical results of various contact angles; i.e., surfaces with the contact angles less than 40° , between 40° and 60° and from 60° to 90° which are referred to as super hydrophilic, hydrophilic and less hydrophilic surfaces, respectively. At first the experimental data from Chen et al. (2008) and He et al. (2009) is used to validate our numerical results for less hydrophilic cases i.e. contact angle 68° , 70° and 93° . Chen et al. (2008) used rectangular microfluidic structures with an expansion angle of 90° which were fabricated of PMMA (polymethylmethacrylate) material using CNC machine. The fluid used in the test was DI-water containing a small amount of red ink. On the other hand, He et al. (2009) used PMMA circular based microstructures, which were manufactured using a microinjection moulding technique. The CYTOP-coated polyaniline nanofibers were used to increase the contact angle of PMMA to 93° . The fluid used in the test was DI-water containing red food dye. The sizes and locations of the microstructures used in our numerical model for validation are set to be equal to that used in the experiment investigations, which are listed in Table 4.2. In Table for, $F_{b)exp}$, $F_{b)theo}$ $F_{b)num}$, denote the experimental, theoretical and numerical burst frequencies, respectively. For the same contact angles i.e., 68° , 70° , 93° and water, as the test liquid, our results are in good agreement with the measurements reported in Chen et al. (2008) and He et al. (2009).

In the second step, the burst pressure measurements for rectangular microstructures by Glière et al. (2006) are used to further validate our numerical results for the hydrophilic and the super hydrophilic cases. In that study, silicon wafer microstructures were fabricated using a single deep etching process (Cho et al., 2004) and sealed with a PDMS substrate. DI-water with a surface tension of 0.072 N/m and a biological buffer solution with a surface tension of 0.03 N/m were used in the test. The contact angle of DI-water on the silicon wafer and PDMS are 60° and 80° and that of the biological buffer is 35° and 75°, respectively. Figure 4.3 shows a comparison between our numerical results and the numerical and measured data from Glière et al. (2006). The numerical results are in good agreement with measured and simulation data reported in Glière et al. (2006) especially for DI-water (Figure 4.3 (a)). The large deviation between our numerical data and experimental data of Glière et al. (2006) for biological buffer (Figure 4.3 (b)) may be due to an alteration of the surface tension in the experiment which causes the increase of burst pressure in comparison with the numerical results. This deviation can also be observed in the numerical data reported by Glière et al. (2006). In fact, in the experiment, during the expansion of a meniscus the surfactant concentration reduces to a value lower than the equilibrium concentration, which causes the increase in surface tension value. In addition, during the relaxation time of the surface tension and surfactant the actual surface tension of the buffer is larger than the equilibrium surface tension. However, the surface concentration value gradually increases back to its equilibrium value (Danov et al., 2002; Glière & Delattre, 2006).

4.6.2 Flow sequence in a super hydrophilic capillary

The difference of flow motion in a hydrophilic and a super hydrophilic capillary is illustrated in Figure 4.4. Before the fluid reaches the valve point, i.e., at $t=0.1s$ and earlier, the meniscus in both capillary has a concave shape due to the hydrophilicity of capillary surfaces. For a hydrophilic capillary with an assumed contact angle of $\theta = 60^\circ$

as shown in Figure 4.4 (a), at $t=1.3s$ due to the capillary pressure barrier, the fluid stops at the very end of the capillary and the meniscus shape is gradually changed into a convex shape. As the rotational speed increases to 275rpm, the centrifugal pressure overcomes the pressure barrier ($t=1.35s$) and the fluid bursts into the right chamber. It flows at the top of the chamber against the clockwise rotational direction probably due to the inertial force and the start of Coriolis effect. After $t=1.5s$, the fluid consistently flows towards the top the chamber. These observations are confirmed in the experimental studies of Cho et al. (2007b) and Man et al. (1998). A small portion of liquid, due to symmetrical advancement of the liquid at lower spinning speeds, may remain on the surface of the T-junction which will eventually flow toward the rest of the liquid in case of increasing the spinning speed.

The fluid motion in a super hydrophilic capillary with an assumed contact angle of $\theta = 20^\circ$ (Case 11) is shown in Figure 4.4 (b). At this low a contact angle, on contrary to Figure 4.4 (a) fluid does not completely stop at the capillary valve. While the meniscus retains its concave shape, the fluid flows on sidewalls and continuously leaks into the expanded volume (right chamber) at very low burst frequencies ($<150rpm$). The fluid flows symmetrically at the top and bottom side walls of the circular chamber, and cause the change of the meniscus shape, as shown at $t=0.2s$ to $t=1s$. Differences seen between hydrophilic and super hydrophilic capillaries are due to the significant influence of the adhesive wall force in the case of a low contact angle, which eases the flow over expansion surfaces at a very low rotational speed. Moreover, the Coriolis force is dependent on the angular velocity (eq. 13) therefore, operating at a low rotational speed results in inadequate Coriolis force to effect on the direction of the flow advancement in circular chamber.

$$F_{co} = 2 \times m \times \omega \times v \quad [24]$$

Similar flow motion to Figure 4.4 (b) is also observed for the rectangular structure under the same model set up (the results are not presented here).

The fact that on contrary to the theoretical studies, the numerical data shows the fluid leakage at the low contact angles can be due to several reasons. The theoretical expressions from Chen et al. (2008) and He et al. (2009) have been verified experimentally for a particular operational parameters e.g., specific geometry of the capillary expansion and specific contact angles i.e., 68°, 70°, 93°. In addition, the theoretical models do not explicitly include the effect of wall adhesion that has a significant influence on fluid interfaces at a low contact angle. However, in the VOF method, the wall adhesion effect is fully considered in the governing equations (see Eq. 23).

Table 4.2: Comparison between the numerical and experimental burst frequencies with dimensions and positions of the capillary valves on the disk.

Case no.	\hat{r} (mm)	σ_{la} (N/m)	θ°	width (μm)	depth (μm)	$F_{b)Num}$ (rpm)	$F_{b)Theo}$ (rpm)	$F_{b)Exp}$ (rpm)	Erro (%)	Exp. Ref.
1	29.25	0.072	68	300	180	250-300	318	284	3.17	(Chen et al., 2008)
2	29.25	0.072	68	300	300	350-400	430	390	3.85	(Chen et al., 2008)
3	29.25	0.072	68	300	400	375-425	465	418	4.31	(Chen et al., 2008)
4	29.25	0.072	68	300	450	425-475	476	439	2.50	(Chen et al., 2008)
16	41.51	0.072	70	426	157	225-275	426	216-270	2.89	(He et al., 2009)
18	41.51	0.072	93	426	157	300-350	331	302-352	0.66	(He et al., 2009)

4.6.3 Effect of dimensions of the capillary channel

Figure 4.5 shows the computed burst frequency against the aspect ratio (AR) for Cases 5-10 where with a constant height of 300 μm , the capillary width is varied from 180 μm to 450 μm . These results are compared with the burst frequencies calculated by the theoretical model developed by Chen et al. (2008). In addition, the influence of capillary height on burst frequencies calculated from the same theoretical model is plotted in Figure 4.6. The results show that for a constant height (300 μm), burst

frequencies increase as the capillary width decreases. It shows similar trend to experiments by Chen et al. (2008) where the capillary height varied and width kept constant (300 μ m). Therefore, lower burst frequencies are always expected for wide capillaries ($w>h$) compared to narrow capillaries ($h>w$).

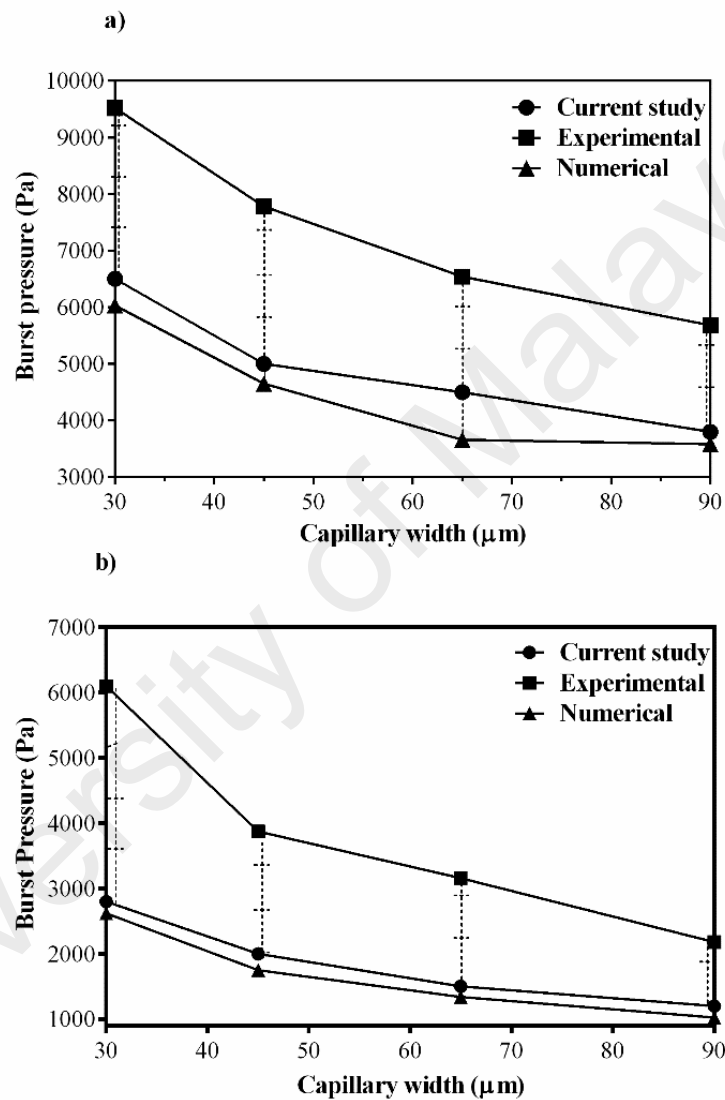


Figure 4.3: Comparison between the present study and experimental and numerical data from Gliere et al. (2006), a) for DI-water (surface tension of 0.072 N/m) and b) biological buffer (surface tension of 0.03 N/m).

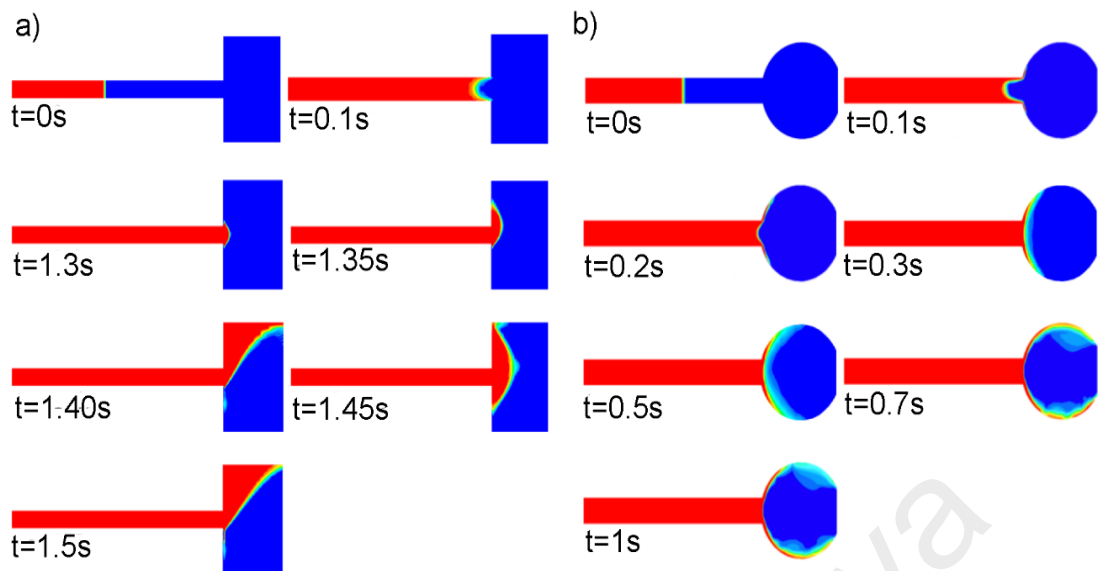


Figure 4.4: Sequences of the fluid motion in a) hydrophilic and b) super hydrophilic capillary.

This probably is because of the microfluidics structures used in the present study and that of the theoretical models. In such structures, alteration in capillary height and its width do not have the identical effect on the burst frequency. In the width direction, the capillary is bounded by solid walls while in its height direction it is not; that results in greater influence of the height on the burst frequencies compared to capillary width (see Figure 4.3). For a large difference between the capillary height and its width (h/w from 0.06 to 0.33) the burst frequency is highly susceptible to capillary height. For instance, with an increase in capillary height from $10\mu\text{m}$ to $100\mu\text{m}$ the burst frequency increases from 250rpm to 1200rpm. On the contrary, when there is a small difference between the height and width of the capillary ($1 < h/w < 3$) a large increase in height ($300\mu\text{m}$ to $900\mu\text{m}$) only increases the burst frequency from 430rpm to 525rpm. Note that, the theoretical expressions have been tested merely for conventional capillary dimensions. A possible reason for the contrary trend can be rather large dimension of the capillaries, which is not commonly used in centrifugal microfluidic platforms. The computed results show the minima burst frequencies for square capillaries ($AR=1$). The minimum burst frequency in square capillaries can be seen in Figure 4.5 where at aspect ratio of 1, our numerical value of the burst frequency is 375rpm. However, these minima are not

predicted by previous theoretical models, they are predicted well in the theoretical model we have developed (Thio et al., 2013). The lower burst frequency of the square capillaries compared to the rectangular capillaries can be seen in our experimental results listed in Table 4.3. This drop in the burst frequency is due to the unique geometrical aspect of the square microchannels where unlike the rectangular channels the meniscus in both width and height of the capillary experiences a symmetrical advancement which accelerate the burst. The experiments were carried out for a constant capillary width of $400\mu\text{m}$ and depth of $200\mu\text{m}$, $300\mu\text{m}$, $400\mu\text{m}$ and $500\mu\text{m}$ to further investigate the burst frequency in square and rectangular capillaries.

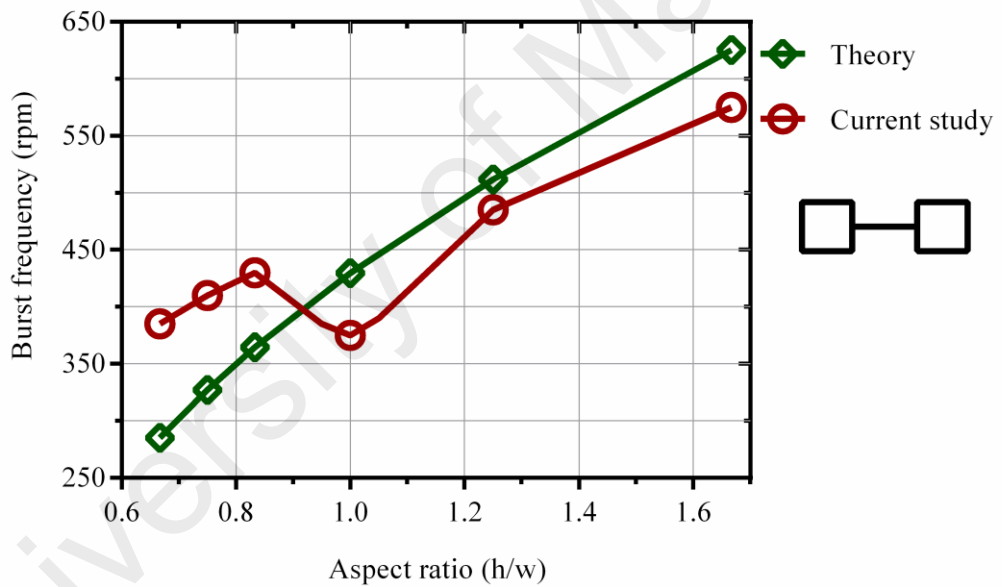


Figure 4.5: Burst frequency of the CFD model and Equation from Chen et al (2008) versus aspect ratio for Cases 5-10.

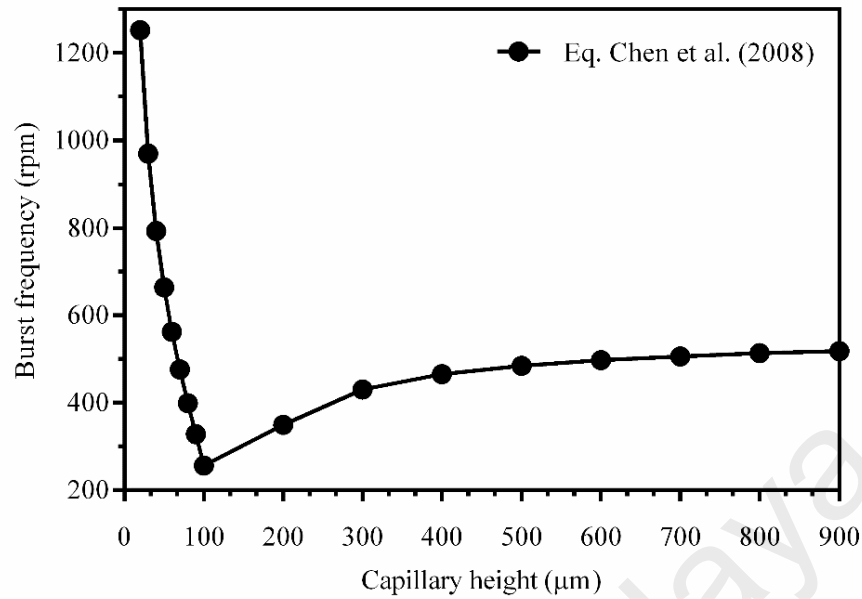


Figure 4.6: The distribution of the burst frequencies using Equation from Chen et al. (2008) versus different capillary height where the capillary width is kept constant of 300μm for a contact of 70.

Table 4.3 shows that the burst frequency lowers in square capillaries in comparison with the rectangular ones. The numerical predictions are presented in the range of 50 rpms due to the gradual increment (interval of 50 rpm) in simulations. These minima can be probably due to the specific symmetrical shape of the capillary that reduces the difference between the liquid-air interfaces on both the horizontal and vertical directions of the capillary. In the same manner, the equal distribution of the centrifugal force on the same directions may cause the minima burst frequencies. Therefore, the meniscus will be exposed to a uniform tension that can cause an early burst.

Table 4.3: A comparison between burst frequencies of square and rectangular capillary valves

Capillary section	\hat{r} (mm)	σ_{la} (N/m)	θ°	width (μm)	depth (μm)	Exp. burst (rpm)	Num. burst (rpm)
Rectangular	45	0.072	77	400	200	350-370	350-400
Rectangular	45	0.072	77	400	300	300-320	300-350
Square	45	0.072	77	400	400	230-260	200-250
Rectangular	45	0.072	77	400	500	290-310	300-350

4.6.4 Effect of contact angles on burst frequency

Figure 4.7, Figure 4.8 show the effect of the contact angles on burst frequencies of wide capillaries ($w>h$) and narrow capillaries, respectively. Figure 4.7 contains numerically computed results for Cases 11-18 where the height to width ratio of the capillaries is 157/426. Experimental results from He et al. (2009) for $\theta=70^\circ$ and $\theta=93^\circ$ and the theoretical models are included for comparison with the numerical results. The computed results are in excellent agreement with those of experimental from He et al. (2009). They show two lowest burst frequencies which occur at $\theta=20^\circ$ ($<150rpm$) and at $\theta=70^\circ$ (240 rpm). For super hydrophilic centrifugal microfluidic platforms ($\theta<40^\circ$), a decreasing trend of burst frequency with the decreasing of the contact angle can be expected due the increase of the wall adhesion effect. With a strong adhesion wall force, the fluid leaks even at a small centrifugal force as shown in Figure 4.4. For contact angles between 40° and 90° , first the burst frequency decreases with increasing contact angle until the minimum burst frequency of 240rpm, which occurs at 70° contact angle. This is quite interesting and we regard this minimum point as an optimum contact angle for the channel's dimensions, i.e., aspect ratio (h/w) of this case. For a different aspect ratio, the minimum burst frequency occurs at a different contact angle. Following the minimum point, the burst frequency only slightly increases with the increase of the contact angle, i.e., from about 250rpm to about 325rpm. The highest burst frequency occurs at the contact angle of 40° (about 450 rpm).

For super hydrophilic centrifugal microfluidic platforms ($<40^\circ$) numerical results and Eq. 10 both show the increase of burst frequencies with the increase of the contact angle which is in contradiction to burst Equation from Chen et al (2008). Despite of the high burst frequencies predicted by theoretical model our numerical results show that fluid flows over the capillary expansion walls before it actually bursts. In fact, the fluid leaks into the desired chamber before applying adequate centrifugal pressure that causes

the change of the meniscus shape in hydrophilic centrifugal microfluidic platforms (Figure 4.4). At the contact angle 70° the significant drop of the burst frequency predicted by theoretical models is on contrary to the experiments from He et al. (2009) (~200rpm difference). This exaggeration in predicting the burst frequency can be expected for other configurations of capillaries especially when the theoretical models calculate an extremely low burst frequency.

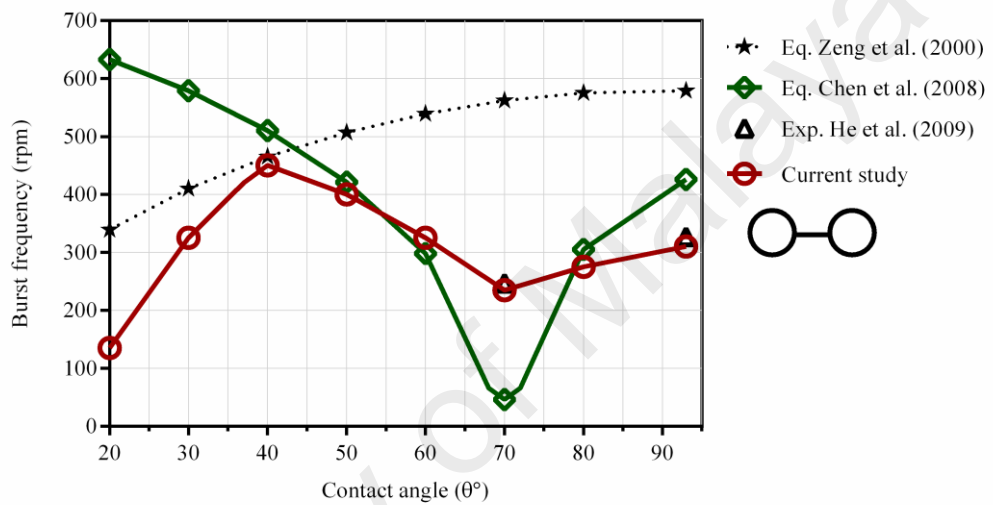


Figure 4.7: Burst frequency from the CFD model, Equation from Zeng et al. (2000b) and Equation from Chen et al. (2008) versus contact angles for Cases 11-18. Experiment results from He et al. (2009) is also given.

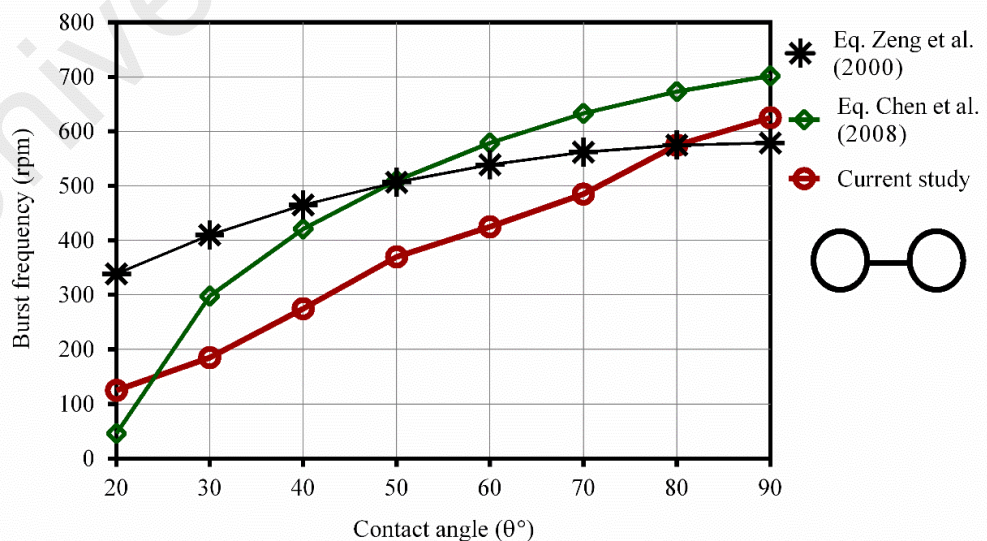


Figure 4.8: Burst frequencies from the CFD model, Equations from Zeng et al. (2000b) and Chen et al. (2008) versus contact angles for Cases 19-26.

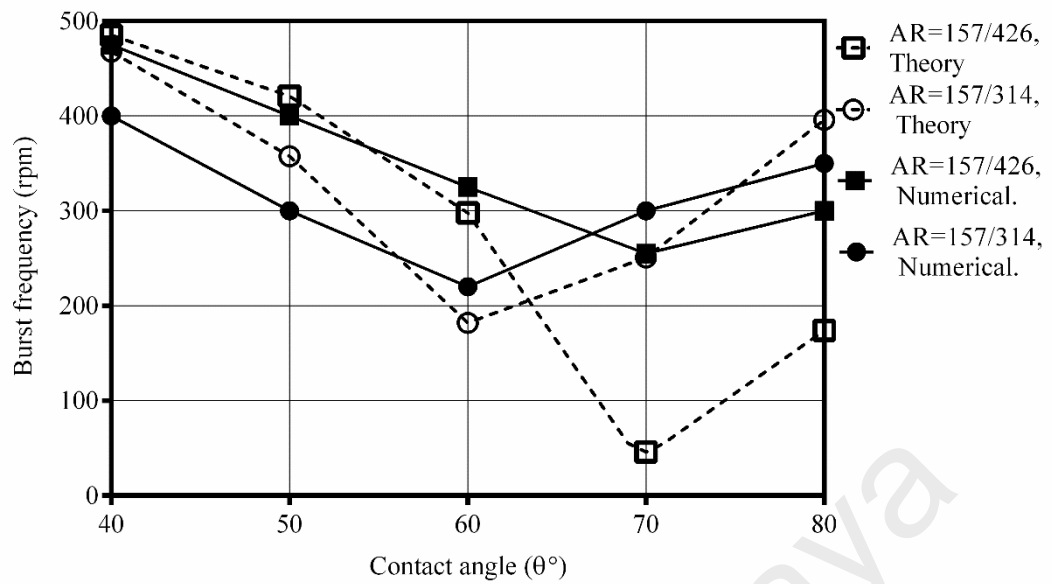


Figure 4.9: The distribution of the burst frequencies from the CFD model and Equation from Chen et al. (2008) with respect to different aspect ratios and contact angles for Cases 27-42.

Figure 4.8 shows the effect of the contact angles on burst frequencies for narrow capillaries ($h > w$). The height/width ratio is $426/157$, which is the opposite of that used in Cases 11-18 (i.e., $157/426$). In general, for narrow capillaries ($h > w$) the numerical results show the increase of burst frequency with the increase of the contact angle. On contrary to wide capillaries ($h < w$), both the numerical and the theoretical models have the similar trends.

Figure 4.9 shows the distribution of the computed burst frequencies for different capillary dimensions versus the contact angles (Cases 27-36). Herein, Geo. 1 has been used instead of Geo. 2 (used in Figure 4.7) to extend our discussion about the minima burst frequencies. Similar to Figure 4.7 computed results show a minimum burst frequency, which changes with the capillary dimensions. Although theoretical models almost successfully predict such minima, the values calculate by these models can be extremely different from those of experiments. These values are considered too small for burst frequencies in any centrifugal microfluidic platforms. The burst frequency of

most of the cases in the literature is above 250rpm with very limited cases below 250rpm (Chen et al., 2008; Cho et al., 2007c; Ducreé et al., 2007; Duffy et al., 1999; Glière & Delattre, 2006; Haeberle et al., 2006; He et al., 2009; Jia et al., 2006; Madou et al., 2001; Yan et al., 2008).

4.7 Summary

Flow in passive capillary valves in centrifugal microfluidic platforms for a wide range of hydrophilic and super hydrophilic contact angles has been studied using the VOF model within the commercial CFD code of ANSYS Fluent. Our experimental data in addition to experiment results from Chen et al. (2008), He et al. (2009) and Gliere et al. (2006) were used for validation and computed results were compared with existing theoretical models. The results obtained from this investigation completes the previous studies on the effect of contact angle and the aspect ratio on the burst frequency of provides holistic view into The findings of the current study can be summarized as:

- In common capillary dimensions ($>100\mu m$) for the cases of a low contact angle especially less than 20° , the capillary valve is unable to retain the fluid from leaking and it loses its function.
- The computed results suggest that the theoretical models cannot be used for super hydrophilic materials since they are unable to predict the fluid leakage. While they predict that high pressure is required for pushing the fluid over capillary valves, the computed results show that fluid flows consistently over the capillary valve into the next chamber at low pressures.
- In general, computed results show that burst frequencies of wide capillaries ($w>h$) are always lower than those of narrow capillaries ($w<h$). Theoretical models predict similar to our computed results for wide and narrow capillaries.

- The computed results for narrow capillaries ($w < h$) show a consistent increase of burst frequencies with the increase of the contact angle. However, for wide capillaries ($w > h$) the computed results predict three divisions of burst frequencies. First, as the contact angle increases, the burst frequency increases to a peak where it starts decreasing at a low burst frequency. After a low burst frequency, it slightly increases with the increase of the contact angle.
- The results show that burst frequencies of square capillaries are lower than those of rectangular shapes. However, the theoretical models used for comparison are not able to predict pressure drops in square capillaries.

University of Malaya

CHAPTER 5: DESIGN OF GATING VALVE, A MICROVALVE TO SWITCH THE FLOW DIRECTION

5.1 Introduction

At this point, the understanding obtained from the investigation of the performance of different capillary valves are used for devising a new passive valve that provides more control on the liquid movement in centrifugal microfluidic platforms. Flow in centrifugal microfluidics is intrinsically unidirectional issuing from the disc center towards its edge, while at T-junctions it is also intended to flow in the direction of the Coriolis force. The ability to employ multi-directional flow on centrifugal microfluidics allows for better use of disc's real estate and increases flexibility of fluidic operations. The switching of flow direction on spinning microfluidic platforms i.e., usually based on Coriolis force enables more sophisticated and flexible assay sequences such as mixing, metering, sample preparation and manipulation of high quality DNA and so on. Thus far flow-switching techniques on centrifugal microfluidic platforms have been accomplished by changing the spinning direction or by exploiting external power sources e.g., pneumatic or thermo-pneumatic pressure (Brenner et al., 2005; Brenner et al., 2003; Ducrée et al., 2004; Kim et al., 2008; Kong & Salin, 2011).

In this chapter a gating microstructure is presented that controls the flow direction in centrifugal microfluidics without the need of changing the direction of the disc rotation, applying surface treatments or employing external sources. The device is a frequency dependent valve that is able to direct the flow to one direction (e.g., c.w.) at low frequency and to the opposite direction (e.g., c.c.w.) at higher frequencies. At low frequencies, the liquid follows a micro path as a consequence of the specific gating microstructure and at higher frequencies liquid follows in the direction of the Coriolis force. The flow behavior of the novel valve for di-water as well as for other liquids with different properties has been investigated experimentally and numerically. The results

show that the new valve is able to control the flow direction on spinning microfluidic platforms for liquids of the wide range of properties. Some of the results of the introduction and characterization of this novel valve have been published in the esteemed technical peer-reviewed journal of *Sensors and Actuators Part B: Chemical* (Kazemzadeh et al., 2014).

5.2 Concept

Unlike Coriolis force, the geometrical structure of microvalve has not been reported as a method to control the flow direction on spinning microfluidic platforms. Here a new concept of gating valves is demonstrated that exploits special geometrical structures of the valve at T-shape junctions. A GV is a flow control means that exploits both geometrical effect and Coriolis force simultaneously to determine flow direction on a spinning platform. At low rotational frequencies, the liquid flow is gated into the opposite direction of the Coriolis force while it flows in direction of the Coriolis force at higher frequencies. Figure 5.1 compares the geometrical structure of a GV (b) and a conventional valve (a) at T-shape junctions. As compared to a conventional valve, GV allows controlling the interaction between the capillary force and the centrifugal force at the fluid/gas interface. GV is fabricated by creating an asymmetrical outlet chamber which produces an offset between the posterior and anterior expansion walls as presented in Figure 5.1 (b) and Figure 5.1 (c). The GV mechanism is investigated by studying the effect of gating parameter G on flow behavior. The capability of the valve to stop and control the flow direction and the effect of G on burst frequency of the valves are discussed in the Results section below.

5.3 Experimental set up

The CD-like microfluidics with the new valve design was fabricated using a Computer Numerical Control (CNC) machine (model VISION 2525, by Vision Engraving and Routing Systems, USA). The microstructures were milled on a 4mm

thick Polymethylmethacrylate (PMMA) layer. To create a microfluidic disc, this plastic layer is bonded by Pressure Sensitive Adhesive (PSA) layer (by FLEXcon, USA) to another 2mm thick PMMA layer that contains venting holes. A cutter plotter (model PUMA II, by GCC, Taiwan) is used to cut the CD-like microfluidic design in the PSA layers corresponding to the design of the PMMA layer. A custom-made system consisting of a digital disc spin test system, laser sensor and a high-speed camera is used to perform the experiments.

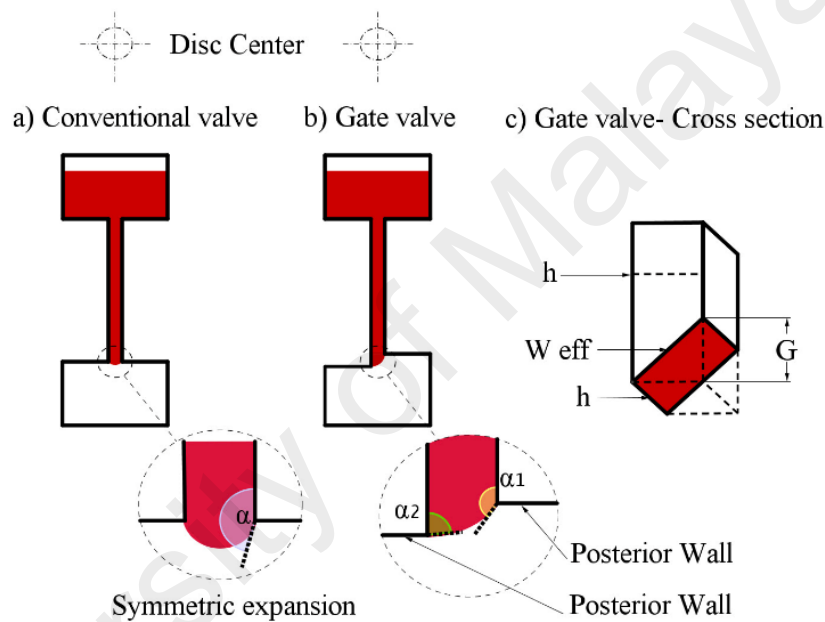


Figure 5.1: A sketch of (a) a conventional capillary valve (b) a Gating valve and (c) isometric view of GV.

5.4 Characterization

The flow switch was experimentally tested by fabricating a number of GVs with G varying from $10\mu\text{m}$ to $300\mu\text{m}$ by a step increase of $10\mu\text{m}$. In order to enhance the visual observation of the flow direction, the outlet chamber was divided by a V-shape wall as shown in Figure 5.2. The figure shows CD-like microfluidic containing both the conventional and GVs with the capillary width and height of $400\mu\text{m}$ and $250\mu\text{m}$, respectively. The figure shows a step-by-step experiment conducted to characterize the valve by comparing liquid motion in a conventional (Figures 5.2 (a) to (d)) valve and in

a GV (Figures 5.2 (e), (f)). The source chambers of the conventional and gated microfluidic systems are primarily loaded with the blue and red dyed di waters, respectively. Thereafter the platform is spun (Figure 5.2 (a)) and the rotational frequency is gradually increased until the fluid bursts (at 250rpm) and flows radially outward on the posterior wall (Figure 5.2 (b)). Here the liquid is gated into direction of the disc rotation and fills the left side of the outlet chamber (Figures 5.2 (c), (d)). In the conventional system, the meniscus is prior to burst when the rotational frequency is increased to 300rpm (Figure 5.2 (e)). Figure 5.2 (f) shows that the meniscus is slightly influenced by the Coriolis effect that is due to a small increase in rotational frequency (to 330rpm). The sudden increase of the rotational frequency to 450rpm causes the flow bends in the direction opposite to that of disc rotation. Figure 5.2 (g) shows that the liquid continuously fills the right side of the outlet chamber. The same procedure has been repeated to define the optimal sizes of G. In order to test the valve performance in different operational conditions the experiments were conducted for various liquids consisted of different solutions of di water and ethanol, 0.9% sodium chloride solution and carboxymethylcellulose sodium 0.5% with boric acid, calcium, magnesium and potassium chloride, purified water, sodium borate and sodium chloride. The water-ethanol mixtures were prepared by mixing di water and ethanol to a total volume of 100 μ L in a clean beaker. The volumetric concentration of ethanol was increased from 5% to 45% in 10% increments. The physicochemical properties of the water-ethanol mixture can be found in reference (Khattab et al., 2012; Leu & Chang, 2004b). Further experiments are conducted to investigate the valving mechanism for specific substances such as Bovine Albumin Solution (BSA) and washing solution used in biological assays (e.g., ELISA). The experiments are carried out several times for each liquid to investigate the consistency of the valving mechanism. The effect of adsorption of proteins and other substances existing in the biological solutions on serial switching is

investigated by consecutively loading the biological solutions into the same microstructure (consisting capillaries, GV and inlet and outlet chamber). In addition, the ability of GV for changing flow direction was numerically simulated for a biological buffer containing 0.1% Triton X-100 surfactant. The mechanical and chemical properties of the biological buffer can be found in reference (Glière & Delattre, 2006).

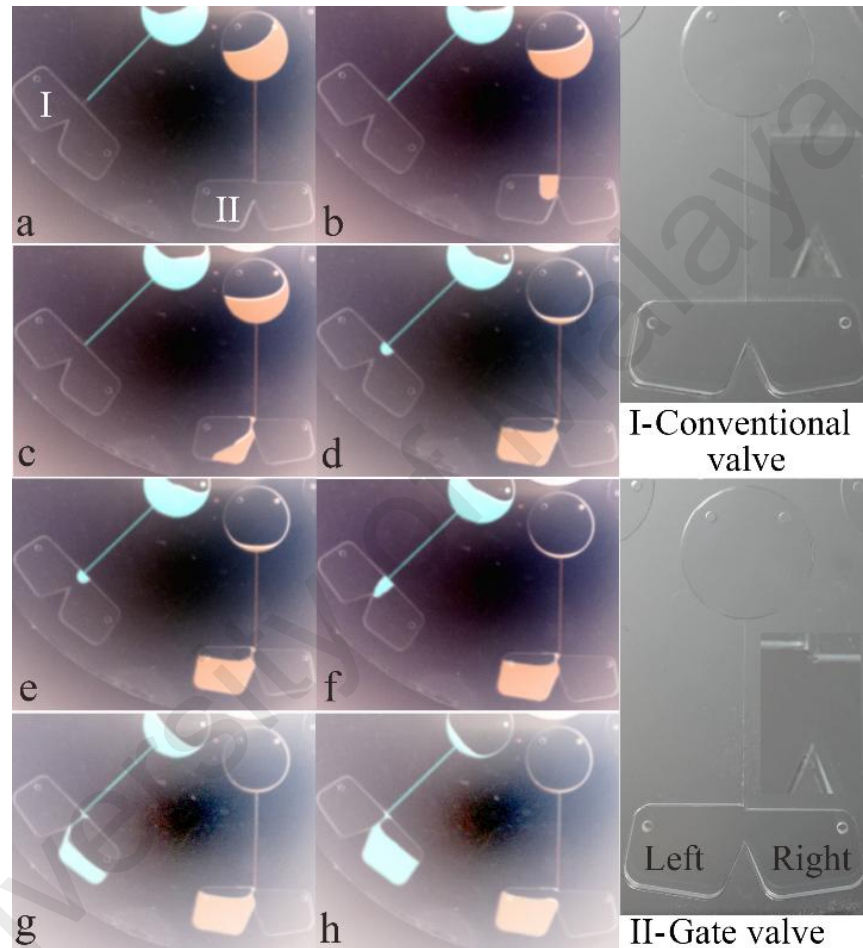


Figure 5.2: Partial top view of the liquid motion in a clockwise rotating disc a) conventional valve b) GV for capillary width of $400\mu\text{m}$ and $G=400\mu\text{m}$.

5.5 Numerical analysis

None of the existing theoretical models e.g., Chen et al. (2008), Lu et al. (2007) are formulated to address asymmetrical expansion of capillaries. Thus, in order to investigate the effect of G on the flow behavior different simulation cases were carried out using the volume of fluid (VOF) method within the commercial ANSYS-Fluent CFD package, version 13.1 (see appendix for more details). Details of the simulation

cases such as capillary dimensions, contact angles are listed in Table 5.1. In general, a uniform quad grid, which is further, refined at the edges adjacent to expansion areas, is used throughout the domains. The grid dependency tests conducted show that the increase of the original mesh to obtain finer grids does not give any significant difference in the results ($<1.3\%$). The grids used for the capillary channel and the right chamber are shown in Figure 5.3. The computational domain is set to rotate clockwise with the starting rotational frequency of 50rpm increasing gradually at intervals of 50rpm. All the solid boundaries of the domains are treated as walls with zero slip velocities. The Pressure Implicit Split Operators (PISO) method which uses the splitting of operations in the solution of discretized momentum and pressure equations is used for the coupling of pressure and velocity (Issa, 1986). The body-force-weighted interpolation scheme is used in the calculation of the explicit body forces at cell faces (e.g., Coriolis, centrifugal, etc.). The equations were solved using the unsteady solver in Fluent with a time step of 0.00005s. The scaled residuals of 1×10^{-6} are set as the convergence criteria for the continuity and other governing equations.

Table 5.1: Details of the simulation cases, where, \hat{r} , θ , σ_{la} are distance from the disc center, contact angle and surface tension of the liquid, respectively.

\hat{r} (mm)	θ ($^{\circ}$)	width (μm)	height (μm)	G (μm)	σ_{la} (N/m)
45	68, 77	100, 150	200	10:10:50	0.072,
		200:100:400		80:30:250	0.035

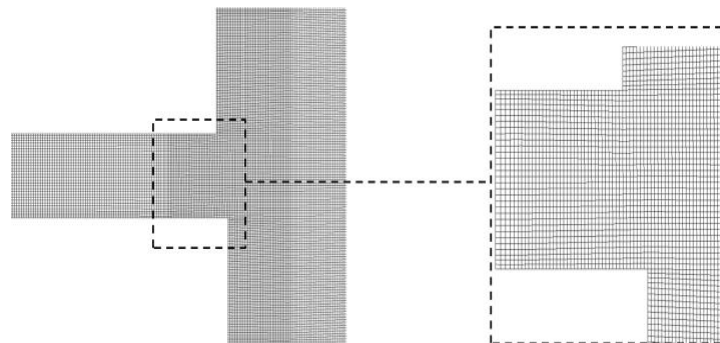


Figure 5.3: Computational mesh adjacent to the outlet of capillary channel.

5.6 Results

5.6.1 Validation

The simulation results are validated by comparing burst frequencies and flow behavior in GV and the conventional valves with our experimental observations. A comparison of the numerical and our experimental burst frequencies is listed in Table 5.2. The table shows that numerical burst frequencies and experimental data are in a good agreement. We have also compared the numerical results for the conventional valves with a theoretical expression from Chen et al. (2008). The comparison between the numerical results and the theoretical model is plotted in Figure 5.4 that shows that shows an excellent agreement between the numerical and theoretically calculated burst frequencies. Further, we have validated the CFD model in our previous study on the flow behavior in super hydrophilic capillaries using our pervious experimental investigations and the theoretical expression and experimental data from different studies (Chen et al., 2008; Glière & Delattre, 2006; He et al., 2009). The details of the validation can be found in Tables 1 and 2 and Figure 4.3 in the previous chapter.

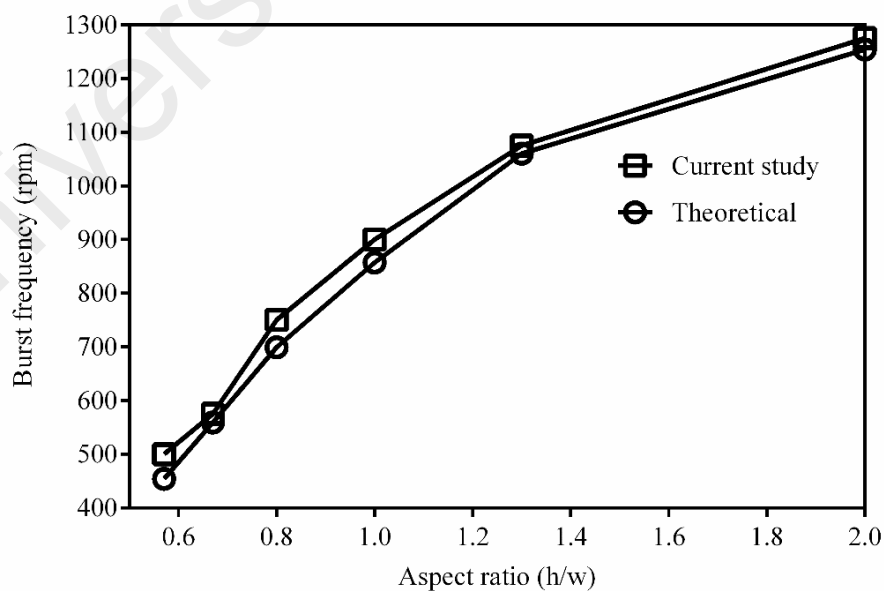


Figure 5.4: Comparison between numerical data and theoretical expression from Chen et al. (2008).

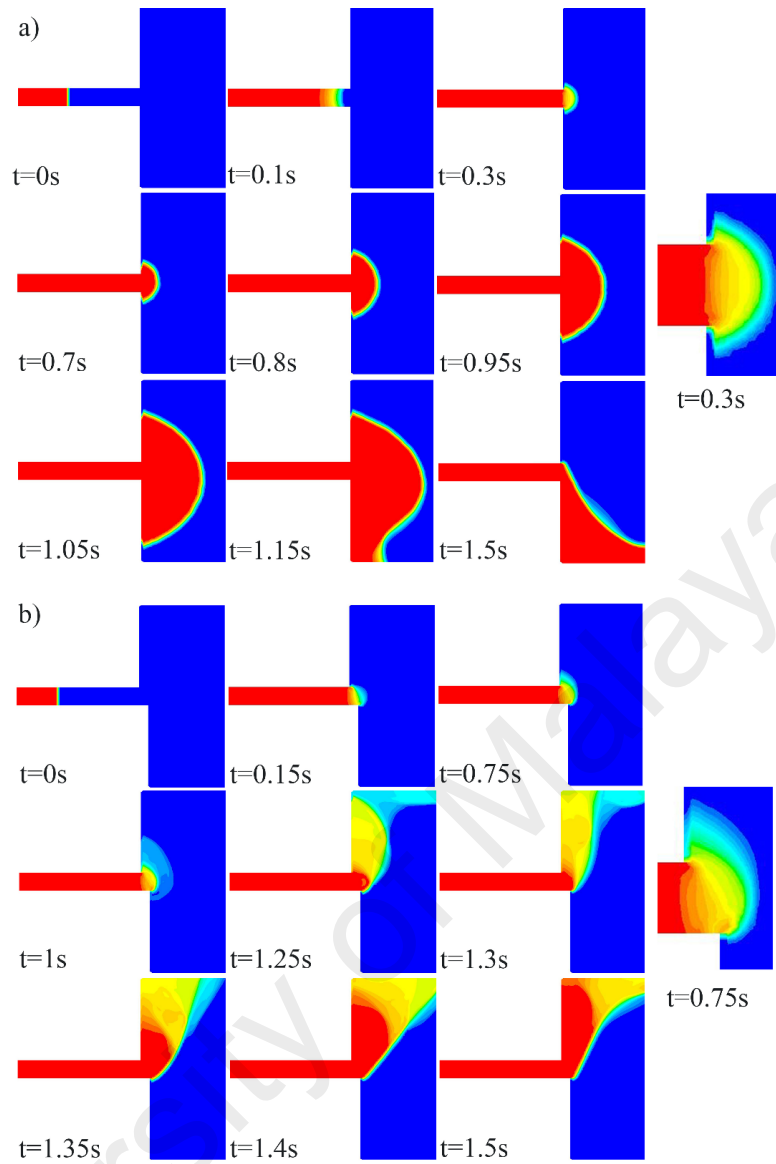


Figure 5.5: Sequences of the liquid motion and meniscus propagation in a) conventional and b) GV ($G=50\mu\text{m}$).

Table 5.2: Comparison between the numerical and experimental burst frequencies of the conventional capillary valves and GVs on the disc.

\hat{f} (mm)	σ_{la} (N/m)	θ (°)	width (μm)	height (μm)	G (μm)	Exp. burst rpm	Num. burst rpm
45	0.072	77	400	200	0	350-370	350-400
45	0.072	77	400	200	100	280-320	300-325
45	0.072	77	400	200	200	240-260	225-275

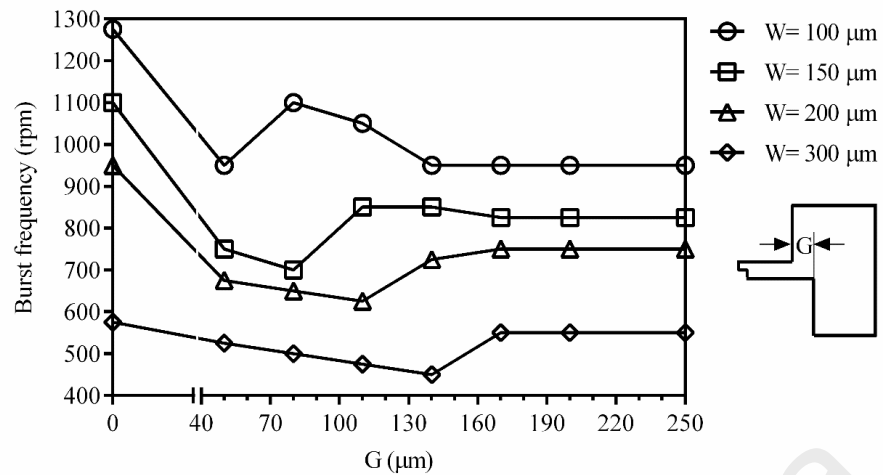


Figure 5.6: The distribution of burst frequencies for different capillary heights and various G s between 0 and 50 μm .

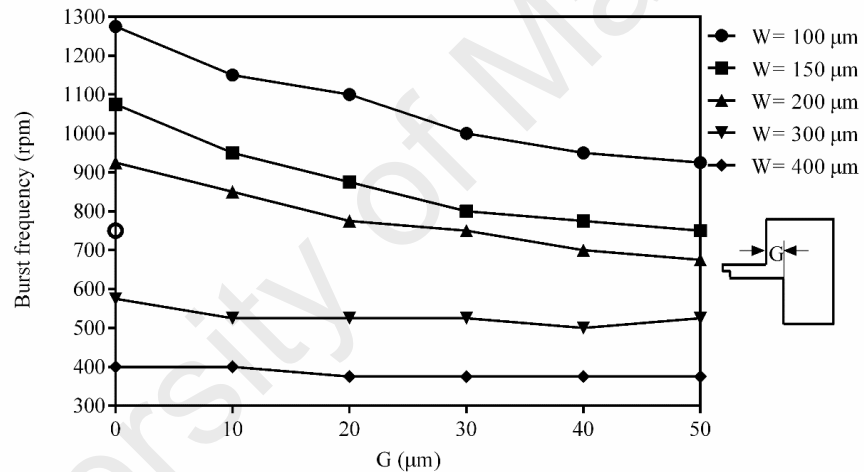


Figure 5.7: The distribution of burst frequencies for different capillary heights and various G s between 50 and 250 μm , for a constant capillary height (200 μm) and contact angle (68°).

5.6.2 Fluid motion

The numerical simulations demonstrate that GV successfully changes the flow direction of di water and biological buffer for various capillary dimensions. It shows that the liquid flows along the posterior wall and bursts in the direction of disc rotation at a lower rotational frequency. The liquid flows in the direction opposite to that of disc rotation with the sudden increase of rotational frequency. The minimum rotational frequency that changes the direction of the liquid flow is dependent on the G value such

that a longer G increases the required rotational frequency for switching flow direction. On average, an increase of 150-400rpm is required to change the flow direction in GVs with G values approaching half of the capillary width.

The gating effect on flow behavior was numerically simulated for a wide range of capillary width of 100 μm to 400 μm . The liquid motion in all capillaries is similar to the experimental observation shown in Figure 5.2. Figure 5.5 illustrates the top view of liquid motion in GV and a conventional capillary valve of 100 μm wide. In the figure the red color demonstrates the water and blue the air, the density of the color shows the volume fraction of each phase. As the centrifugal pressure overcomes the capillary pressure barrier, the liquid begins to burst into the outlet chamber. Thereafter, the liquid flow in conventional valve is different than that in GV. Figure 5.5 (a) shows that in the conventional valves liquid flow is advancing equally and by increasing the rotational frequency it is inclined into opposite direction of the rotational frequency under the influence of Coriolis force. The liquid bursts into the left side of the outlet chamber when rotational frequency is increased to 1050rpm. Further details of the liquid motion in the conventional valves can be found in in the pervious chapter. Figure 5.5 (b) shows that in GV the liquid is gated in the direction of rotational frequency due to slanted shape of the meniscus (see the inset in Figure 5.5 (b)). The advancing gated liquid eventually draws entire liquid from the inlet chamber to the outlet chamber in the direction of the rotational frequency. Note that, at $t=0.1s$ and earlier the meniscus has a concave shape due to the hydrophilic surface of the microchannel in both conventional and GVs; at $t=0.3s$ the point where the advancing liquid meniscus is trapped at the very end of the capillary channel due to the capillary pressure barrier; after the valve bursts the liquid motion in GV is different than in the conventional valve.

The liquid bursts into the right side of the outlet chamber when the rotational frequency is 775 rpm (~26% less than the conventional valve). The effect of G on the

burst frequency is discussed in below. The numerical study was repeated for various capillary dimensions and different fluids and the results show a similar fluid motion. For negligible value of G compared to capillary width (i.e., $20\mu\text{m}$ vs $350\mu\text{m}$) however, the liquid motion in a GV is more alike the conventional valves. The meniscus shape for minor G s is slightly inclined to the posterior expansion wall but the inclination is not enough for gating the liquid. In order to accomplish gating, G must be large enough to cause the meniscus to burst at the posterior expansion wall. The experimental and numerical data show that the critical value of G that enables liquid gating is when gating parameter approaches half of the hydraulic diameter of the capillaries.

5.6.3 Burst frequency in GVs

Introducing the gating ratio i.e., α that is the ratio of G to the hydraulic diameter D_h assists in comprehending the flow behavior in GVs. Burst frequencies of $0 < \alpha < 0.37$ that represents G s less than $50\mu\text{m}$ for the capillary width of $100\mu\text{m}$ to $400\mu\text{m}$ are studied with a constant capillary depth of $200\mu\text{m}$. Figure 5.6 shows that Gate Valving decreases the burst frequency, especially in narrow capillaries e.g., capillary width 100 and $150\mu\text{m}$ where a small gating ratio, e.g., $\alpha = 0.11$ is reducing the burst frequency up to 200rpm . For such gating ratio the burst frequency is decreased from 1275rpm to 1125rpm and from 1075rpm to 875rpm for capillary width of $100\mu\text{m}$ and $150\mu\text{m}$, respectively. The difference in burst frequencies between the conventional and GVs of such capillaries increases with the decrease of the gating ratio α . The maximum difference between burst frequencies in the conventional and gated capillaries for the capillary width of $100\mu\text{m}$ is about 350rpm at G of $50\mu\text{m}$. Note that the geometrical structure and the effective aspect ratio of the capillary valve change at the expansion (see the width w and effective width w_{eff} of the capillary in Figure 5.1 (c)) as a result of change in G . Also, there will be a gradient between the advancing contact angles on the posterior and the anterior wall which increases with the increase of G . The effect of capillary dimensions

(aspect ratio), the contact angle, and the expansion angle on the burst frequency of the capillary valves has been studied extensively (Chen et al., 2008; Glière & Delattre, 2006; Leu & Chang, 2004a; Li et al., 2010). The meniscus curvature in GVs is similar to that of heterogeneous capillaries studied by Lu et al. (2007). In that study differences in the surface properties of capillary walls caused deviations in advancing contact angles on the bottom and on the top of the capillary walls while such difference in the gating valves is due to asymmetric expansion of the capillaries. Employing the expression proposed by Lu et al. (2007) that takes into account the effect of different advancing contact angles facilitates a realistic prediction of the burst frequencies in GVs. Utilization of the effective capillary width is suggested especially for larger G s. The results show that as the width of capillary increases, the sensitivity of the burst frequency to G decreases. For instance, for a $400\mu\text{m}$ wide capillary, the difference between burst frequencies of GV with the gating ratio of 0.11 and the conventional valve is less than 50rpm. Such a difference for a $200\mu\text{m}$ wide capillary is about 80rpm. The larger effect of G on capillaries of the smaller hydraulic diameter (narrower capillaries) is due to the larger difference between the advancing contact angles on the posterior and the anterior walls (see Figures 5.1 (a), (b)). In comparison with wider capillaries, there is a significant difference between the advancing contact angle on the posterior wall and the advancing contact angle on the anterior wall in narrow capillaries as a result of a small value of G . Scaling considerations, such as the fact that for small capillaries a larger fraction of fluid is in contact with channel walls, can also play a role. Figure 5.7 illustrates the effect of larger G ($0 < \alpha < 1.5$) on burst frequency and the flow behavior in capillaries with hydraulic diameter of $130\mu\text{m}$ to $270\mu\text{m}$. For all capillaries, burst frequency consistently decreases as the gating ratio increases, except when G has almost half of the value of capillary width i.e., $0.37 < \alpha < 0.57$ for capillaries studied. The results show a minimum burst frequency when the gating ratio approaches half of the

capillary hydraulic diameter. For instance, the burst frequency drops from 950rpm to 650rpm for capillary width of $200\mu\text{m}$ at $G\sim 100\mu\text{m}$ and from 1275rpm to 950rpm at $G\sim 50\mu\text{m}$ for a capillary width of $200\mu\text{m}$. Next to a sudden increase of the burst frequencies at $0.37 < \alpha < 0.57$, a stable burst frequency is seen for all capillaries. The sudden increase is due to the effect of aspect ratio (height/width of capillaries) of the capillary on burst frequencies (Chen et al., 2008; Kazemzadeh et al., 2013). The reduction in burst frequency seen in Figure 5.7 is similar to our experimental observations of capillaries with different aspect ratios and those found in references (Chen et al., 2008; Li et al., 2010). The figure shows that the sensitivity of burst frequency to the aspect ratio is reduced with the increase of aspect ratio, which is in agreement with observations by other researchers (Chen et al., 2008; Cho et al., 2007a; Li et al., 2010).

5.6.4 Flow switch

In the previously introduced technique of Coriolis flow switching on rotational platforms, the liquid stream flows radially outward as it reaches T-shape junction for discs spinning at low rotational frequencies (Brenner et al., 2005; Haeberle et al., 2006). As the rotational frequency is increased, the flow rate is increased as well and the Coriolis force becomes large enough to affect the flow direction at the T-junction. Brenner et al. (2003) have shown that by changing the direction of the disc rotation (e.g., c.w to c.c.w) it is possible to direct liquid to the either side of a T-shape junction. To avoid stopping the platform a more recent technique proposed by Kong & Salin (2011) employs compressed air to switch the flow direction. However, the technique has enabled switching the flow at low of rotational frequencies and without changing the direction of disc rotation it may introduce more cost and complexity and causes contamination to the system. We suggest using GVs to direct the liquid flow, after the valve bursts, against the typical liquid flow direction prompted by the Coriolis force.

GV is able to direct entire liquid in the direction opposite to that of Coriolis force at low rotational velocities and in the direction of Coriolis force at high rotational velocities. In comparison with the previously introduced methods, GV successfully directs entire liquid in the desired direction without the need to change the direction of disc rotation or employment of external power sources.

Figure 5.8 shows partial top view of the liquid motion on clockwise rotating disc consisted of capillaries of width $200\mu\text{m}$ (connects the blue dyed chamber to the main channel), $400\mu\text{m}$ (connects the red dyed chamber to the main channel) and $700\mu\text{m}$ (connects the distributions chamber to outlets). In order to explicitly show the performance of the new valve a microfluidic network consisted of two inlet chambers and capillaries, which connect the inlet and the destination chambers to the distribution chamber, are designed and fabricated. The red (primary) and the blue (secondary) dyed di water are filled into the primary and secondary inlet chambers. The capillaries have different dimensions in order to further increase the difference between the burst frequencies of the red and the blue dyed liquids. The smaller capillary has the width of $200\mu\text{m}$ and the height of $100\mu\text{m}$, whereas the larger capillary has the width of $400\mu\text{m}$ and the height of $300\mu\text{m}$. Figure 5.8 (a) shows that the primary liquid stops at the anterior expansion wall due to the capillary pressure barrier while the secondary liquid is still pinned at the capillary due to the difference in radial position of two inlet chambers and the capillary dimensions and the air trapped. The rotational frequency is gradually increased in order to overcome the pressure barrier and direct the primary liquid toward the desired direction. The red dyed liquid bursts at approximately 310rpm and gated into the direction of the disc rotation (Figures 5.8 (b), (c)). The spinning speed is gradually increased further until the entire liquid is displaced to the destination chamber. Thereafter, the rotational frequency is increased to 1300rpm and the Coriolis force overcomes the effect of geometrical structure of GV and the flow reverts to move

against the disc rotation (i.e. in the direction of the Coriolis force). Figure 5.8 (d) shows that the secondary liquid travels to the destination chamber at 1300rpm. Figures 5.8 (e), (f) show that the entire liquid is transferred into the destination chamber. The liquid retention ability of GVs similarly to conventional capillary valves depends on the valve geometry, surface properties and surface energy of the liquids. The liquids mentioned in the methodology section (such as BSA blocking buffer, washing solution, and di water-ethanol mixture) are employed to investigate the variation in liquid properties and as well as effects of protein adsorption on the valving mechanism. Protein adsorption onto PMMA reduces the hydrophobicity of the capillary valves which can cause failure of capillary valves (He et al., 2009). Table 5.3 lists the burst and switching frequencies of different liquids when GV is operated in the regime when the listed fluids are dispensed sequentially. The results demonstrate that the burst frequencies of di water-ethanol mixture are increased with the decrease of volumetric percentage of ethanol. The reduction of the burst frequency is due to the decrease in surface energy of the mixture. The burst frequencies of mixtures of di water-ethanol vary from 250 to 120rpm for volumetric ethanol concentration of 5% to 45% while the increase of rotational speed to 450rpm reverses the flow direction. The repeated experiments yielded a small variation in switching frequencies – around 20rpm. When the blocking buffer BSA is used, the adsorption of the proteins from the solution onto the plastic surface reduces subsequent burst frequency of the valve. For example, for a 400 μ m wide capillary valve, the initial burst frequency for blocking BSA buffer is about 230rpm and for the sequentially released washing solution it is about 270rpm. Repetition of the experiments (up to six times) in the same capillary evidences the reduction of the burst frequencies of the blocking buffer and washing solution to 170rpm and 210rpm, respectively.

Note that only the burst frequency of the primary liquid is dependent on G . The switching frequency (i.e., burst frequency of the secondary liquid) remains essentially

unchanged since the vent holes of the secondary inlet chamber are sealed. Sealing the vent holes of the secondary inlet leads to the retention of the secondary liquid until the complete exit of the primary liquid. The burst frequency of the secondary liquid (switching frequency) is thus independent from the capillary properties and the secondary liquid will be able to travel only when all of the liquid leaves the GV and the air trapped between the secondary chamber and outlet is removed.

Table 5.3: Burst and switching frequencies of different liquids before and after protein adsorption.

Liquid	\hat{f}_1	\hat{f}_2	σ_{la}	W_1	W_2	H	Burst (rpm)		Switch (rpm)	
							B.P.A, A.P.A		B.P.A, A.P.A	
di water-ethanol (5%-45%)	45	28	0.072 0.028	200	400	200	120-250, 80-220	390-450, 370-450		
0.9% sodium chloride	45	28	200	400	200	260-230		450-430	
Blocking buffer	45	28	200	400	200	230, 170		880, 850	
Washing solution	45	28	200	400	200	250, 210		870, 850	

*B.P.A, A.P.A: before and after protein adsorption

For the centrifugal microfluidic platforms containing capillary valves that are affected by the adsorption of the proteins onto to the plastic substrate, it is advisable to use fish-bone valves or implement surface treatments designed to create a super hydrophobic valve surfaces where the contact angle is less affected by the protein adsorption as evidenced by published studies (He et al., 2009; Lu et al., 2007). In complex biological assays routing a discrete liquid volume to designated channels/chambers is a common task e.g., in preparative protocols where different solutions e.g., wash, sample, etc. have to be directed to the waste or a receiving chamber after passing a common stationary phase (Beebe et al., 2002; Gorkin et al., 2010; Oh & Ahn, 2006). In the centrifugal microfluidics the proposed flow switch technique allows for switching the flow direction instantaneously from the direction of disc rotation to the opposite by the abrupt increase of the rotational speed. It can be employed to separate different substances existing in a common chamber (i.e., previously disintegrated such as RBC from plasma) to a particular destination channel/chamber. In addition, it has the

potential to be employed for mixing large macroscopic volume of liquids by splitting and recombining the liquids.

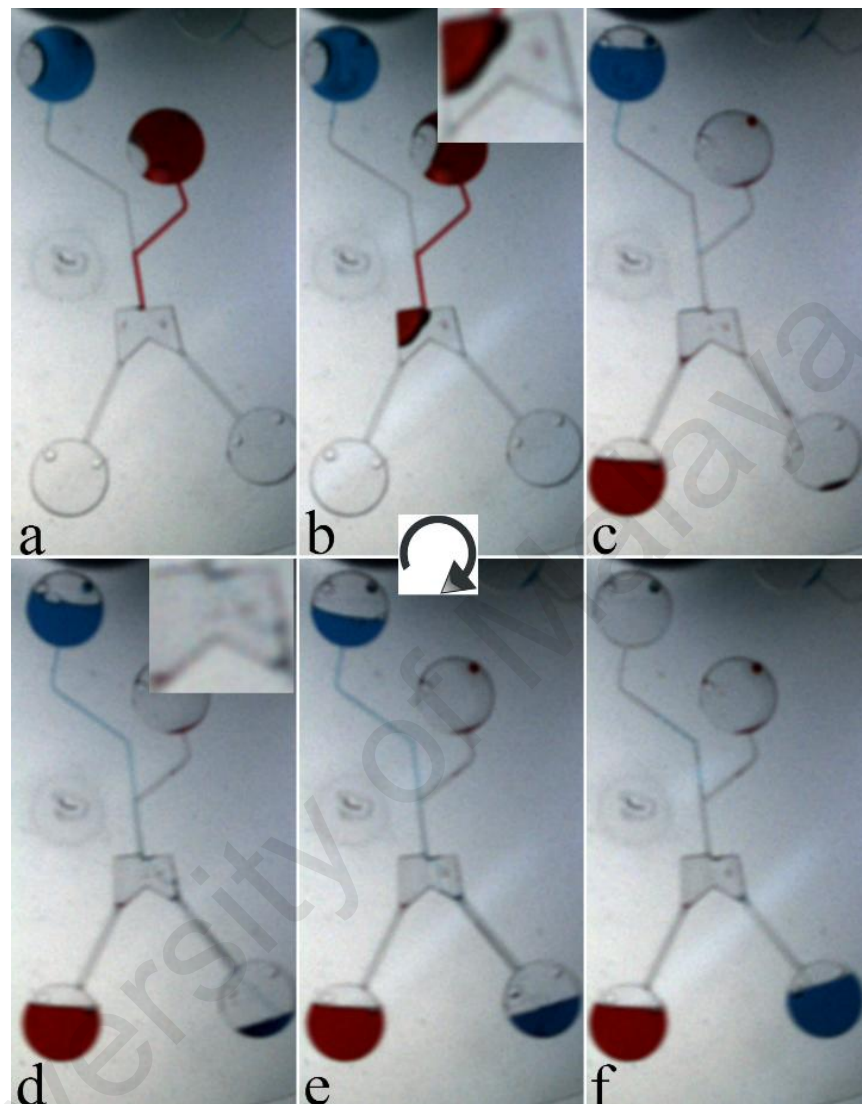


Figure 5.8: Switching the flow direction by increasing the rotational speed.

5.7 Summary

Gating valve as a powerful means to control flow direction at the T-junction has been introduced to control and manipulate flow in microfluidic systems. In comparison with the previously introduced techniques of flow, switching Gate Valve enables switching the flow direction without employing external power sources, applying surface treatments or changing the direction of disc rotation. It directs entire liquid in the direction opposite to that of Coriolis force at low rotational velocities and in the

direction of Coriolis force at high rotational velocities. It allows for multiplexed and more sophisticated assays on the centrifugal microfluidic platforms without interrupting other operations. The effect of gating parameter on flow behavior and burst frequency in the CD-like microfluidics has been studied experimentally and numerically. The results show that GV changes the flow direction when the gating parameter G is approximately half of the capillary width (0.4-0.5 width). The results show that as the gating parameter approaches to half of the channel width the burst frequency rapidly decreases however the rate of decrement decrease significantly for the gating parameter values greater than half of the capillary width.

University of Malaya

CHAPTER 6: DESIGN OF GUIDED ROUTING VALVE, A MICROVALVE FOR FLOW SWITCH AND ROUTING

6.1 Introduction

The flow switch has been a really tough problem for centrifugal microfluidics. The centrifugal microfluidics often encounter switching of the liquid flow between two or more pathways in order to separately direct them to different chambers e.g., where a specimen such as DNA, protein and or antigen has to be discharged into a clean buffer solution. In general, the centrifugal and the fictitious Coriolis force have been often used to determine the flow direction in microchannels and at T-junctions. Several methods have been introduced for propelling liquid against both the centrifugal force (Abi-Samra et al., 2011a; Aeinehvand et al., 2014; Kinahan et al., 2014; Madou et al., 2006; Siegrist et al., 2010b; Soroori et al., 2013) and the Coriolis force (Brenner et al., 2003; Kazemzadeh et al., 2014; Kim et al., 2008; Kong & Salin, 2011). The Coriolis force determines the movement of a liquid when it reaches a T-junction i.e., a point where a channel splits into two channels. By exploiting the Coriolis force (Brenner et al., 2003), fluid at a T-junction can be switched to flow in either one of the channels or through both exit channels simultaneously (at low rotational frequencies). The flow switch in this method is based on the direction of the Coriolis force at high rotational frequencies that is dependent on the direction of the disc rotation; the reversal of the direction of rotation is needed to change the flow direction at T-junctions. A liquid can also be routed first into one branching channel and then into a different branching channel when asymmetrical channels and chamber geometries are used. When the liquid filling a first chamber rises to a level that prevents the connection of the air in the branching channel with the vent hole in the first reservoir, the fluid in the main channel will be routed to a second reservoir (Kim et al., 2008). Because the flow switch is based on the air trapped in the system, it is incapable of switching the flow direction between

exit channels more than once. More recently, an active flow switch method employing a periodically activated air supply was proposed to allow changing the flow direction without altering the direction of disc rotation (Kong & Salin, 2011). In the previous chapter, an attempt has been made into solving this problem. We showed that by performing small geometrical changes in the structure of capillary valves we could devise a novel asymmetric valve. The asymmetric valve, named gate valve, showed for the first time, that geometrical changes allow for switching the flow direction by altering the disc rotational frequency virtually without occupying any space on the valuable disc's real estate. However, the valve can be less suitable when a continuous switching of the flow direction is required.

In this chapter we describe a novel frequency depended approach to route liquids and control the flow direction on a spinning disc that employs a robust guiding microstructure. It allows for routing sample and reagents to designated reservoirs at a given flow rate, to a given flow direction and subsequently to a selection of receiving reservoirs. With this routing method, we will be able to switch the flow direction instantaneously from the direction along the disc rotation to the opposite direction by immediate increasing of the rotational speed and switch the liquid flow back to its previous direction by reduction of the spinning speed. In addition, this novel method, by performing some enhancements, has a high potential to be used for sorting particles and cells in the micro channels or in the reservoirs on the centrifugal microfluidic platforms. The distinctive feature that makes this approach different from other types of passive capillary valves is the robust control of liquid movement by employing two adjustable sequential burst valves called a primary valve and a secondary burst valve. In this chapter flow routing by the proposed technique will be studied theoretically and experimentally, and the flow behavior will be numerically investigated. The performance of the novel valve will be experimentally demonstrated for a wide range of

capillary sizes and for liquids with different properties. The results of the introduction and characterization of this novel valve have been published in the esteemed technical peer-reviewed journal of RSC advances (Kazemzadeh et al., 2015).

6.2 Concept

Capillary valves on a LabDisc prevent liquid from flowing as long as the rotational speed (rpm) is below an rpm corresponding to a critical burst frequency, above that critical rpm the flow rate and direction is based on the magnitude of the centrifugal and Coriolis forces. In order to improve the control over flow direction on a LabDisc we introduce a new technique that does not require changing the spinning direction of the platform, applying surface treatments and/or employing external forces. This new passive flow control technique we call guided routing (GR) relies on a two stage valve comprised of (i) an auxiliary inlet which is a recess that overlaps the capillary and the chamber it feeds into and (ii) a bent auxiliary outlet which is an extension of the auxiliary inlet recess leading into the chamber as seen in Figure 6.1. The first capillary valve that advancing fluid encounters is located at the junction of the capillary and the recessed auxiliary inlet and that valve will burst when the rotational frequency of the disc exceeds a primary burst frequency (ω_p). The second capillary valve is formed at the junction of the recessed auxiliary outlet and the chamber and it will burst when the rotational speed of the disc exceeds a secondary burst frequency (ω_s). By adjusting the spinning frequency of the disc after the primary burst frequency has been breached one can control the direction of the secondary burst that occurs when liquid flows into the chamber through the auxiliary outlet. When ω_p is smaller than ω_s the fluid meniscus remains pinned at the auxiliary inlet/chamber interface while the fluid can advance in the auxiliary outlet and be guided by the bend of that outlet. When ω_p is larger than ω_s or when the angular velocity exceeds both ω_p and ω_s the fluid will not stop at the auxiliary inlet/chamber interface and will flow into the chamber. The materials selection

and geometries of the chamber and channels of the described fluidic network determine the relative relationship between the primary and the secondary burst frequencies. Figure 6.1 illustrates the mechanism of GR in controlling the direction of flow in centrifugal microfluidic platforms. The flow behavior in GR capillaries with different geometries corresponding to a wide range of rotational frequencies is investigated and discussed in the Results section below. In a GR valve the liquid flow is controlled by confining the liquid stream temporarily into a specifically designed guided routing (GR) structure which is comprised of two sections: an (i) auxiliary inlet and (ii) auxiliary outlet; In panel a) and b) (Top view and Side view) we show a traditional capillary valve on a centrifugal microfluidic platform that, in panel a) rotates clockwise with a spinning speed (ω) below its burst frequency (ω_p) and the liquid is pinned at the interface, in panel b) as the platform rotates at a spinning speed above the burst frequency (where the Coriolis force is the predominant force), the liquid flows towards the Coriolis force. Panel c) to e) illustrate what happens in the case of a GR valve again with the platform rotating clockwise. In panel c) the spinning speed is below the primary frequency ($\omega < \omega_p$) and the liquid is pinned at the auxiliary inlet; in panel d) the platform rotates at a spinning speed above the secondary burst frequency and below or equal to the primary burst frequency and the liquid is guided by the auxiliary outlet and in panel e) the liquid is routed towards the direction of the Coriolis force in two manner: a) spinning the platform with a speed above the primary burst frequency if ω_p is larger or equal to the ω_s , b) spinning the platform with a speed above the secondary burst frequency if ω_s is larger or equal to the ω_s .

6.3 Fabrication and Experimental setup

The centrifugal microfluidic platforms with the GR valves were fabricated using a Computer Numerical Control (CNC) machine i.e., model VISION 2525, by Vision Engraving and Routing Systems, USA.

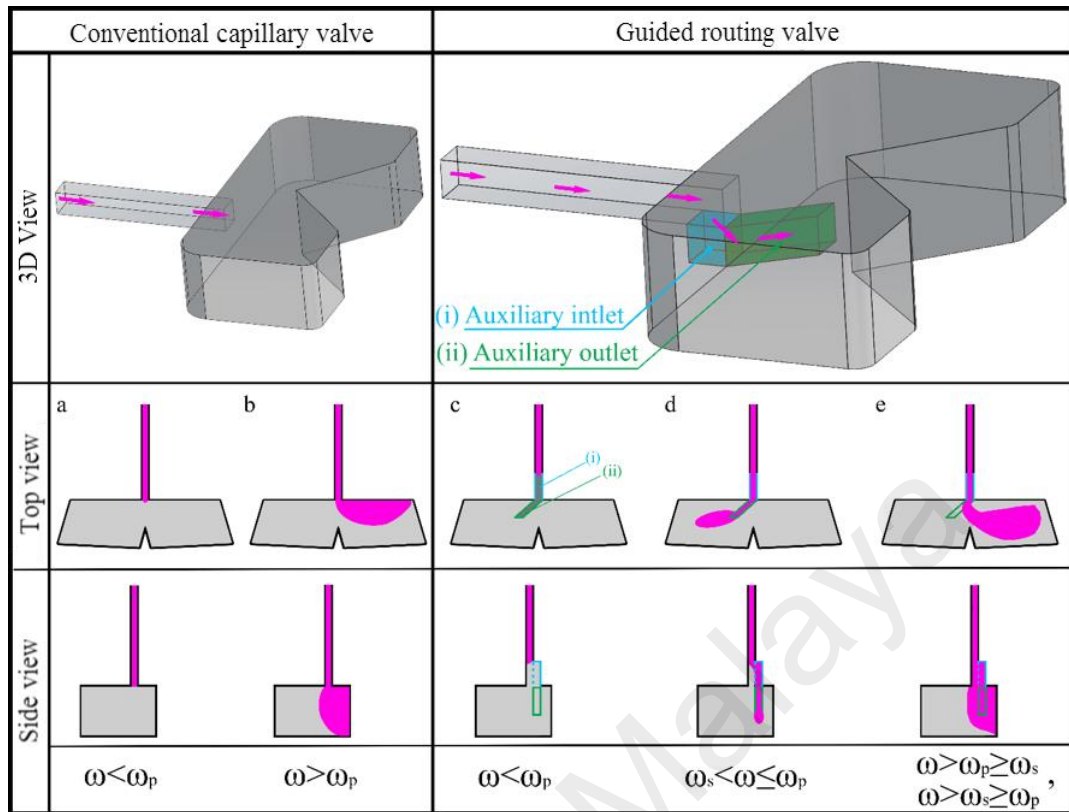


Figure 6.1: A sketch of 3D view, top and side views of a conventional capillary and a GR valve. Fabrication and Experimental setup.

Microstructures were milled in three 2mm thick Polymethyl methacrylate (PMMA) layers that were bonded together with two 0.056mm thick Pressure Sensitive Adhesive (PSA) layers (by FLEXcon, USA). Figure 6.3 shows an exploded view of the thus assembled five-layer CD-like device used in the current study. The first substrate containing vent holes is bonded to the middle substrate, which contains microchannels, inlet and outlet chambers. The guided routing valves are milled on the lowest layer and bonded to the middle substrate layer. The microstructures formed in the PSA layers conforming to the designs in the PMMA layer are cut by a cutter plotter i.e., model PUMA II, by GCC, Taiwan.

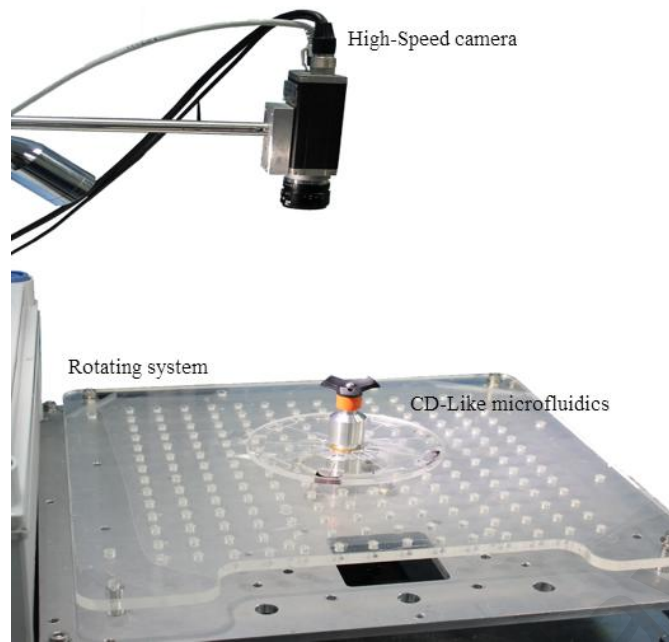


Figure 6.2: The custom-made experimental setup.

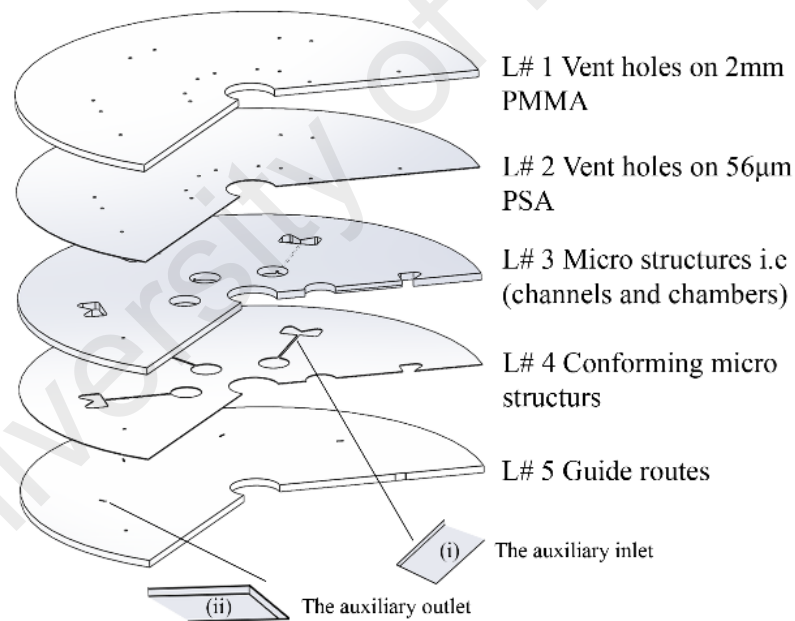


Figure 6.3: An exploded view of the disc assembly, Guided routing valves (GR) are located on layer fourth and fifth of the assembled disc.

6.4 Theory

Apart from the use of hydrophobic patches, liquid routing in most passive techniques depends on the direction of the disc rotation and the ratio of the centrifugal to the

Coriolis force. In addition to these parameters, Kazemzadeh et al. (2014) have shown the effect of an asymmetric expansion of a capillary channel on the liquid flow direction and on the performance of the capillary valves. The present technique relies on a balance between the centrifugal and Coriolis forces and the distinctive capillary pressures at the GR valve. The valving technique benefits from two adjustable sequential bursts; a primary and secondary burst occurring at the auxiliary inlet and the auxiliary outlet, respectively. The body forces applied to fluidic elements on a rotating reference frame include the sum of total pressure and viscous forces (see Figure 6.4). For a non-inertial, incompressible system the Navier-Stokes equations are (Acheson, 1990):

$$\sum F_x = ma_x = -F_{co} + \mu \left(\frac{\partial^2 v_x}{\partial x^2} + \frac{\partial^2 v_x}{\partial y^2} + \frac{\partial^2 v_x}{\partial z^2} \right) = \rho \left(\frac{\partial v_x}{\partial t} + v_x \frac{\partial v_x}{\partial x} + v_y \frac{\partial v_x}{\partial y} + v_z \frac{\partial v_x}{\partial z} \right) \quad [24-a]$$

a]

$$\sum F_z = ma_z = -F_{\omega} + \mu \left(\frac{\partial^2 v_z}{\partial x^2} + \frac{\partial^2 v_z}{\partial y^2} + \frac{\partial^2 v_z}{\partial z^2} \right) = \rho \left(\frac{\partial v_z}{\partial t} + v_x \frac{\partial v_z}{\partial x} + v_y \frac{\partial v_z}{\partial y} + v_z \frac{\partial v_z}{\partial z} \right) \quad [24-b]$$

Where ρ , $a_{x, z}$, μ , and $v_{x, z}$ are density, acceleration in the x and z directions, viscosity and velocity in the x and z directions, respectively. The forces per unit volume in x and z direction are due to the vector product of Coriolis and centrifugal accelerations, respectively. The centrifugal force per unit volume is given as:

$$F_{\omega} = \frac{\rho \omega^2}{\Delta r} \int_{r_1}^{r_2} r dr = \frac{\rho \omega^2}{2 \Delta r} (r_2^2 - r_1^2) = \frac{\rho \omega^2}{2 \Delta r} (r_2 - r_1)(r_2 + r_1) = \rho \omega^2 \bar{r} \quad [25]$$

$$\bar{r} = \frac{r_1 + r_2}{2}$$

Where ω is the spinning frequency of the disc, r_1 and r_2 are the inner and outer radial position of a liquid plug, and \bar{r} is the mean radial position of the liquid, respectively. The primary burst frequency of a GR valve, similar to the burst frequency of a regular

capillary valve, can be obtained from the Young-Laplace equation. However, the specific geometry of a GR valve features two contact angles (θ_1 on the bottom surface and θ_2 on the top surface of the valve structure) that change dynamically as a function of the length of the auxiliary inlet and the centrifugal pressure (see Figure 6.4 (a)). In order to cause the liquid to flow in the auxiliary inlet before it reaches the expansion, the advancing contact angle of the bulged meniscus θ_2 must be higher than $\theta_1 - 90^\circ$. The optimum value of θ_2 is when the length of the auxiliary inlet λ_i is equal to the channel height which is when $\theta_2 = \theta_1 + 90^\circ$. In these circumstances, the liquid will flow into the auxiliary inlet instead of flowing along the top surface of it and will avoid the unfavorable valve burst which occurs when the liquid continues to flow along the top surface of the auxiliary outlet (when $\theta_2 > \theta_1 - 90^\circ$). Figure 6.5 demonstrates that when $\lambda_i = h$ the primary burst pressure can be predicted based on the cross-sectional height of the GR valve (ρ):

$$\Delta P_b = 2\sigma_{la} \left(\frac{\cos(\theta + \beta)}{h_e} + \frac{\cos\theta}{w} \right) \quad [26]$$

Where, σ_{la} , θ , β , w and h_e are liquid surface tension, the contact angle, the channel width and the expansion angle and effective height of the channel (see Figure 6.5 (a)). It can be gleaned from Figure 6.5 (b) that the secondary burst in a GR valve occurs when the liquid is released from the recessed area of the auxiliary outlet and can be calculated from equations presented earlier in other studies (Chen et al., 2008; Cho et al., 2007a). In order to determine the flow direction based on the spinning frequency of the disk the maximum radial velocity is required to determine the dominant force acting on the liquid at the GR junction. The maximum radial velocity is solved by writing the Navier-Stokes equation in the plane parallel to the disc surface. Typically, the gravitational force is significantly smaller than other forces on a spinning disc and thus can be ignored. We also assume fluid of constant density and since the walls are impermeable,

the liquid is confined to flow in the z direction and there are no changes of the fluid velocity except in the direction of the flow:

$$-\rho\omega^2\bar{r} + \mu\left(\frac{\partial^2 v_z}{\partial x^2} + \frac{\partial^2 v_z}{\partial z^2}\right) = \rho\left(v_z \frac{\partial v_z}{\partial z}\right) \quad [27]$$

Now, considering that the flow is fully developed, the velocity of the fluid in the direction of the flow is constant:

$$-\rho\omega^2\bar{r} + \mu\left(\frac{\partial^2 v_z}{\partial x^2}\right) = 0 \rightarrow v_z = \rho\omega^2\bar{r} \frac{1}{2\mu} x^2 + C_1x + C_2 \quad [28]$$

Due to no-slip at the wall, $v_z=0$ at $x=0$ and $x=w$:

$$v_z = \rho\omega^2\bar{r} \frac{1}{2\mu} x(x-w) \quad [29]$$

The maximum velocity is at $x=0.5w$ and it is equal to:

$$v_z = \frac{\rho\omega^2\bar{r}}{8\mu} w^2 \quad [30]$$

The ratio of Coriolis to centrifugal force is then given by:

$$\frac{F_{co}}{F_{\omega}} = \frac{\rho\omega w^2}{4\mu} \quad [31]$$

The liquid flows in the direction of the Coriolis force if $\frac{F_{co}}{F_{\omega}} \gg 1$ (Brenner et al., 2003), therefore increasing the spinning frequency to meet that condition makes it possible for the liquid to flow in the direction of the Coriolis force without having to reverse the spinning direction of the disc. In addition, the Euler force $F_{Eu} = -\rho\alpha \times r$ assists in instantaneous switching of the flow direction from the direction of the auxiliary outlet to the opposite direction when $\frac{F_{Eu}}{F_{\omega}} \gg 1$.

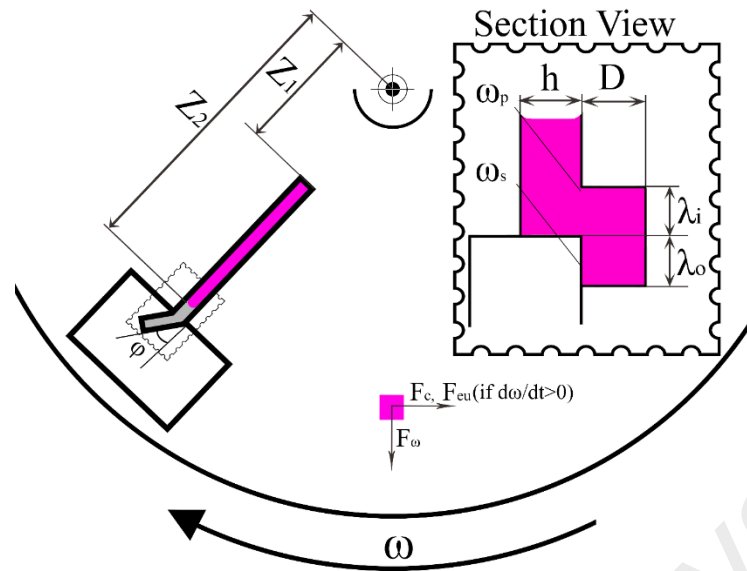


Figure 6.4: Partial view of a disc spinning at ω containing GR valve of the auxiliary inlet and outlet length of λ_i and λ_o respectively, a liquid plug exposed to radial centrifugal and transversal Coriolis force.

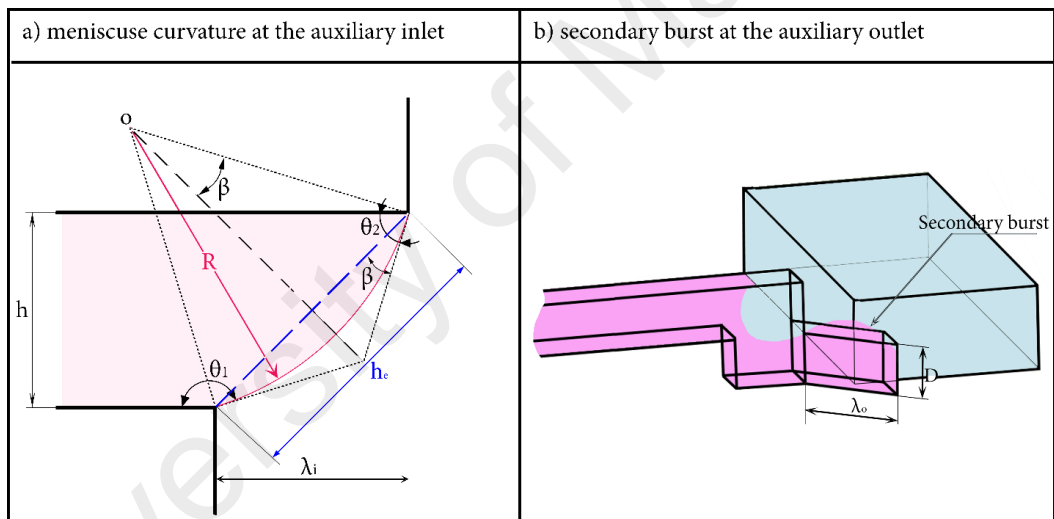


Figure 6.5: The burst frequencies of GR valve a) primary burst occurring at the auxiliary inlet when λ_i is equal to the microchannel height, b) secondary burst at the auxiliary outlet.

6.5 Numerical analysis

The volume of fluid (VOF) method from the commercial ANSYS-Fluent CFD package, version 13.1 was used to simulate the flow behavior within the fluidic network under study. The details of the method and formulations of the numerical analysis are given in the previous chapter. Briefly, the computational domain was set to rotate clockwise with an initial rotational frequency of 50rpm, which was increased in steps of 50rpm. Zero fluid velocity is set at all the walls of the microstructures (in accordance

with the no-slip boundary condition). In order to consider the effects of surface tension, centrifugal and Coriolis forces the body-force-weighted interpolation scheme was used in the numerical calculation. The scaled residuals were set at 1×10^{-6} as the convergence criteria for the continuity and other governing equations. The area adjacent to the GR was simulated using a uniform quad grid and the accuracy of the simulation results was evaluated by comparing the numerical with our experimental data and theoretical analyses.

6.6 Results

6.6.1 Flow behavior

Capillary valves are typically fabricated by either a one or two-dimensional expansion in microchannels due to their ease of fabrication (see Figure 6.6). The difference between the commonly used capillaries (two-dimensional) and GR valves is that in common capillaries, the meniscus is pinned in the plane perpendicular to the disc surface holding its convex shape at the expansion point and the meniscus expands on the surfaces of the outlet chambers (for more details on conventional capillaries refer to (Cho et al., 2007a). In a GR valve, on the other hand the meniscus expands in the perpendicular plane and simultaneously advances in the parallel plane retaining its convex shape. In comparison with a conventional capillary valve, a GR valve generates an either slightly weaker or a slightly stronger blockage to the flow depending on the capillary width (i.e., due to the effect of channel aspect ratio on the burst pressure studied in references (Chen et al., 2008; He et al., 2009)). However this difference can often be neglected in designing of sequential operations since the interval between the burst frequencies in sequential processes on a LabDisc is kept at about 200rpm to avoid unwanted release of samples/reagents (He et al., 2009).

Figure 6.7 shows the sequential movement of the liquid adjacent to a GR valve for a capillary of $200 \times 200 \mu\text{m}$ and GR with the auxiliary inlet and outlet of $200 \mu\text{m}$

and the outlet chamber where the rotational frequency is gradually increased to the burst frequency of the valve. The meniscus experiences a two-dimensional motion due to the geometrical condition of the capillary. The maximum distance that the meniscus is able to expand in the radial direction (x_m) before the valve bursts into the auxiliary inlet is proportional to the height of the capillary, and the radial length that the meniscus can expand before reaching the outlet chamber is proportional to the groove height and the capillary height. Figure 6.7 (a) shows that as the rotational frequency is gradually increased and liquid reaches the GR expansion the meniscus continues its radial advancement along the capillary with its initial convex shape however, the meniscus expands in the perpendicular direction to the disc surface. Figure 6.7 (b) shows the occurrence of first bursting in GR valve and Figure 6.7 (c) shows that while the liquid meniscus is pinned at the top surface of GR valve, the meniscus continues its expansion from the bottom surface and flows into the auxiliary inlet and later into the auxiliary outlet. At this point a fluctuating movement of the meniscus is observed and the portion of meniscus previously advanced is pulled back due to the advancement of the portion of meniscus previously pinned (Figures 6.7 (c), (d)). By increasing the rotational speed, the liquid will flow in the groove (Figures (e), (f)).

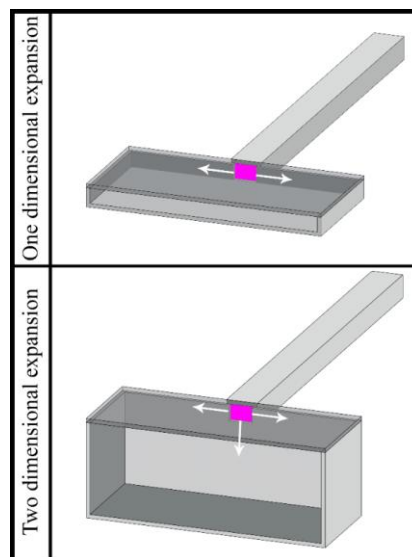


Figure 6.6: Three dimension view of the possible methods of fabricating capillary valves.

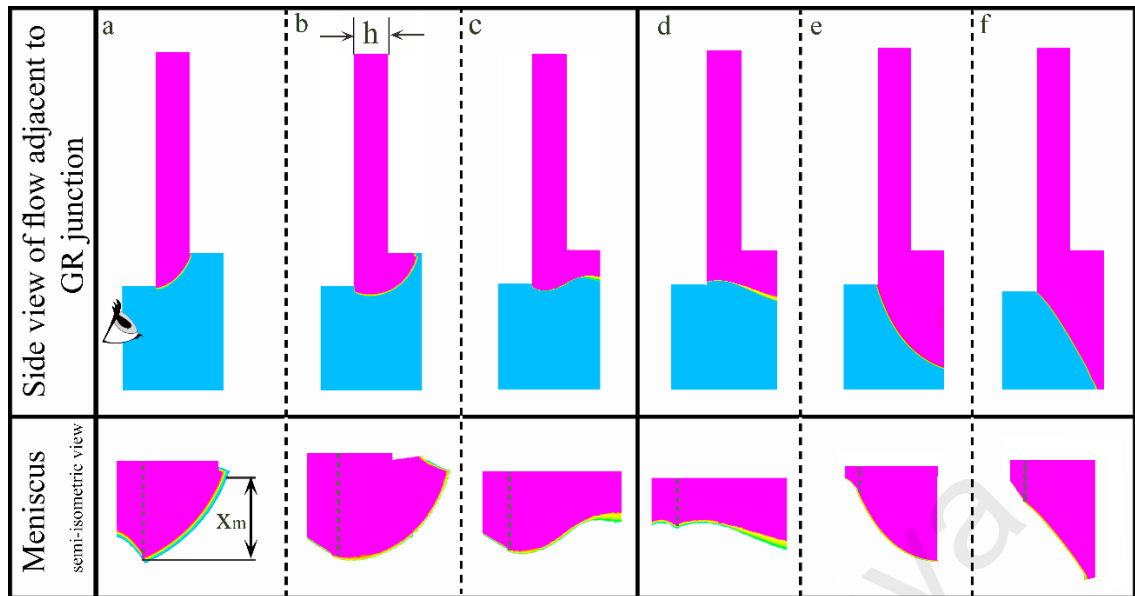


Figure 6.7: Numerically obtained sequential images of meniscus advancement in response to increasing the rotational frequency.

The mechanism of GR valve is characterized by investigating experimentally and numerically the influence of λ_i and λ_o on the burst frequency, when employing different liquids (where λ_i and λ_o are the length of the auxiliary inlet and the auxiliary outlet respectively, see Figure 6.4). The optimum length of the auxiliary inlet (λ_i) and the auxiliary outlet (λ_o) is defined by constructing several GRs with different λ_i and λ_o . The minimum λ_i and λ_o are equal to $h/2$ and are increased in a step size of 0.1mm. The effect of surface tension and protein absorbance on the GR valve operation is investigated by conducting several experiments using different liquids such as di-water, a mixture of ethanol-water and with bovine serum albumin (BSA). A comparison between burst frequencies of di-water and BSA in normal capillaries and capillaries equipped with GR is compiled in Table 6.1. The table shows the effect that λ_i and λ_o have on the burst frequency of GR valves with cross sections of $200 \times 200 \mu\text{m}$ and $400 \times 400 \mu\text{m}$. The burst frequency reduces dramatically when $x_c > h$ which can be explained by the manner in which the meniscus advances. As long as $x_c \neq h$ the meniscus advances along the top surface until it is pinned at the incline where a higher centrifugal pressure is required to continue the advance of the liquid front. The increase in the length of the groove ($x_c > h$)

facilitates a smooth advancement of the liquid meniscus on the top surface until θ_1 reaches the value of 180° and the GR valve bursts. At $x_m \approx h$, the meniscus is pinned at the top surface with the contact angle θ_2 much lower than the angle required for bursting, while at the bottom the contact angle θ_1 is at the threshold to burst.

6.6.2 Guided Routing applications

6.6.2.1 Flow switch

In many types of microfluidic functions such as separation and many other preparative protocols, separated samples, washing and elution buffers are required to be directed to the waste or other receiving chambers. Several techniques (e.g., Coriolis based strategies or hydrophobic patches) have been pursued for routing of a sequence of distinct volumes to designated vessels as a common task in preparative protocols or more specific assignments on intricate assays in LabDisc systems (Ouyang et al., 2013; Strohmeier et al., 2014). As a demonstration for one of the many possible applications, different microchannels equipped with GR valves were fabricated in order to control the flow direction on a spinning microfluidic disc that contains inlet and outlet chambers connected via a fluidic network of microchannels. The GR flow switching experiments are conducted for various sizes of microchannels, GR dimensions, and types of liquids. The height and the length of GRs vary from $0.5h$ to $2h$ where h is the height of the capillary. The width of the grooves is kept identical to the width of the corresponding capillary microchannel on the same disc. Black dyed di-water is dispensed into the inlet chamber of a GR capillary and the experiment commences by spinning the disc and gradually increasing the angular velocity in 10rpm increments until the capillary valve bursts. Figure 6.8 shows the partial top view of sequential movement of liquids in a capillary of $w=h=400\mu\text{m}$ without and with a GR valve of $\lambda_i=\lambda_o=400\mu\text{m}$ (these terms are explained in Figure 6.1). Figures 6.8 (a), (b) show the sequences of liquid movement before the first and second burst frequencies of a GR valve. The gradual increase of the

spinning frequency up to ~ 170 rpm causes the liquid to flow in the direction of the auxiliary outlet (Figures 6.8 (c), (d)). The abrupt increment in the spinning frequency (to 370rpm) causes the liquid to detour from the tip of the route channel toward the direction of the Coriolis forces (Figures 6.8 (e), (f)). At any moment after the abrupt increase in spinning frequency, a reduction of the spinning frequency to its previous value will cause the liquid to flow along the auxiliary outlet and toward its previous direction (the supporting video can be seen in the supplementary section). For the current capillary dimension and $\bar{r} = 39\text{mm}$ the flow is switched to the direction of Coriolis at $\sim 350\text{rpm}$ and in the direction of the auxiliary outlet at $\sim 170\text{rpm}$. The performance of the GR valve under continuous operation was investigated for several liquids with different physicochemical properties and the results show that the GR valve successfully guided all those liquids. The effect of protein adsorption on the PMMA surfaces, which occurs in most of the clinical assays where biological substances are used, was investigated by conducting the experiments using Bovine Albumin Solution (BSA). The consecutive loading and emptying of the same microstructure up to 5 times with 10 minutes interval between each experiment shows up to 50-60rpm reduction of the initial burst frequency. Note that the switching frequency is independent of the burst frequency of the capillary valve since the GR controls the fluid flow after bursting. The experimental observations presented in Table 6.2 confirm that the optimum length of the auxiliary inlet is when $\lambda_i = h$ and that for $\lambda_i > h$, the GR valve is unable to take control of the flow. It can be understood from the data presented in the table that a minimum value of the auxiliary outlet is equal to the height of the channel however a $\lambda_o > h$ will guarantee a consistent control on the liquid flow in the direction of the auxiliary outlet.

Table 6.1: The effect of GR on the burst frequency for different liquids for $\check{r}=39\text{mm}$

Substance	Width = Height (μm)	λ_i (mm)	λ_2 (mm)	F_b)Num. (rpm)*	F_b)Exp. (~ rpm)**
Di-Water	200	0	0	450-500	480
		0.2	0.1, 0.2, 0.3	450-500	450-460
		0.3	0.2, 0.3, 0.4	300-350	340
	400	0	0	150-200	190
		0.4	0.3, 0.4, 0.5	150-200	160-170
		0.6	0.5, 0.6, 0.7	100-150	120-130
BSA	200	0	0	400-450	410-420
		0.2	0.1, 0.2, 0.3	350-400	380
		0.3	0.2, 0.3, 0.4	250-300	300
	400	0	0	150-200	140-150
		0.4	0.4, 0.5, 0.6	100-150	110
		0.6	0.5, 0.6, 0.7	100-150	100

* The numerical rotational speed increased in steps of 50rpm, ** Values after conducting several experiments.

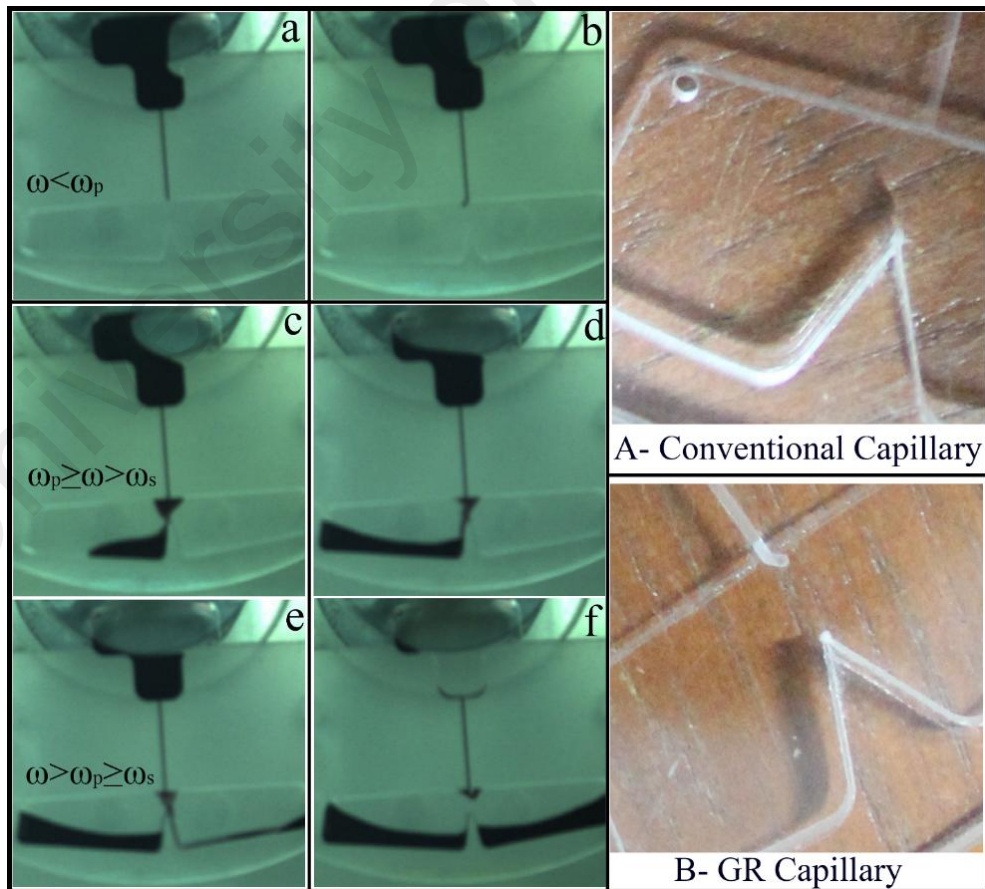


Figure 6.8: switch and switching back the flow direction in centrifugal microfluidics.

Table 6.2: The response of flow to the auxiliary inlet and outlet dimensions and experimental flow switch frequencies.

Microchannel height (μm)	λ_i (μm)	λ_o (μm)	Frequency (rpm)	C.W.	Frequency (rpm)	C.C.W.
200	>200	<200	≤ 420	*	>700	\checkmark
	~ 200	≥ 200	≤ 460	**		\checkmark
400	>400	<400	≤ 150		>370	\checkmark
	~ 400	≥ 400	≤ 170			\checkmark
700	>700	<700	≤ 110		>350	\checkmark
	~ 700	≥ 700	≤ 140			\checkmark

* x: failure to guide the liquid, ** \checkmark : Success in guiding liquid.

6.6.2.2 Fluid distribution

As a demonstration of another application of GR valving, we describe the function of a GR valve for dividing a liquid flow into several side streams with a given flow rate after the burst without applying surface treatments or employing external power sources. The capability of a GR valve in flow control and distribution of the liquid is investigated by conducting a simple experiment where the auxiliary inlet of a GR valve is connected to several outlet branches with the same dimensions engraved in the outlet chamber. Figure 6.9 shows a microfluidic structure consisting of an inlet and an outlet chamber connected by a GR capillary. The inlet chamber is loaded with red died di-water and the experiment commences by spinning the disc until the GR valve bursts. As it is gleaned from Figure 6.9 as a consequence of using a GR, after the secondary burst of the valve the liquid flows into the designated paths. This capability of a GR valve can be employed to regulate and distribute liquids with different flow rates to different directions. Figure 6.10 shows the free body diagram of a GR with two branch channels splitting at a junction. At the point where the main channel meets two branch channels the overall propelling force can be written as components of the centrifugal and Coriolis forces in the direction of the branching outlet channels (as indicated in Figure 6.10):

$$\begin{aligned}
F_{z_1} &= F_{\omega} \cos\theta_1 - F_{co} \sin\theta_1 \\
F_{z_2} &= F_{\omega} \cos\theta_2 + F_{co} \sin\theta_2
\end{aligned}
\tag{32}$$

Where F_{Z1} and F_{Z2} are total propelling forces in the direction of each outlet branch. The splitting of the incoming fluid between two outlet branches of equal hydraulic diameters is regulated by the ratio of the forces:

$$\frac{\sum F_{z_1}}{\sum F_{z_2}} = k
\tag{33}$$

The flow will be equally divided into two outlet branches when $k=1$. The equal division of the liquid into two streams can be used to reduce the consumption of samples by duplicating the detection chambers for example in the CD-like-ELISA chips (Lin, 2010). Substituting Equation 29 in Equation 30, the difference between angles of two outlet branches is:

$$\Delta\theta = 2 \tan^{-1}\left(\frac{\rho\omega w^2}{4\mu}\right)
\tag{34}$$

Where θ_1 and θ_2 are the separation angle against the direction and in the direction of Coriolis force. In addition, as the flow in most of the microfluidic platforms is laminar, the branch channel dimensions can be employed to manipulate the flow resistance and regulate the flow distribution to each branch (Takagi et al., 2005). The Poiseuille law can be rewritten in terms of the flow rate ($Q=A.V$) (Bird et al., 2007):

$$Q = \Delta P \frac{D_h^2 \cdot A}{32\mu L} = \frac{\Delta P}{R}
\tag{35}$$

Where L , D_h , A , V and R are the branch channel length, the hydraulic diameter, the cross sectional area of the channel, the velocity and the resistance to flow, respectively:

$$R = \frac{32\mu L}{D_h^2 \cdot A}
\tag{36}$$

Thus, for a fluid of uniform viscosity and channels of given dimensions, the flow rate for the splitting branches can be calculated. In order for the parabolic velocity profile to develop completely within the branching channels, the length of the auxiliary outlet λ_o (see Figure 6.1) has to be greater than entrance length (l_e) of (Bird et al., 2007):

$$\lambda_o > l_e = 0.035 D_h \text{ Re} \quad [37]$$

The accuracy of Eq. 10 in predicting the flow rate in branch channels have been evaluated by carrying out several simulations according to the angles predicted based on Eq. 34. Figure 6.11 shows the velocity distribution in branch channels of a $200 \times 200 \mu\text{m}$ GR spinning at rotational frequency of (i) 500, (ii) 1000 and (iii) 1500rpm and $\theta_1=40^\circ$. Branch channels (a, b) are bifurcated evenly and are simulated according the angle calculated from Eq. 10. The figure shows that using the suggested separation angles (calculated by Eq. 33) enhances the accuracy of the uniform distribution of liquid for branch channels up to 99.5, 97.4 and 94% for the rotational frequency of 500, 1000 and 1500rpm respectively. The small difference between the velocities of branch channels at high rotational speed may be possibly reduced by small geometrical changes at the point where branches are separated from the main channel. Equation 34 can be also used to define different velocity rates at each branch channel by integrating it with flow resistance equation.

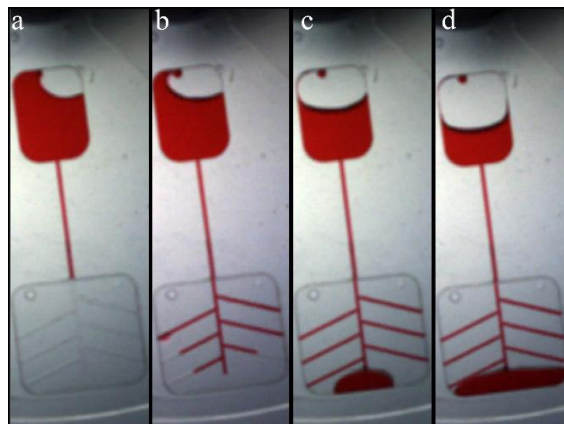


Figure 6.9: A partial view of a rotating disc indicate showing the distribution of the liquid by using GR valve.

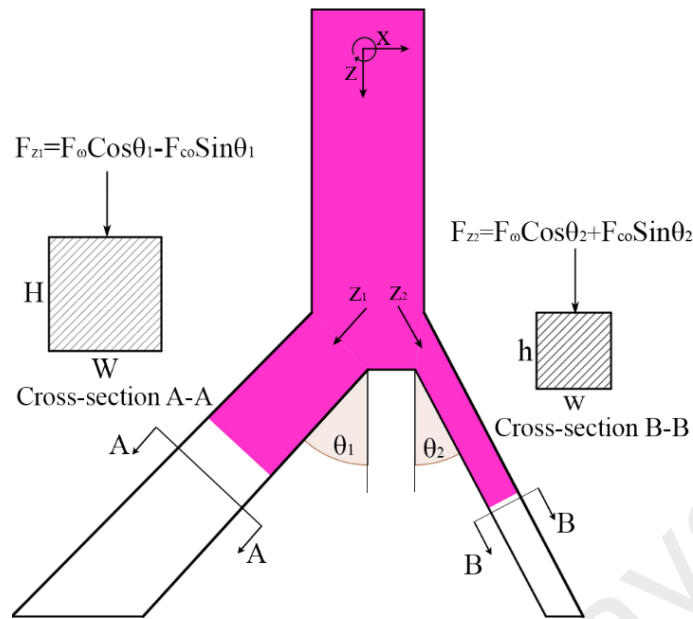


Figure 6.10: Free body diagram of a GR with two branch channels splitting at a junction.

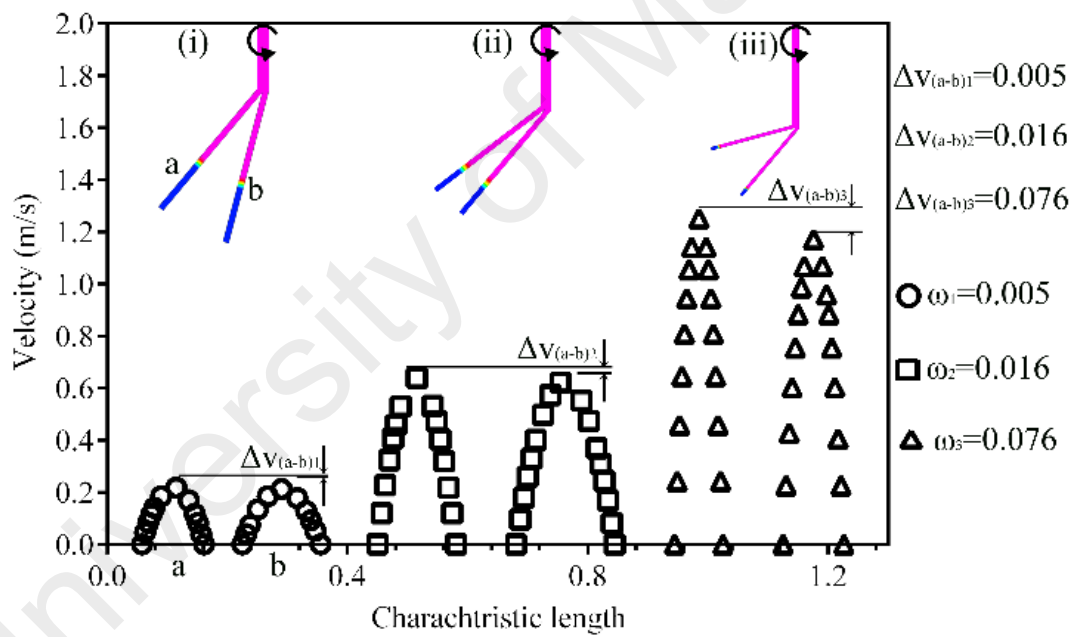


Figure 6.11: Numerically obtained velocity magnitudes in branch channels.

6.7 Summary

This Chapter introduced a novel technique called guided routing (GR) to control and manipulate the flow after capillary valve bursting on a centrifugal microfluidic disc. The introduced method is capable of determining the direction of the flow in T-junctions as well as guiding the liquid into several branches. The experimental results show that GR is able to continuously switch the flow to one direction i.e., in the direction of disc

rotation at low rotational speeds and instantaneously change it to the opposite direction by an abrupt increase of the rotational speed. Also the capability of the valve to equally distribute the flow into two branches has been theoretically and numerically presented. This valving technique is applicable to clinical and chemical operations where switching the flow direction or equal and non-equal dividing the liquid is required.

University of Malaya

CHAPTER 7: THE EFFECT OF MOMENT OF INERTIA AND HETEROGENEITY

7.1 Introduction

In this chapter, for the first time two novel methods for controlling the flow direction on centrifugal microfluidics are introduced. It includes the concepts, methods and preliminary numerical and experimental results.

7.2 Moment of inertia in centrifugal microfluidics

In many biomedical, chemical and clinical applications, samples and reagents often experience sequential and complicated processes, including preparative microfluidics procedures, mixing and separation and complete with detection or the ultimate chemical reactions. These processes can occupy a large space on the centrifugal discs that increases the costs and limits parallel processing of assays. In order to efficiently use the disc real estate and facilitate parallel processing, several active and passive techniques have been introduced by researchers, which are able to push liquids radially inward such as siphoning, pneumatic and thermo-pneumatic pumping. Most of these techniques such as pneumatic pumping, siphoning, etc. have specific operational frequency range or require additional instruments and external power sources. In addition, the diversity of chemical and biomedical applications motivates researchers to develop new techniques to manipulate fluids in lab-on-a-disc devices. In this chapter for the first time, the role of the effective angular moment of inertia of the liquid in centrifugal microfluidics is investigated theoretically and experimentally. The effective angular moment of inertia of the liquid inside a chamber on a rotating disc can be used for pushing the liquid towards specific lateral or/and radial directions by suddenly pausing or reducing the rotational velocity of the disc.

7.2.1 Concept

Figure 7.1 shows a top view of the design, which illustrates how the inertia and Euler forces can be employed in centrifugal microfluidics in order to drive liquid towards the disc center. The design is comprised of an inlet chamber, which is connected by a V-shape microchannel to an outlet chamber. The inlet chamber and the outlet chamber (which can be located at any position on the disc) are located at the periphery of the disc. Figure 7.1 (a) shows a partial top view of a disc rotating clockwise at a spinning frequency below the burst frequency of the capillary valve. The increase of the spinning speed causes the liquid to pass the capillary valve and move slightly towards the disc center. It will stop in the V-shape micro channel because of the balance between the centrifugal force exerting on the volume of the liquid in the inlet chamber and the centrifugal force acting on the volume of the liquid in the micro channel (Figure 7.1 (b)). Further increment of the spinning speed does not propel the liquid towards the disc center, but it will increase the potential energy stored in the liquid. At such circumstances, stopping the rotating disc will release the stored energy in the liquid and the liquid will propel towards the disc center. The distance that liquid is able to flow towards the disc center depends on the spinning speed of the disc at the time exactly before the abrupt reduction of the rotational speed, the higher the speed the longer the distance. It also depends on the deceleration rate of the rotating disc; with a higher the deceleration the liquid will flow a longer distance. Figures 7.1 (c), (d) show that the liquid flow in the V-shape micro channel and reaches the entrance of the outlet chamber where additional pressure is needed to overcome the capillary valve. At this point, by rotating the disc and increasing the spinning speed to a special frequency, the centrifugal and Coriolis forces acting on the liquid in the inlet chamber provides adequate pressure to breach the capillary valve and liquid fills the outlet chamber (Figures 7.1 (e),

(f). Note that in order to enhance the flow manipulation, a siphoning like mechanism can be designed for the proposed method.

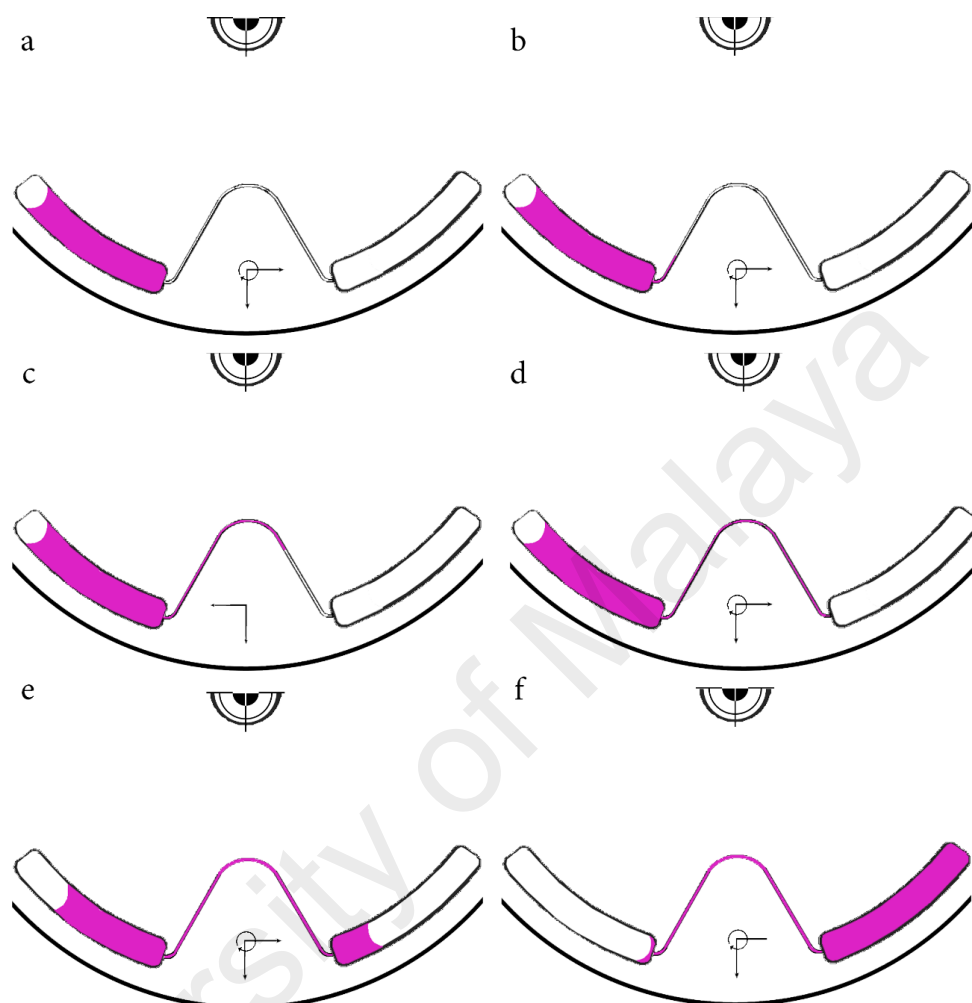


Figure 7.1: A partial top view of the liquid flow.

7.2.2 Theory

The on-board storage and on-demand release of samples or reagents in centrifugal microfluidics can increase the efficiency of these devices and improve their portability. Pre-stored samples on the disc are ready to use and can be propelled to the test chambers by using different liquid handling techniques. Because of the unidirectional nature of the flow in centrifugal microfluidics, storing samples or reagents in the chambers, which are located closer to the disc rim assists in the efficient use of the disc real estate. The liquid, stored in a container located on a place close to the disc

periphery is propelled to an inlet chamber, which is close to disc center where it can participate in different biomedical or chemical tasks. The stored samples can be driven back to the disc center by using some passive techniques and different active pumping techniques such as thermo pneumatic pumps (Abi-Samra et al., 2011a). The present method introduces a passive technique that employs the energy stored in the liquid, the Euler and Coriolis forces to propel liquids towards the disc center. The Navier-Stokes equation can be written for a non-inertial, incompressible system (see Eq. 24). The forces per unit volume in a two-dimensional plane for a disc rotating with a constant spinning speed are the vector product of Coriolis and centrifugal accelerations, respectively (see Eq. 25). The Coriolis force acting on the liquid is calculated by solving the Navier-Stokes equations in the plane parallel to the disc surface. Assuming a fluid of constant density and the impermeable walls and ignoring the gravitational force, which is significantly smaller than other forces on a spinning disc, the Coriolis force is:

$$F_{co} = -2\rho \times r\omega \times ru \quad [38]$$

When the disc abruptly stops i.e., which requires a large rate of deceleration (α) the Euler force is acting on the liquid. The Euler force can be written as:

$$F_{Eu} = -\rho\alpha \times \bar{r} \quad [39]$$

Where, ρ , α and \bar{r} are density of the liquid, angular deceleration and mean radial position of the liquid, respectively. The minimum force required for propelling the liquid towards the disc center is:

$$F_{eu} + F_{co} = \Delta P_{cap} \quad [40]$$

In the hydrophobic microchannels, aqueous liquids do not flow spontaneously in the microchannel due to the existence of the negative capillary pressure. This capillary pressure has been extensively studied and for a rectangular capillary is (McNeely et al., 1999):

$$\Delta P_{cap} = 2\sigma \cos\theta \left(\frac{1}{w} + \frac{1}{h} \right) \quad [41]$$

Where, w and h are the capillary width and height respectively. The minimum force required to push the liquid back towards the disc center have to be greater than this negative capillary pressure.

7.2.3 Fabrication method and experiments

The fabrication method of the disc is similar to the technique used in the previous chapters. Briefly, the microstructures are fabricated on layers of PMMA and PSA using a CNC machine and cutter plotter, respectively (see fabrication in chapter 6). The design of centrifugal microfluidic platform is composed of three PMMA layers and two PSA layer. The PSA layers are sandwiched between the PMMA layers and the platform is formed. In general, most of the centrifugal microfluidics are fabricated from at least two different materials e.g., PMMA and PSA layers that are used to bound different layers of the disc together.

The experimental setup used to carry out the experiments is the same as that used in Chapter 6. Briefly, it consists of a CNC machine, a high-speed camera and a custom-made disc rotating system. Figure 7.2 shows the disc at rest state before and after the experiment. The disc is rotated up to 3500 rpm and its rotational velocity suddenly decreased to zero with a high deceleration rate of $\sim 45 \text{ Hz} \cdot \text{s}^{-1}$. Figure 7.2 (a) shows that the black dyed di-water is initially dispensed into two chambers one close to the disc center and the other close to the disc periphery in order to investigate the effect of the radius on the Euler and inertial forces. The disc is begun to rotate with a gradual increment in the rotational velocity until it reaches to spinning speed equal to 3500 rpm (the figure is not presented). Figure 7.2 (b) shows the liquid displacement after the sudden deceleration when the disc is at rest. As it can be grasped from the figure depending on the direction of rotation the liquid can flow towards the disc center via

one of which V-shape microchannels (microchannel 1, 2). First the disc rotated clockwise direction and stops with a high deceleration rate and as a result the liquid will flow towards the disc center through microchannel 2 and stops in the crest of V-shape of microchannel. Repeating the experiment will cause the liquid to fill the other outlet chamber located close to the disc periphery. It can be grasped that when the disc rotates in the opposite direction and it suddenly stops the liquid begins to flow towards the disc center via microchannel 1.

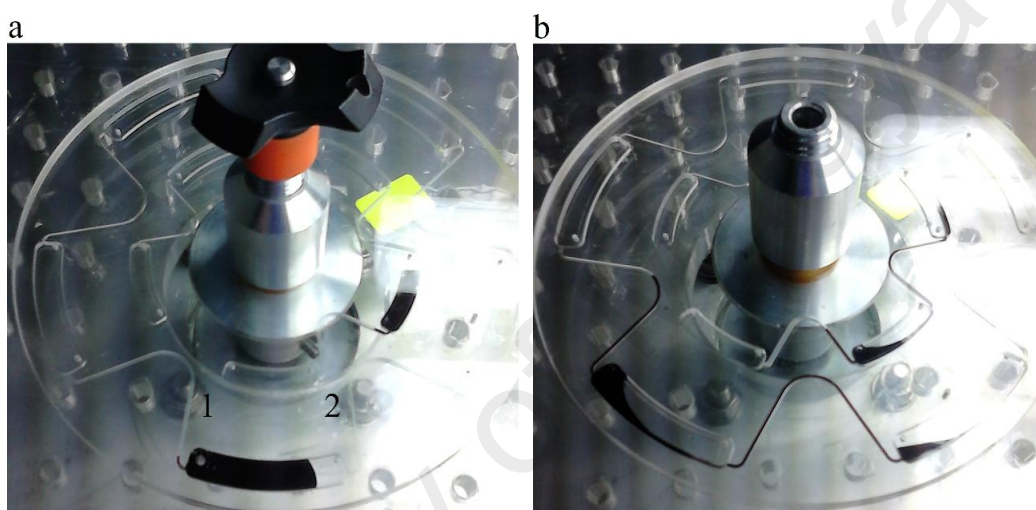


Figure 7.2: Propelling liquid towards the disc center using Euler and inertial forces.

7.2.4 Preliminary results

The experiment results confirmed that utilizing the effective moment of inertia of the liquid i.e., as a result of a sudden reduction of the rotational speed (~ 45 Hz/s), propels the entire liquid volume from a chamber adjacent to the disc's periphery to a chamber close to the disc center. The experiment was carried out for chambers connected with square hydrophobic capillaries ($400 \times 400 \mu\text{m}$) and disc rotational velocities of ~ 58 Hz. This technique can be used to propel the samples/reagents stored in the liquid storage devices on the disc peripheral towards the disc center.

7.3 Effect of surface heterogeneity on the liquid flow

A centrifugal microfluidic platform is usually a heterogeneous product since it is often fabricated by bounding layers of different materials e.g., PMMA and PSA that have different surface properties and contact angles. Herein, the effect of surface heterogeneity of micro channels and micro chambers on the flow pattern in stationary and rotating microfluidic platforms is investigated. In order to simulate the effect of surface heterogeneity on the flow pattern it is assumed that the different micro chambers and micro channels have different surface properties and contact angles. The contact angle of the bottom surface of the micro chambers/channels is assumed to be different (contact 80° - 130°) from that of the other surfaces (70°). The results reveal that building microstructures with a careful selection of materials allows for equal bifurcation of a liquid samples inside a micro chamber or a micro channel. The bifurcation occurs as a spontaneous response of the liquid to the surface properties of its container. In addition, the effect of geometry of the micro chambers and the ratio of the liquid volume to the micro chamber volume on bifurcation of liquid is simulated. This technique can be used in micro mixing by split and recombination of the liquid in consecutive micro chambers and also for liquid distribution when equal volume of liquids needs to be delivered to different destinations.

7.3.1 Concept

The instantaneous response of a liquid on solid surfaces is based on the wettability of the surface. The liquid tends to spread and flow spontaneously on a hydrophilic surface whereas the spontaneous response of the same liquid on a hydrophobic surface is to contract and minimize its free energy by taking bubble-like form. This phenomenon can be utilized to separate liquid in a chamber and distribute the separated volume of liquids into different destination chamber. In order to separate liquid, it is required to design and fabricate micro chambers of different materials with relatively large difference

between their contact angles. A careful arrangement of the heterogeneous surfaces forming a micro chamber will cause two opposite responses of the liquid to hydrophilic and hydrophobic surfaces, which can lead to a complete separation of the liquid into two even parts.

7.3.2 Numerical method and simulation cases

The numerical method used to simulate the effect of heterogeneity on the flow pattern is the same to that used to simulate the effect of contact angles on the flow behavior (see section 3.4.2). Briefly, the volume of fluid method (VOF) from ANSYS-Fluent software has been used to investigate the flow pattern. Structural mesh was used and the mesh sensitivity study was carried out to reduce the effect of meshing error in predicting the flow behavior.

The dimensional effects and the effects of micro chamber shape on the flow pattern in the heterogeneous micro chambers are simulated. Table 7.1 lists the simulation cases used to investigate the flow pattern in different shape of micro chamber with different dimensions. The volume of the liquid and the ratio of the liquid volume to the volume of the micro chamber in the different cases are kept constant. The contact angles of the bottom surface of the micro chamber is considered to be 70° and is increased to 130° with the step size of 10° ; the contact angles of the other surfaces are kept constant value of 70° . The table lists the total number of different simulation cases studied and it contains three different micro chamber cases, which are the most common micro chamber shapes namely, rectangular, trapezoid and circular.

Table 7.1: Simulation cases used to study the effect of heterogeneity on the flow pattern.

Case	HxWxL	$\theta_{t,s}^{\circ}$	θ_b°	Micro chamber
1- 35	5x6x0.5 10x6x0.5	70	70- 130	Rectangular
36- 71	13x7x0.5 13x7x1	70	70- 130	Trapezoid
72- 103	R5.7x0.5 R5.7x1	70	70- 130	Circular

7.3.3 Flow behavior

Figure 7.3 shows a step-by-step flow movement in a rectangular micro chamber of 5x6x0.5mm in the rest condition at different times. The top and side surfaces of the micro chamber are hydrophobic with contact angle of 120 and the bottom surface is hydrophilic with contact angle of 70. The micro chamber is partially filled with water with surface tension of 0.073 N/m. The response of the liquid to the hydrophobic surfaces causes spontaneous liquid flow from the surfaces with higher contact angles towards the surfaces of lower contact angle. Figures 7.3 (b), (c) show the decrease of the liquid-solid interface between the liquid and the top surface and the increase of the interface between the liquid and the bottom surface. Figures 7.3 (d), (e) show the process of formation and development of scattered wet areas on the top surface. The scattered wet areas on the top surface join due to the intermolecular and surface tension forces and a larger dry area on the top surface of the micro chamber is formed (see Figures 7.3 (f), (g)). The process of development of the new dry areas on the top surface of the micro chamber varies depending on the ratio of the liquid volume to the micro chamber volume (see Figures 7.3 (h), (i)). Following the development of new wet areas on the top surface the scattered wet areas are recombined and form a larger continuous dry area (see Figures 7.3 (j), (k)). The fluid continues its movement until it reaches its balance where the liquid is separated into two even parts as shown in Figures 7.3 (l), (o).

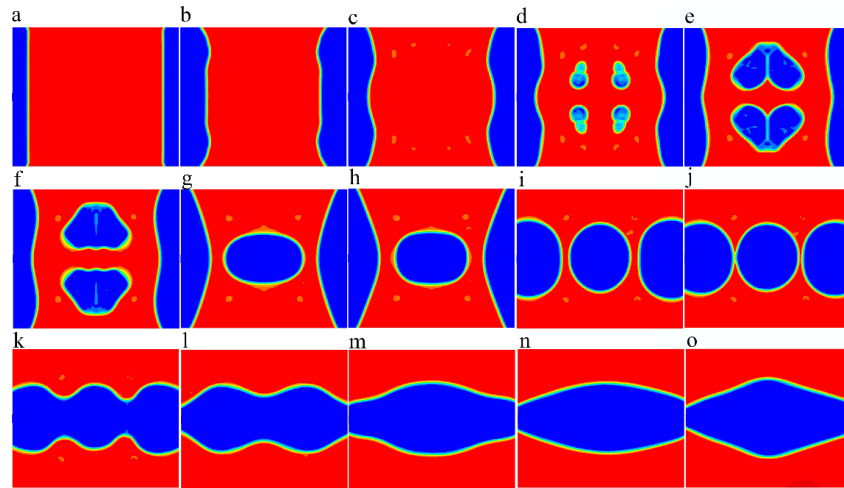


Figure 7.3: Top view of a heterogeneous micro chamber, $\theta=70^\circ$ and $\beta=120^\circ$.

Figure 7.4 shows a step-by-step fluid response to heterogeneous surfaces in a trapezoid micro chamber of $13 \times 7 \times 2 \text{ mm}$ in the rest condition at different times. The top and side surfaces of the micro chamber are hydrophobic with contact angle of 130° and the bottom surface is hydrophilic with contact angle of 70° . The liquid is initially dispensed into the micro chamber and the simulation starts (the liquid cannot be seen in Figure 7.4 (a), because it is spread on the bottom surface). The liquid starts to flow from the hydrophobic surface towards the hydrophilic surfaces. It reaches the top surface of the micro chamber from its corners due to the larger surface liquid interface at the corners (see Figure 7.4 (b)). The liquid continues its movement and spreads on the top surface of the micro chamber, which creates a larger wet area (Figures 7.4 (c), (d)). The development of wet areas on the top surface is corresponding to the development of dry area on the bottom surface (the hydrophobic surface) that cannot be seen in the figure. Figure 7.4 (e) shows that the wet areas on the top surface gradually combine and create a large continuous wet area on the top surface. However, due to the special shape of the micro chamber the liquid gradually splits from the larger base of the trapezoid and stays continues on the smaller base (Figures 7.4 (f), (g)). Unlike the rectangular shape the

liquid separation only occurs on the bottom surface (not shown) and on the top surface it is partially separated as shown in the Figure 7.4 (h).

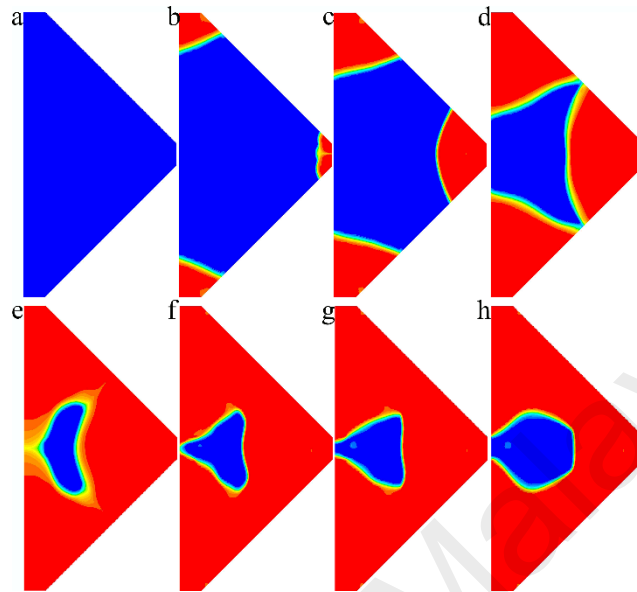


Figure 7.4: Top view of a trapezoid heterogeneous micro chamber.

7.4 Summary

For the first time the effect of moment of inertia of the liquids in the rotating microfluidic platforms on the liquid flow control and manipulation was investigated experimentally and theoretically. The preliminary results show that the moment of inertia of the liquid can be used to efficiently propel liquids towards any lateral or radial direction. For instance, it was shown that abruptly pausing or reducing the spinning speed of a rotating disc can transfer the entire liquid inside a chamber close to the disk rim to a chamber near the disc center.

In addition, the effect of surface heterogeneity of the micro channels and micro chambers on the flow pattern in stationary and rotating systems were investigated. The preliminary results revealed that a careful selection of materials for building multi-layer microstructures can be used in micro mixing or in even bifurcation of liquids.

CHAPTER 8: CONCLUSIONS

The research in this PhD thesis is motivated by the importance of precise microflow control in transforming various laboratory-based chemical and clinical assays into portable centrifugal microfluidics based devices. Efficient and inexpensive flow control techniques based on new principles and operations are introduced and compared with state of the art industrial approaches. Unlike previously introduced techniques our novel flow control methods are not dependent on the direction of the disk rotation and do not require special surface treatments or external power sources. The hardware to enable these techniques is easy to implement and provides robust control of the flow in centrifugal microfluidic platforms.

In order to be able to develop inexpensive novel flow control microstructures, a comprehensive investigation of the relationship between contact angles and capillary dimensions on the performance of passive capillary valves has been carried out. The effects of different contact angles (20° to 90°) and capillary dimensions ($100\mu\text{m}$ to $700\mu\text{m}$) on the burst frequency of capillary valves were investigated numerically and experimentally. As a result, a holistic insight into the performance of a wide range of capillary valves made from different materials from super hydrophilic to hydrophobic was acquired. The output of this research can be summarized as follows:

The results show that the existing theoretical models for predicting the burst frequency in capillary valves cannot be used for super hydrophilic materials since they are unable to predict the fluid leakage. While they predict that, a high pressure is required for pushing the fluid over super hydrophilic capillary valves, our computed results show that fluid flows consistently over such capillary valves into the next outlet at low pressures. The results also show that, generally burst frequencies of square capillaries are lower than those of rectangular shapes.

For the first time, a new valving technique named gate valve is introduced that exploits a geometrical effect on the surface tension to control and switch the flow direction in centrifugal microfluidics. The new valve is a frequency dependent device that is able to direct the flow to one direction (e.g., c.w.) at low frequencies and to the opposite direction (e.g., c.c.w.) at higher frequencies without using external power sources or applying surface treatments. At low frequencies, the liquid follows a path dictated by the specific gating microstructure and at higher frequencies; liquid follows the direction of the Coriolis force. The flow behavior of the new valve for distilled water as well as for liquids with different properties was investigated experimentally and numerically. The results show that the new valve is able to control the flow direction on a spinning microfluidic platform for liquids of widely varying properties. In comparison with the previously introduced techniques of flow, switching gate valve enables switching the flow direction without employing external power sources, applying surface treatments or changing the direction of disc rotation. It directs entire liquid in the direction opposite to that of Coriolis force at low rotational velocities and in the direction of Coriolis force at high rotational velocities. Gate valve by introducing minimal complexity and minimal occupation of the disc's real estate allows for implementing larger number of multiplexed and more sophisticated assays on the centrifugal microfluidic platforms without interrupting other operations.

Another novel microvalve is presented that allows for the efficient routing of samples and controlling the flow direction on centrifugal microfluidic platforms. The distinctive feature that makes this approach different from other types of passive capillary valves is the robust control of liquid movement, which is achieved by employing two adjustable sequential burst valves i.e., a primary and a secondary burst valve. This valve configuration can be used to route samples and reagents at given flow rates to selected receiving reservoirs, determined by the spinning frequency of the disc.

It is capable of guiding the liquid into several outlet branches as well as determining the direction of the flow in T-junctions. The technique also allows for switching the flow direction instantaneously from the direction along the disc rotation and to the opposite direction by immediate increasing of the rotational speed and switches the liquid flow back to its previous direction by reduction of the spinning speed. The performance of this novel valve configuration was experimentally tested, the flow behavior was numerically studied using the VOF method and a theoretical model for their burst frequency was presented. In addition, the capability of the valve to equally distribute the flow into two branches has been discussed theoretically and numerically. This valving technique is applicable to clinical and chemical operations where switching the flow direction or equal and non-equal liquid distribution is required. Example of these operations are switching of the liquid flow between two or more pathways in order to separately direct them to different chambers e.g., where a specimen such as DNA, protein and or antigen has to be discharged into a clean buffer solution.

For the first time, the role of the effective moment of inertia of the liquid in centrifugal microfluidics was investigated. The effective moment of inertia of the liquid inside a chamber on a rotating disc can be used for pushing the liquid towards specific lateral or/and radial directions by suddenly pausing or reducing the rotational velocity of the disc. The experiment results confirmed that utilizing the effective moment of inertia of the liquid i.e., as a result of a sudden reduction of the rotational speed (~ 45 Hz/s), propels the entire liquid volume from a chamber adjacent to the disc's periphery to a chamber close to the disc center. The experiment was carried out for chambers connected with square hydrophobic capillaries ($400 \times 400 \mu\text{m}$) and disc rotational velocities of ~ 58 Hz. This technique can be used to propel the samples/reagents stored in vessels on the disc periphery towards chambers in lateral directions or the disc center.

The effect of surface heterogeneity of micro channels and micro chambers on the flow pattern in stationary and rotating microfluidic platforms was investigated numerically. In order to simulate the effect of surface heterogeneity on the flow pattern it was assumed that the different micro chambers and micro channels have different surface properties and contact angles. The contact angle of the bottom surface of the micro chambers/channels was assumed to be different (80° - 130°) from that of the other surfaces (70°). The results reveal that building microstructures with a careful selection of materials allows for equal bifurcation of a liquid samples inside a micro chamber or a micro channel. The bifurcation occurs as a spontaneous response of the liquid to the surface properties of its container. In addition, the effect of geometry of the micro chambers and the ratio of the liquid volume to the micro chamber volume on the bifurcation of liquid was simulated. This technique can be used in micro mixing by split and recombination of the liquid in consecutive micro chambers and also for liquid distribution when equal volume of liquids needs to be delivered to different destinations.

8.1 Suggestions for future study

The preliminary results of the effect of moment of inertia on the fluid flow have been presented in Chapter 7. These results implied that the moment of inertia can be used as an inexpensive passive pumping technique in the centrifugal microfluidics. The effect of the moment of inertia required to be profoundly analyzed using theoretical and numerical methods to characterize the mechanism of the micropumps which can be developed based on the effect of the moment of inertia.

As well, the simulation results of the effect of the surface heterogeneity in the vessels on centrifugal microfluidics presented in the last chapter showed that using smart combination of different contact angles when fabricating these vessels can be used for

mixing or separating purposes. Further simulations to observe the effect of the surface heterogeneity in microchannels is recommended to investigate the effect of different contact angles on the fluid motion in heterogeneous microchannels. These simulations need to be experimentally verified to validate the results obtained.

University of Malaya

REFERENCES

- Abi-Samra, K., Clime, L., Kong, L., Gorkin, R. I., Kim, T. H., Cho, Y. K., & Madou, M. (2011a). Thermo-pneumatic pumping in centrifugal microfluidic platforms. *Microfluidics and Nanofluidics*, 11(5), 643-652.
- Abi-Samra, K., Hanson, R., Madou, M., & Gorkin, R. I. (2011b). Infrared controlled waxes for liquid handling and storage on a CD-microfluidic platform. *Lab on a Chip*, 11(4), 723-726.
- Acheson, D. J. (1990). *Elementary fluid dynamics*. New York City: Oxford University Press.
- Aeinehvand, M. M., Ibrahim, F., harun, S. W., Al-Faqheri, W., Thio, T. H. G., Kazemzadeh, A., & Madou, M. (2014). Latex micro-balloon pumping in centrifugal microfluidic platforms. *Lab on a Chip*, 14(5), 988-997.
- Aeinehvand, M. M., Ibrahim, F., Harun, S. W., Kazemzadeh, A., Rothan, H. A., Yusof, R., & Madou, M. (2015). Reversible thermo-pneumatic valves on centrifugal microfluidic platforms. *Lab on a Chip*, 15(16), 3358-3369.
- Aguirre, G., Efremov, V., Kitsara, M., & Ducreé, J. (2014). Integrated micromixer for incubation and separation of cancer cells on a centrifugal platform using inertial and dean forces. *Microfluidics and Nanofluidics*, 1-14.
- Amasia, M., Cozzens, M., & Madou, M. J. (2012). Centrifugal microfluidic platform for rapid PCR amplification using integrated thermoelectric heating and ice-valving. *Sensors and Actuators B: Chemical*, 161(1), 1191-1197.
- Anderson, N. G. (1969). Computer Interfaced Fast Analyzers. *Science*, 166(3903), 317-324.
- Ansgar, W., Stefan, R., & Lienhard, P. (2001). Fluidic microsystems based on printed circuit board technology. *Journal of Micromechanics and Microengineering*, 11(5), 528.
- ANSYS-FLUENT, H. (2011). 36.5.4 *Phase Interaction Dialog Box*.
- Ashish, S. A., & Mitra, S. K. (2009). Effect of dynamic contact angle in a volume of fluid (VOF) model for a microfluidic capillary flow. *Journal of Colloid and Interface Science*, 339(2), 461-480.

- Auroux, P. A., Iossifidis, D., Reyes, D. R., & Manz, A. (2002). Micro total analysis systems. 2. analytical standard operations and applications. *Analytical Chemistry*, 74(12), 2637-2652.
- Beebe, D. J., Mensing, G. A., & Walker, G. M. (2002). PHYSICS AND APPLICATIONS OF MICROFLUIDICS IN BIOLOGY. *Annual Review of Biomedical Engineering*, 4(1), 261-286.
- Bird, R. B., Stewart, W. E., & Lightfoot, E. N. (2007). *Transport phenomena*. Wisconsin, Madison: John Wiley & Sons.
- Blake, T. D. (2006). The physics of moving wetting lines. *Journal of Colloid and Interface Science*, 299(1), 1-13.
- Bouchard, A. P., Duford, D. A., & Salin, E. D. (2010). Non-contact Addition, Metering, and Distribution of Liquids into Centrifugal Microfluidic Devices in Motion. *Analytical Chemistry*, 82(20), 8386-8389.
- Brackbill, J. U., Kothe, D. B., & Zemach, C. (1992). A continuum method for modeling surface tension. *Journal of Computational Physics*, 100(2), 335-354.
- Brenner, T. (2005). *Polymer Fabrication and Microfluidic Unit Operations for Medical Diagnostics on a Rotating Disk*.
- Brenner, T., Glatzel, T., Zengerle, R., & Ducree, J. (2005). Frequency-dependent transversal flow control in centrifugal microfluidics. *Lab on a Chip*, 5(2), 146-150.
- Brenner, T., Glatzel, T., Zengerle, R., & Ducreé, J. (2003). A Flow Switch Based on Coriolis Force. Proceedings of 7th international conference on micro total analysis systems (pp. 5-9).
- Brogger, A. L., Kwasny, D., Bosco, F. G., Silaharoglu, A., Tumer, Z., Boisen, A., & Svendsen, W. E. (2012). Centrifugally driven microfluidic disc for detection of chromosomal translocations. *Lab on a Chip*, 12(22), 4628-4634.
- Burtis, C. A., Mailen, J. C., Johnson, W. F., Scott, C. D., Tiffany, T. O., & Anderson, N. G. (1972). Development of a Miniature Fast Analyzer. *Clinical Chemistry*, 18(8), 753-761.
- Chen, J., Huang, P. C., & Lin, M. G. (2008). Analysis and experiment of capillary valves for microfluidics on a rotating disk. *Microfluidics and Nanofluidics*, 4(5), 427-437.

- Chen, J. J., Liu, W. Z., Lin, J. D., & Wu, J. W. (2006). Analysis of filling of an oval disk-shaped chamber with microfluidic flows. *Sensors and Actuators A: Physical*, 132(2), 597-606.
- Cho, H., Kim, H.-Y., Kang, J. Y., & Kim, T. S. (2007a). How the capillary burst microvalve works. *Journal of Colloid and Interface Science*, 306(2), 379-385.
- Cho, H., Kim, H. Y., Kang, J. Y., & Kim, T. S. (2004). Capillary passive valve in microfluidic system. Proceedings of Nanotechnology Conference and Trade Show (pp.), Boston, Massachusetts
- Cho, H., Kim, H. Y., Kang, J. Y., & Kim, T. S. (2007b). How the capillary burst microvalve works. *Journal of Colloid and Interface Science*, 306(2), 379-385.
- Cho, Y. K., Lee, J. G., Park, J. M., Lee, B. S., Lee, Y., & Ko, C. (2007c, 10-14 June 2007). One-Step Pathogen Specific DNA Extraction from Whole Blood on a Centrifugal Microfluidic Device. Proceedings of Solid-State Sensors, Actuators and Microsystems Conference, 2007. TRANSDUCERS 2007. International (pp. 387-390).
- Danov, K. D., Valkovska, D. S., & Kralchevsky, P. A. (2002). Adsorption Relaxation for Nonionic Surfactants under Mixed Barrier-Diffusion and Micellization-Diffusion Control. *Journal of Colloid and Interface Science*, 251(1), 18-25.
- Ducrée, J., Glatzel, T., Brenner, T., & Zengerle, R. (2004). Coriolis-Induced Flow Control for Micro-and Nanofluidic Lab-on-a-Disk Technologies. In: H. Knobloch & Y. Kaminorz (Eds.), *MicroNano Integration* (pp. 147-153): Springer Berlin Heidelberg.
- Ducrée, J., Haeberle, S., Brenner, T., Glatzel, T., & Zengerle, R. (2006). Patterning of flow and mixing in rotating radial microchannels. *Microfluidics and Nanofluidics*, 2(2), 97-105.
- Ducrée, J., Haeberle, S., Lutz, S., Pausch, S., von Stetten, F., & Zengerle, R. (2007). The centrifugal microfluidic Bio-Disk platform. *Journal of Micromechanics and Microengineering*, 17(7), S103.
- Duffy, D. C., Gillis, H. L., Lin, J., Sheppard, N. F., & Kellogg, G. J. (1999). Microfabricated centrifugal microfluidic systems: characterization and multiple enzymatic assays. *Analytical Chemistry*, 71(20), 4669-4678.
- Ekstrand, G., Holmquist, C., Örlfors, A., Hellman, B., Larsson, A., & Andersson, P. (2000). Microfluidics in a Rotating CD. In: A. van den Berg, W. Olthuis & P. Bergveld (Eds.), *Micro Total Analysis Systems 2000* (pp. 311-314): Springer Netherlands.

- Erickson, D., Li, D., & Park, C. B. (2002). Numerical simulations of capillary-driven flows in nonuniform cross-sectional capillaries. *Journal of Colloid and Interface Science*, 250(2), 422-430.
- Feng, G.-H., & Chou, Y.-C. (2011). Fabrication and characterization of thermally driven fast turn-on microvalve with adjustable backpressure design. *Microelectronic Engineering*, 88(2), 187-194.
- Feng, Y., Zhou, Z., Ye, X., & Xiong, J. (2003). Passive valves based on hydrophobic microfluidics. *Sensors and Actuators A: Physical*, 108(1-3), 138-143.
- Focke, M., Stumpf, F., Faltin, B., Reith, P., Bamarni, D., Wadle, S., Muller, C., Reinecke, H., Schrenzel, J., Francois, P., Mark, D., Roth, G., Zengerle, R., & von Stetten, F. (2010). Microstructuring of polymer films for sensitive genotyping by real-time PCR on a centrifugal microfluidic platform. *Lab on a Chip*, 10(19), 2519-2526.
- Frederick, M. F. (1964). *Contact Angle, Wettability, and Adhesion* (Vol. 43): American Chemical Society.
- Fulcher, R. A., Jr., Ertekin, T., & Stahl, C. D. Effect of Capillary Number and Its Constituents on Two-Phase Relative Permeability Curves. *Journal of Petroleum Technology*, 37(02), 249-260.
- Garcia-Cordero, J. L., Dimov, I. K., O'Grady, J., Ducree, J., Barry, T., & Ricco, A. J. (2009, 25-29 Jan. 2009). Monolithic Centrifugal Microfluidic Platform for Bacteria Capture and Concentration, Lysis, Nucleic-Acid Amplification, and Real-Time Detection. Proceedings of Micro Electro Mechanical Systems, 2009. MEMS 2009. IEEE 22nd International Conference on (pp. 356-359).
- Glière, A., & Delattre, C. (2006). Modeling and fabrication of capillary stop valves for planar microfluidic systems. *Sensors and Actuators A: Physical*, 130-131(0), 601-608.
- Godino, N., Gorkin Iii, R., Linares, A. V., Burger, R., & Ducree, J. (2013). Comprehensive integration of homogeneous bioassays via centrifugo-pneumatic cascading. *Lab on a Chip*, 13(4), 685-694.
- Gorkin III, R., Nwankire, C. E., Gaughran, J., Zhang, X., Donohoe, G. G., Rook, M., O'Kennedy, R., & Ducreé, J. (2012). Centrifugo-pneumatic valving utilizing dissolvable films. *Lab on a Chip*, 12(16), 2894-2902.
- Gorkin, R., Park, J., Siegrist, J., Amasia, M., Lee, B. S., Park, J.-M., Kim, J., Kim, H., Madou, M., & Cho, Y.-K. (2010). Centrifugal microfluidics for biomedical applications. *Lab on a Chip*, 10(14), 1758-1773.

- Gorkin, R., Soroori, S., Southard, W., Clime, L., Veres, T., Kido, H., Kulinsky, L., & Madou, M. (2012). Suction-enhanced siphon valves for centrifugal microfluidic platforms. *Microfluidics and Nanofluidics*, 12(1-4), 345-354.
- Grader, L. (1986). On the modelling of the dynamic contact angle. *Colloid and Polymer Science*, 264(8), 719-726.
- Grumann, M., Geipel, A., Riegger, L., Zengerle, R., & Ducree, J. (2005). Batch-mode mixing on centrifugal microfluidic platforms. *Lab on a Chip*, 5(5), 560-565.
- Guo-Hua, F., & Eun Sok, K. (2004). Micropump based on PZT unimorph and one-way parylene valves. *Journal of Micromechanics and Microengineering*, 14(4), 429.
- Haerberle, S., Brenner, T., Zengerle, R., & Ducree, J. (2006). Centrifugal extraction of plasma from whole blood on a rotating disk. *Lab on a Chip*, 6(6), 776-781.
- Haerberle, S., Mark, D., von Stetten, F., & Zengerle, R. (2012). Microfluidic Platforms for Lab-On-A-Chip Applications. In: Z. Zhou, Z. Wang & L. Lin (Eds.), *Microsystems and Nanotechnology* (pp. 853-895): Springer Berlin Heidelberg.
- Handique, K., Burke, D. T., Mastrangelo, C. H., & Burns, M. A. (2001). On-Chip Thermopneumatic Pressure for Discrete Drop Pumping. *Analytical Chemistry*, 73(8), 1831-1838.
- Handique, K., Gogoi, B. P., Burke, D. T., Mastrangelo, C. H., & Burns, M. A. (1997). Microfluidic flow control using selective hydrophobic patterning. *Proceedings of SPIE* (pp. 185-195).
- Harrison, D. J., Manz, A., Fan, Z., Luedi, H., & Widmer, H. M. (1992). Capillary electrophoresis and sample injection systems integrated on a planar glass chip. *Analytical Chemistry*, 64(17), 1926-1932.
- He, H., Yuan, Y., Wang, W., Chiou Nan-Rong, N. R., Epstein, A. J., & Lee, L. J. (2009). Design and testing of a microfluidic biochip for cytokine enzyme-linked immunosorbent assay. *Biomicrofluidics*, 3(2), 022744.
- Hirt, C. W., & Nichols, B. D. (1981). Volume of fluid (vof) method for the dynamics of free boundaries. *Journal of Computational Physics* 39(1), 201-225.
- Hwang, H., Kim, H.-H., & Cho, Y.-K. (2011). Elastomeric membrane valves in a disc. *Lab on a Chip*, 11(8), 1434-1436.

- Issa, R. I. (1986). Solution of the implicitly discretised fluid flow equations by operator-splitting. *Journal of Computational Physics* 62, 40-65.
- Jenison, R., Jaeckel, H., Klonoski, J., Latorra, D., & Wiens, J. (2014). Rapid amplification/detection of nucleic acid targets utilizing a HDA/thin film biosensor. *Analyst*, 139(15), 3763-3769.
- Jens, D., Stefan, H., Sascha, L., Sarah, P., Felix von, S., & Roland, Z. (2007). The centrifugal microfluidic Bio-Disk platform. *Journal of Micromechanics and Microengineering*, 17(7), S103.
- Jeon, N. L., Chiu, D. T., Wargo, C. J., Wu, H., Choi, I. S., Anderson, J. R., & Whitesides, G. M. (2002). Microfluidics section: design and fabrication of Integrated passive valves and pumps for flexible polymer 3-dimensional microfluidic systems. *Biomedical Microdevices*, 4(2), 117-121.
- Jia, G., Ma, K. S., Kim, J., Zoval, J. V., Peytavi, R., Bergeron, M. G., & Madou, M. J. (2006). Dynamic automated DNA hybridization on a CD (compact disc) fluidic platform. *Sensors and Actuators B: Chemical*, 114(1), 173-181.
- Jinlong, Z., Qiuquan, G., Mei, L., & Jun, Y. (2008). A lab-on-CD prototype for high-speed blood separation. *Journal of Micromechanics and Microengineering*, 18(12), 125025.
- Johnson, R. D., Badr, I. H. A., Barrett, G., Lai, S., Lu, Y., Madou, M. J., & Bachas, L. G. (2001). Development of a Fully Integrated Analysis System for Ions Based on Ion-Selective Optodes and Centrifugal Microfluidics. *Analytical Chemistry*, 73(16), 3940-3946.
- Kazarine, A., & Salin, E. D. (2014). Volumetric measurements by image segmentation on centrifugal microfluidic platforms in motion. *Lab on a Chip*, 14(18), 3572-3581.
- Kazemzadeh, A., Ganesan, P., Ibrahim, F., Aeinehvand, M. M., Kulinsky, L., & Madou, M. J. (2014). Gating valve on spinning microfluidic platforms: A flow switch/control concept. *Sensors and Actuators B: Chemical*, 204(0), 149-158.
- Kazemzadeh, A., Ganesan, P., Ibrahim, F., He, S., & Madou, M. J. (2013). The Effect of Contact Angles and Capillary Dimensions on the Burst Frequency of Super Hydrophilic and Hydrophilic Centrifugal Microfluidic Platforms, a CFD Study. *PLoS ONE*, 8(9), e73002.
- Kazemzadeh, A., Ganesan, P., Ibrahim, F., Kulinsky, L., & Madou, M. J. (2015). Guided routing on spinning microfluidic platforms. *RSC Advances*, 5(12), 8669-8679.

- Khattab, I., Bandarkar, F., Fakhree, M., & Jouyban, A. (2012). Density, viscosity, and surface tension of water+ethanol mixtures from 293 to 323K. *Korean Journal of Chemical Engineering*, 29(6), 812-817.
- Kim, D. S., Lee, K. C., Kwon, T. H., & Lee, S. S. (2002). Micro-channel filling flow considering surface tension effect. *Journal of Micromechanics and Microengineering*, 12(3), 236.
- Kim, J., Kido, H., Rangel, R. H., & Madou, M. J. (2008). Passive flow switching valves on a centrifugal microfluidic platform. *Sensors and Actuators B: Chemical*, 128(2), 613-621.
- Kinahan, D. J., Kearney, S. M., Dimov, N., Glynn, M. T., & Ducree, J. (2014). Event-triggered logical flow control for comprehensive process integration of multi-step assays on centrifugal microfluidic platforms. *Lab on a Chip*, 14(13), 2249-2258.
- Koch, M., Evans, A. G. R., & Brunnschweiler, A. (1997). Simulation and fabrication of micromachined cantilever valves. *Sensors and Actuators A: Physical*, 62(1-3), 756-759.
- Kong, M. C. R., & Salin, E. D. (2011). Pneumatic Flow Switching on Centrifugal Microfluidic Platforms In Motion. *Analytical Chemistry*, 83(3), 1148-1151.
- Kunert, C., & Harting, J. (2008). Simulation of fluid flow in hydrophobic rough microchannels. *Int. J. Comput. Fluid Dyn.*, 22(7), 475-480.
- Lai, S., Wang, S., Luo, J., Lee, L. J., Yang, S.-T., & Madou, M. J. (2004). Design of a Compact Disk-like Microfluidic Platform for Enzyme-Linked Immunosorbent Assay. *Analytical Chemistry*, 76(7), 1832-1837.
- Lee, B. S., Lee, J.-N., Park, J.-M., Lee, J.-G., Kim, S., Cho, Y.-K., & Ko, C. (2009). A fully automated immunoassay from whole blood on a disc. *Lab on a Chip*, 9(11), 1548-1555.
- Lee, B. S., Lee, Y. U., Kim, H.-S., Kim, T.-H., Park, J., Lee, J.-G., Kim, J., Kim, H., Lee, W. G., & Cho, Y.-K. (2011). Fully integrated lab-on-a-disc for simultaneous analysis of biochemistry and immunoassay from whole blood. *Lab on a Chip*, 11(1), 70-78.
- Lee, L. J., Madou, M. J., Koelling, K. W., Daunert, S., Lai, S., Koh, C. G., Juang, Y.-J., Lu, Y., & Yu, L. (2001a). Design and Fabrication of CD-Like Microfluidic Platforms for Diagnostics: Polymer-Based Microfabrication. *Biomedical Microdevices*, 3(4), 339-351.

- Lee, L. J., Madou, M. J., Koelling, K. W., Daunert, S., Lai, S., Koh, C. G., Juang, Y. J., Lu, Y., & Yu, L. (2001b). Design and fabrication of CD-Like microfluidic platforms for diagnostics: polymer-based microfabrication. *Biomedical Microdevices*, 3(4), 339-351.
- Lee, W., Jung, J., Hahn, Y. K., Kim, S. K., Lee, Y., Lee, J., Lee, T.-H., Park, J.-Y., Seo, H., Lee, J. N., Oh, J. H., Choi, Y.-S., & Lee, S. S. (2013). A centrifugally actuated point-of-care testing system for the surface acoustic wave immunosensing of cardiac troponin I. *Analyst*, 138(9), 2558-2566.
- Leslie, D. C., Easley, C. J., Seker, E., Karlinsey, J. M., Utz, M., Begley, M. R., & Landers, J. P. (2009). Frequency-specific flow control in microfluidic circuits with passive elastomeric features. *Nat Phys*, 5(3), 231-235.
- Leu, T.-S., & Chang, P.-Y. (2004a). Pressure barrier of capillary stop valves in micro sample separators. *Sensors and Actuators A: Physical*, 115(2-3), 508-515.
- Leu, T. S., & Chang, P. Y. (2004b). Pressure barrier of capillary stop valves in micro sample separators. *Sensors and Actuators A: Physical*, 115(2-3), 508-515.
- Leung, W. W.-F., & Ren, Y. (2013). Crossflow and mixing in obstructed and width-constricted rotating radial microchannel. *International Journal of Heat and Mass Transfer*, 64(0), 457-467.
- Li, G., Chen, Q., Li, J., Hu, X., & Jianlong Zhao, J. (2010). A compact disk-like centrifugal microfluidic system for high-throughput nanoliter-scale protein crystallization screening. *Anal Chem*, 82(11), 4362-4369.
- Li, X., Chen, W., Liu, G., Lu, W., & Fu, J. (2014). Continuous-flow microfluidic blood cell sorting for unprocessed whole blood using surface-micromachined microfiltration membranes. *Lab on a Chip*, 14(14), 2565-2575.
- Lin, G., & Jing, L. (2004). Ice valve for a mini/micro flow channel. *Journal of Micromechanics and Microengineering*, 14(2), 242.
- Lin, S. E. (2010). A novel splitter design for microfluidic biochips using centrifugal driving forces. *Microfluidics and Nanofluidics*, 9(2-3), 523-532.
- Lu, C., Xie, Y., Yang, Y., Cheng, M. M.-C., Koh, C.-G., Bai, Y., Lee, L. J., & Juang, Y.-J. (2007). New valve and bonding designs for microfluidic biochips containing proteins. *Analytical chemistry*, 79, 994-1001.

- Ma, S., Loufakis, D. N., Cao, Z., Chang, Y., Achenie, L. E. K., & Lu, C. (2014). Diffusion-based microfluidic PCR for "one-pot" analysis of cells. *Lab on a Chip*, 14(16), 2905-2909.
- Madou, M., Zoval, J., Jia, G., Kido, H., Kim, J., & Kim, N. (2006). Lab on a CD. *Annual Review of Biomedical Engineering*, 8(1), 601-628.
- Madou, M. J. (2002). *Fundamentals of Microfabrication: The Science of Miniaturization, Second Edition*. Washington, D.C.: Taylor & Francis.
- Madou, M. J., & Kellogg, G. J. (1998). LabCD: a centrifuge-based microfluidic platform for diagnostics. Proceedings of SPIE 3259, Systems and Technologies for Clinical Diagnostics and Drug Discovery (pp. 80-93), San Jose, CA.
- Madou, M. J., Lee, L. J., Daunert, S., Lai, S., & Shih, C.-H. (2001). Design and Fabrication of CD-like Microfluidic Platforms for Diagnostics: Microfluidic Functions. *Biomedical Microdevices*, 3(3), 245-254.
- Man, P. F., Mastrangelo, C. H., Burns, M. A., & Burke, D. T. (1998, 25-29 Jan 1998). Microfabricated capillarity-driven stop valve and sample injector. Proceedings of Micro Electro Mechanical Systems, 1998. MEMS 98. Proceedings., The Eleventh Annual International Workshop on (pp. 45-50).
- Manz, A., Graber, N., & Widmer, H. M. (1990). Design of an open-tubular column liquid chromatograph using silicon chip technology. *Sensors and Actuators B: Chemical*, 1(1-6), 244-248.
- Marchalot, J., Fouillet, Y., & Achard, J.-L. (2014). Multi-step microfluidic system for blood plasma separation: architecture and separation efficiency. *Microfluidics and Nanofluidics*, 17(1), 167-180.
- McNeely, M. R., Spute, M. K., Tusneem, N. A., & Oliphant, A. R. (1999). Hydrophobic microfluidics. Proceedings of (pp. 210-220).
- Meijer, H. E. H., Singh, M. K., Kang, T. G., den Toonder, J. M. J., & Anderson, P. D. (2009). Passive and Active Mixing in Microfluidic Devices. *Macromolecular Symposia*, 279(1), 201-209.
- Melin, J., Roxhed, N., Gimenez, G., Griss, P., van der Wijngaart, W., & Stemme, G. (2004). A liquid-triggered liquid microvalve for on-chip flow control. *Sensors and Actuators B: Chemical*, 100(3), 463-468.

- Mohan, R., Schudel, B. R., Desai, A. V., Yearsley, J. D., Apblett, C. A., & Kenis, P. J. A. (2011). Design considerations for elastomeric normally closed microfluidic valves. *Sensors and Actuators B: Chemical*, 160(1), 1216-1223.
- Nan, L., Jiang, Z., & Wei, X. (2014). Emerging microfluidic devices for cell lysis: a review. *Lab on a Chip*, 14(6), 1060-1073.
- Noroozi, Z., Kido, H., Peytavi, R., Nakajima-Sasaki, R., Jasinskas, A., Micic, M., Felgner, P. L., & Madou, M. J. (2011). A multiplexed immunoassay system based upon reciprocating centrifugal microfluidics. *Review of Scientific Instruments*, 82(6), 064303.
- Oh, K. W., & Ahn, C. H. (2006). A review of microvalves. *Journal of Micromechanics and Microengineering*, 16(5), R13.
- Ouyang, Y., Wang, S., Li, J., Riehl, P. S., Begley, M., & Landers, J. P. (2013). Rapid patterning of 'tunable' hydrophobic valves on disposable microchips by laser printer lithography. *Lab on a Chip*, 13(9), 1762-1771.
- Pethig, R., Burt, J. P. H., Parton, A., Rizvi, N., Talary, M. S., & Tame, J. A. (1998). Development of biofactory-on-a-chip technology using excimer laser micromachining. *Journal of Micromechanics and Microengineering*, 8(2), 57.
- Popescu, M. N., Ralston, J., & Sedev, R. (2008). Capillary Rise with Velocity-Dependent Dynamic Contact Angle. *Langmuir*, 24(21), 12710-12716.
- Reboud, J., Bourquin, Y., Wilson, R., Pall, G. S., Jiwaji, M., Pitt, A. R., Graham, A., Waters, A. P., & Cooper, J. M. (2012). Shaping acoustic fields as a toolset for microfluidic manipulations in diagnostic technologies. *Proceedings of the National Academy of Sciences*, 109(38), 15162-15167.
- Ren, Y., & Leung, W. W.-F. (2013). Flow and mixing in rotating zigzag microchannel. *Chemical Engineering Journal*, 215–216(0), 561-578.
- Reyes, D., Iossifidis, D., Auroux, P. A., & Manz, A. (2002). Micro total analysis systems 1. Introduction, theory, and technology. *Analytical Chemistry*, (74), 2623–2636.
- Ritzi-Lehnert, M., Himmelreich, R., Attig, H., Claußen, J., Dahlke, R., Großhauser, G., Holzer, E., Jeziorski, M., Schaeffer, E., Wende, A., Werner, S., Wiborg, J., Wick, I., Drese, K., & Rothmann, T. (2011). On-chip analysis of respiratory viruses from nasopharyngeal samples. *Biomedical Microdevices*, 13(5), 819-827.

- Rosengarten, G., Harvie, D. J. E., & Cooper-White, J. (2006). Contact angle effects on microdroplet deformation using CFD. *Applied Mathematical Modelling*, 30(10), 1033-1042.
- Schönfeld, F., & Hardt, S. (2009). Dynamic contact angles in CFD simulations. *Computers & Fluids*, 38(4), 757-764.
- Schumacher, S., Nestler, J., Otto, T., Wegener, M., Ehrentreich-Forster, E., Michel, D., Wunderlich, K., Palzer, S., Sohn, K., Weber, A., Burgard, M., Grzesiak, A., Teichert, A., Brandenburg, A., Koger, B., Albers, J., Nebling, E., & Bier, F. F. (2012). Highly-integrated lab-on-chip system for point-of-care multiparameter analysis. *Lab on a Chip*, 12(3), 464-473.
- Schwarz, A., Rossier, J. S., Bianchi, F., Reymond, F., Ferrigno, R., & Girault, H. H. (1998). Micro-TAS on Polymer Substrates Micromachined by Laser Photoablation. In: D. J. Harrison & A. van den Berg (Eds.), *Micro Total Analysis Systems '98* (pp. 241-244): Springer Netherlands.
- Shikhmurzaev, Y. D. (1997). Spreading of drops on solid surfaces in a quasi-static regime. *Physics of Fluids*, 9(2), 266-275.
- Shoji, S., & Esashi, M. (1994). Microflow devices and systems. *Journal of Micromechanics and Microengineering*, 4(4), 157.
- Shravanthi, R., P. Randall, S., & Roger, T. B. (2005). Dynamic of low capillary number interfaces moving through sharp features. *Physics of Fluids*, 17, 1-6.
- Siegrist, J., Amasia, M., Singh, N., Banerjee, D., & Madou, M. (2010a). Numerical modeling and experimental validation of uniform microchamber filling in centrifugal microfluidics. *Lab on a Chip*, 10(7), 876-886.
- Siegrist, J., Gorkin, R., Clime, L., Roy, E., Peytavi, R., Kido, H., Bergeron, M., Veres, T., & Madou, M. (2010b). Serial siphon valving for centrifugal microfluidic platforms. *Microfluidics and Nanofluidics*, 9(1), 55-63.
- Soroori, S., Kulinsky, L., Kido, H., & Madou, M. (2013). Design and implementation of fluidic micro-pulleys for flow control on centrifugal microfluidic platforms. *Microfluidics and Nanofluidics*, 1-13.
- Steigert, J., Grumann, M., Brenner, T., Mittenbühler, K., Nann, T., Rühle, J., Moser, I., Haerberle, S., Riegger, L., Riegler, J., Bessler, W., Zengerle, R., & Ducrée, J. (2005). Integrated Sample Preparation, Reaction, and Detection on a High-Frequency Centrifugal Microfluidic Platform. *Journal of the Association for Laboratory Automation*, 10(5), 331-341.

- Strohmeier, O., Marquart, N., Mark, D., Roth, G., Zengerle, R., & von Stetten, F. (2014). Real-time PCR based detection of a panel of food-borne pathogens on a centrifugal microfluidic "LabDisk" with on-disk quality controls and standards for quantification. *Analytical Methods*, 6(7), 2038-2046.
- Takagi, J., Yamada, M., Yasuda, M., & Seki, M. (2005). Continuous particle separation in a microchannel having asymmetrically arranged multiple branches. *Lab on a Chip*, 5(7), 778-784.
- Terry, S. C., Jerman, J. H., & Angell, J. B. (1979). A gas chromatographic air analyzer fabricated on a silicon wafer. *Electron Devices, IEEE Transactions on*, 26(12), 1880-1886.
- Thio, T., Soroori, S., Ibrahim, F., Al-Faqheri, W., Soin, N., Kulinsky, L., & Madou, M. (2013). Theoretical development and critical analysis of burst frequency equations for passive valves on centrifugal microfluidic platforms. *Medical & Biological Engineering & Computing*, 51(5), 525-535.
- Tingrui, P., Scott, J. M., Eleanor, M. K., & Babak, Z. (2005). A magnetically driven PDMS micropump with ball check-valves. *Journal of Micromechanics and Microengineering*, 15(5), 1021.
- Tseng, F. G., Yang, I. D., Lin, K. H., Ma, K. T., Lu, M. C., Tseng, Y. T., & Chieng, C. C. (2002). Fluid filling into micro-fabricated reservoirs. *Sensors and Actuators A: Physical*, 97-98(0), 131-138.
- van Remoortere, P., & Joos, P. (1991). The kinetics of wetting: The motion of a three phase contactline in a capillary. *Journal of Colloid and Interface Science*, 141(2), 348-359.
- Wang, G. R., Yang, F., & Zhao, W. (2014). There can be turbulence in microfluidics at low Reynolds number. *Lab on a Chip*, 14(8), 1452-1458.
- Wang, Y., & Dimitrakopoulos, P. (2012). Low-Reynolds-number droplet motion in a square microfluidic channel. *Theoretical and Computational Fluid Dynamics*, 26(1-4), 361-379.
- Whitesides, G. M. (2006). The origins and the future of microfluidics. *Nature*, 442(7101), 368-373.
- Yamahata, C., Lacharme, F., Burri, Y., & Gijs, M. A. M. (2005). A ball valve micropump in glass fabricated by powder blasting. *Sensors and Actuators B: Chemical*, 110(1), 1-7.

- Yan, H., Zhang, B., & Wu, H. (2008). Chemical cytometry on microfluidic chips. *Electrophoresis*, 29(9), 1775-1786.
- Ymbern, O., Sandez, N., Calvo-Lopez, A., Puyol, M., & Alonso-Chamarro, J. (2014). Gas diffusion as a new fluidic unit operation for centrifugal microfluidic platforms. *Lab on a Chip*, 14(5), 1014-1022.
- Zehnle, S., Schwemmer, F., Roth, G., von Stetten, F., Zengerle, R., & Paust, N. (2012). Centrifugo-dynamic inward pumping of liquids on a centrifugal microfluidic platform. *Lab Chip*, 12(24), 5142-5145.
- Zeng, J., Banerjee, D., Deshpande, M., Gilbert, J., Duffy, C. D., & Kellog, D. J. (2000a). Design analysis of capillary burst valves in centrifugal microfluidics. *μTAS conf*, 579–582.
- Zeng, J., Deshpande, M., Greiner, B. K., & Gilbert, R. J. (2000b). Fluidic capacitance model of capillary-driven stop valves. Proceedings of ASME International Mechanical Engineering Congress and Exposition (pp. 1-7), Orlando, USA
- Zengerle, R., Ulrich, J., Kluge, S., Richter, M., & Richter, A. (1995). A bidirectional silicon micropump. *Sensors and Actuators A: Physical*, 50(1–2), 81-86.
- Zoval, J. V., & Madou, M. J. (2004). Centrifuge-based fluidic platforms. *Proceedings of the IEEE*, 92(1), 140-153.

LIST OF PUBLICATIONS AND PAPERS PRESENTED

As a result of this thesis and in collaboration with other researchers five technical peer-reviewed articles have been published in highly reputed journals, and two posters/papers have been presented in the international conferences. The first page of the published papers and the details of the conferences are shown here.

The details of the published articles are arranged by the publishing year as following:

a) articles:

1. Kazemzadeh, A., Ganesan, P., Ibrahim, F., Kulinsky, L., & Madou, M. J. (2014). Guided routing on spinning microfluidic platforms. RSC Advances.
2. Kazemzadeh, A.; Ganesan, P.; Ibrahim, F.; Aeinehvand, M. M.; Kulinsky, L.; Madou, M. J. (2014). "Gating valve on spinning microfluidic platforms: A flow switch/control concept." Sensors and Actuators B: Chemical 204(0): 149-158.
3. Aeinehvand, M. M.; Ibrahim, F.; Harun, S. W.; Al-Faqheri, W.; Thio, T. H. G.; Kazemzadeh, A.; Madou, M. (2014). "Latex micro-balloon pumping in centrifugal microfluidic platforms." Lab on a Chip 14(5): 988-997.
4. Kazemzadeh, A.; Ganesan, P.; Ibrahim, F.; He, S.; Madou, M. (2013). "The Effect of Contact Angles and Capillary Dimensions on the Burst Frequency of Super Hydrophilic and Hydrophilic Centrifugal Microfluidic Platforms, a CFD Study." PLoS ONE 8(9): e73002.
5. Aeinehvand, M., M., Ibrahim, F., Harun, S., Kazemzadeh, A., Rothan, H. A., Yusof, R., Madou, M. (2015) Reversible Thermo-Pneumatic Valves on Centrifugal Microfluidic Platforms, DOI: 10.1039/C5LC00634A

b) conferences:

1. Kazemzadeh, A.; Ganesan, P.; Ibrahim, F.; Aeinehvand, M. M.; Kulinsky, L.; Madou, M. J., Guide Routing On Spinning Microfluidic Platforms: A Passive Flow

Switch/Control, 24th Anniversary World Congress on Biosensors, 2014, Melbourne, Australia

2. Kazemzadeh, A.; Ganesan, P.; Ibrahim, F.; Madou M., Micro valves on CD platforms: partial investigation into influential aspects in burst frequency, 8th International Symposium on Heat Transfer ISHT-8, 2012, Beijing, China

University of Malaya